Telomere-dependent Interleukin-1 signalling promotes immunosuppression in tumor micro-environment

Ananda Kishore Mukherjee[1,2], Subhajit Dutta[1,2,$], Ankita Singh[1,$], Shalu Sharma[1,2], Shuvra Shekhar Roy[1,2], Antara Sengupta[1,2], Megha Chatterjee[1], Soujanya Vinayagamurthy[1,2], Sulochana Bagri[1,2], Divya Khanna[1], Meenakshi Verma[1], Dristhi Soni[1,2], Anshul Budharaja[3], Sagar Kailasrao Bhisade[4], Vivekanand[,2,6], Ahmad Perwez[1],Nija George[7], Ajay Pratap Singh[2,5],Mohammed Faruq[,2,5,6], Ishaan Gupta[3,4], Radhakrishnan Sabarinathan [7], Debasish Dash[2,5,] and Shantanu Chowdhury[1,2,5,8*]

$ Equal contribution

[1]Integrative and Functional Biology Unit, CSIR-Institute of Genomics and Integrative Biology, New Delhi 110026, India

[2]Academy of Scientific and Innovative Research (AcSIR), Ghaziabad 201002, India

[3]IIT Delhi, Hauz Khas, Delhi

[4]IISER Bhopal, Bhauri, Bhopal

[5]GNR Knowledge Centre for Genome and Informatics, CSIR-Institute of Genomics and Integrative Biology, New Delhi 110026, India

[6] Genomics and molecular medicine, CSIR-Institute of Genomics and Integrative Biology, New Delhi 110026, India

[7]National Centre for Biological Sciences, Tata Institute of Fundamental Research, Bellary Road, Bangalore 560065,Karnataka,India

[8]Lead contact *Correspondence: shantanuc@igib.in

Abstract

Telomere maintenance is crucial for cancer progression[1–5]. Anti-tumor immune response, on the other hand, is important for prognosis in cancer[6–10]. How telomeres affect anti-tumor immunity however is poorly understood. Here, we observed significant variation in cancer cell telomeres within the tumor microenvironment (TME) across cancer types. Infiltration of tumor-associated-macrophages (TAM) was sensitive to cancer cell telomeres. Using breast cancer tissue (>90 patients), tumor-derived organoids, cancer cells and xenograft tumors with either long or short telomeres we show interleukin-1 signalling is telomere-sensitive. Mechanistically, non-telomeric TRF2 binding at the IL-1-receptor-1 (*IL1R1*) promoter was telomere-dependent; enhanced TRF2 binding in case of short telomeres directly recruited the histone-acetyl-transferase p300; and, consequent H3K27 acetylation activated *IL1R1*. This enhanced IL-signalling, which induced secretion of the cytokine IL-1-beta resulting in increased TAM infiltration in tumors with shorter telomeres. M2-type macrophage infiltration was significantly reduced in presence of the receptor antagonist IL1RA, and *IL1R1*-knockout compromised TRF2-induced IL-1 activation, supporting specificity of the TRF2-IL1R1 axis in telomere-dependent TAM infiltration. Together these reveal a heretofore unknown function of telomeres in immunosuppression within the TME implicating telomeres as a key factor in the often-reported variation in patient response to immunotherapy.

Main

Introduction

Telomeres are composed of DNA repeats (TTAGGG) and proteins that constitute the end of each eukaryotic chromosome. Gradual shortening of telomeres and change in the telomeric structure with cell division leads to cellular senescence/death, which is crucial for tissue homeostasis[11–13]. During oncogenic transformation this process is affected resulting in uncontrolled cell proliferation and cancer progression underlining the impact of telomeres in cancer[14,15]. Major advances show how immune cells including tumor-infiltrating-lymphocytes (TIL), tumor-associated-macrophages (TAM), natural-killer and dendritic cells impact cancer progression[7,10]. TAMs - typically M2 macrophage-like – predominantly promote immunosuppressive TME through secretion of anti-inflammatory cytokines[16,17], implicating the role of TAMs in aggressive tumor growth[17,18]. However, despite the relevance in cancer prognosis and intervention[4,19], how telomeres influence anti-tumor immune response is poorly

understood. Here, upon finding variation in tumor-cell telomere length (TL) within the TME, we asked whether and how this affects TAM infiltration. Interestingly, non-telomeric TRF2 transcriptionally activated Interleukin-1-receptor-1 (IL1R1) in a telomere-dependent fashion. Resulting NFKappaB (p65)-phosphorylation-mediated IL1-signaling enhanced TAM infiltration within the TME in tumors with relatively short telomeres. Together these implicate telomere-sensitive immune-microenvironment in tumors.

Results

Variation in cancer cell telomere length within the tumor microenvironment

Fluorescently-labeled telomere-specific probes showed significant variation in cellular telomeric DNA within the TME in breast cancer (Figure 1A-B and Supplementary Figure 1A-B). We found similar variation in telomeric DNA in colon, gastric, ovarian, prostate and kidney TMEs (Figure 1C). Telomeric staining was optimized using cells with either long or short telomeres; and, pixel-by-pixel normalization of FITC (telomere) to DAPI (cellular DNA) showed variation in telomeric DNA was unlikely from cell density in the TME (details of staining including optimization in Supplementary Figure 1B). In addition to intra-tumor, variation in telomeres across tumors was evident (Figure 1A-C).

We measured TL in tissues from 94 breast cancer (triple-negative (TNBC)) patients for detailed analysis: Median length was ~3.6 kb (quantitative-telomeric-RTPCR[20] (Telo-qPCR); Figure 1D, Supplementary Table 1). Tumors with TL <50% of median were designated TNBC-short-telomeres (TNBC-ST) and >50% of median length TNBC-long-telomeres (TNBC-LT) (Figure 1D). TLs were confirmed by flow-cytometry and in-situ hybridization (Figure 1E-F). Further, reads from whole genome sequence of the TNBC samples were analyzed by TelSeq[21]: TL difference between TNBC-ST and LT was clear, and cancer tissue had lower TL than adjacent normal tissue consistent with earlier reports[19] (Supplementary Figure 1C). EpCAM^{+ve} (tumor-cell marker)[22] cells within the TME had significant heterogeneity in TL (lower in TNBC-ST vis-a-vis LT), whereas difference in TL of EpCAM^{-ve} cells was insignificant indicating TL variation in TME was primarily from cancer cells (Figure 1G and Supplementary Figure 1D).

Immunosuppressive tumor-associated-macrophage infiltration is telomere-dependent

To understand the functional significance of variation in cancer cell telomeres we used TNBC with long/short telomeres and focused on immune signaling. First, pro- and anti-inflammatory cytokines including IL-1 signaling was screened in TNBC tissue (12 patients), patient-derived organoids (TNBC-organoids from short (TNBO-ST) or long (TNBO-LT) telomeres), and cancer cells or mouse-xenograft tumors with long/short telomeres. *IL1B* and *IL1R1* expression was significantly low in case of tumors/cells with relatively long telomeres and notably consistent across clinical tissue, organoids, xenografts and cells, in contrast to the other cytokines (Supplementary Figure 1E). Additionally, 34 TNBC samples further confirmed the inverse correlation of *IL1R1* with TL; positive correlation between *IL1R1* and *IL1B* (Supplementary Figure 1F); and, RNA-seq in cancer cells with short/long telomeres showed key IL1 signaling genes largely upregulated in the short-telomere cells (Supplementary Figure 1G).

Based on consistent change in IL1 signaling in long versus short telomere tumors, and because tumor cell IL1 signaling has been widely implicated for TAM infiltration in multiple cancers[23–26], we checked TAM in TNBC-ST vis-à-vis TNBC-LT. Nine TNBC-ST and nine TNBC-LT tumors were analyzed for M2-type TAMs by double-positive CD11b (monocyte-derived cells)[27] and CD206 (M2-specific)[28] labeling: TNBC-LT had relatively low TAM infiltration (mean 1.78%, range: 0.18 – 5.41%) than TNBC-ST (mean 7.34%, range: 3.76-16.80%; Figure 1H). Accordingly, both CD206 levels within the TME (Figure 1I) and *CD206* expression was significantly low in TNBC-LT relative to TNBC-ST tumors (Supplementary Figure 1H).

TAM infiltration was further tested using patient tumor-derived organoids from five long and five short telomere cases. First, following organoid formation TL in each case was confirmed (Supplementary Figure 1I). M2-type macrophage derived from THP1 cells (Supplementary Figure 1J) were labeled (red-tracker dye) before co-incubating with each of the five TNBO-ST or five TNBO-LT: Following 12 hr incubation TNBO-ST had on average 8.56% infiltration of M2-type macrophages (range: 6.54-10.9%) compared to 3.14% (range: 0.99-4.88%) for TNBO-LT (Figure 1J).

Next tumor xenografts in NOD-SCID mice from cancer cells with either long or short telomeres were checked for TAM infiltration. We resorted to previously well-characterized cancer cells with short/long telomeres in cell-isogenic backgrounds: Fibrosarcoma HT1080 or corresponding long-telomere HT1080-LT cells with ~2 to 2.5-fold higher TL[29] (Supplementary Figure 1K). All the five HT1080-LT-derived xenograft tumors had increased proportion of cells with long

telomeres, and enhanced *hTERT* and *TERC* compared to the five HT1080 tumors as expected (Supplementary Figure 1L-M). We found average 5.21% $CD11b^{+}CD206^{+}$ cells (TAM infiltration) in HT1080 compared to 1.67% in case of the xenografts from HT1080-LT cells (Figure 1K). Consistent with this, expression of TAM-specific markers *CD163* and *CD206* was relatively low in LT xenografts (Supplementary Figure 1N); $F4/80^{+}$ cells representing the total macrophage lineage in mice[27] did not change significantly in long vs short-telomere xenografts Supplementary Figure 1O). Together these showed TAM infiltration was relatively low in tumors with long vis-à-vis short telomeres.

Secreted IL1B was significantly low in tumor-organoids TNBO-LT relative to TNBO-ST (Supplementary Figure 1P). Consistent with relatively lower *IL1R1* expression in TNBO-LT than TNBO-ST (Supplementary Figure 1E) and lower IL1R1 in xenograft tumors with long compared to short telomeres (Supplementary Figure 1Q) supporting IL1R1-dependent IL1B secretion noted in tumor cells[25]. Further, we used the IL1R1-receptor antagonist IL1RA to directly test IL1R1 dependence. Organoids treated with IL1RA before co-incubating with dye-labeled M2-type macrophages showed >50% reduction in macrophage infiltration (Figure 1L).

Non-telomeric TRF2 binding at the IL1 receptor R1 promoter is telomere-dependent

Next, we sought to understand how telomeres might affect *IL1R1*. First, reads from TRF2 ChIP-seq performed earlier[30] mapped ~200 bp upstream of the *IL1R1* TSS (transcription start site) (Supplementary Figure 2A); ChIP-qPCR spanning +200 to -1000 bp of the *IL1R1* TSS confirmed promoter TRF2 binding in HT1080 xenograft tumors and HT1080 cells (Supplementary Figure 2B). Second, we tested telomere-dependence of TRF2 binding based on TL-sensitive non-telomeric TRF2 binding observed earlier[31]. TRF2-ChIP in cells obtained from xenograft tumors or ex-vivo cultured HT1080-LT/HT1080 cells showed TRF2 occupancy at the *IL1R1* promoter was significantly reduced in cells with long relative to short telomeres (Figure 2A). IL1R1 was significantly low in HT1080-LT relative to HT1080 cells (IF/western/FACS; Figure 2B and Supplementary Figure 2C; mRNA expression in Supplementary Figure 2C); consistent with this, both expression and secretion of IL1B was significantly low in HT1080-LT compared to HT1080 cells (Supplementary Figure 2D).

Telomere-dependent TRF2 binding at the *IL1R1* promoter was further checked using *hTERT*-inducible HT1080 cells that gradually increased telomeres by ~50% over 12 days following

hTERT induction (Figure 2C, Supplementary Figure 2E): gradual reduction of *IL1R1* promoter TRF2 binding (Figure 2D) and *IL1R1* expression with telomere elongation over the 12 days was notable (Supplementary Figure 2F) consistent with HT1080/HT1080-LT cells (Figure 2A-B). An alternative telomere elongation model was made from TNBC MDAMB-231 cells using G-rich-telomere-repeat (GTR) oligonucleotides as reported earlier[31,32]. In resulting MDAMB-231-LT cells with ~1.8-2-fold increase in TL (Supplementary Figure 2G), *IL1R1* promoter TRF2 occupancy and *IL1R1* expression was significantly lower (Supplementary Figure 2H).

TRF2 transcriptionally activates *IL1R1*

TRF2 induction (Flag-TRF2 or stable-doxycycline-inducible-TRF2) showed increase in *IL1R1* expression and protein, and TRF2 silencing reduced *IL1R1* in HT1080 cells (Figure 2E, and Supplementary Figure 2I). *IL1R1* promoter activity was induced/repressed on TRF2 expression/silencing respectively (Supplementary Figure 2J); and, flag-TRF2-full-length, or without the B-domain (TRF2-delB) or M-domain (TRF2-delM) necessary for DNA binding, showed both promoter occupancy and activation was compromised in case of the mutants indicating TRF2 DNA binding as necessary (Figure 2F and Supplementary Figure 2K). Further, promoter TRF2 binding and TRF2-dependent activation of *IL1R1* was clearly evident in cancer MDAMB-231, and normal MRC5 fibroblasts or HEK293T cells (Supplementary Figure L-N).

G-quadruplex DNA secondary structure necessary for TRF2 binding to the *IL1R1* promoter

We reported TRF2 binding to G-quadruplex (G4) DNA secondary structures within promoters throughout the genome[30]; further, role of G4s in epigenetic regulation was noted[33]. Here, we found two G4s within the *IL1R1* promoter TRF2-binding site (Supplementary Figure 2O). BG4 antibody (against G4s[34]) ChIP was enriched ~200 bp upstream on the *IL1R1* promoter (Figure 2G); TRF2-dependent *IL1R1* promoter activity was compromised on introducing G4-deforming G>T substitutions (Figure 2H); and, in presence of the intracellular G4-binding ligand 360A[35] TRF2-induced IL1R1 promoter activity, expression/protein was significantly reduced (Figure 2I). Using CRISPR we artificially inserted a *IL1R1* luciferase-reporter-cassette (-1500 bp) at the CCR5 safe-harbor locus in HEK293T cells; TRF2 binding and TRF2-dependent promoter activity from the inserted *IL1R1* promoter-reporter was clear supporting earlier results (Figure

2J). Next, on making base substitutions that deformed the G4 motif B in the inserted reporter, TRF2 binding and promoter activity was significantly reduced showing G4 dependence (Figure 2J). Furthermore, CRISPR-mediated G>T editing in the promoter G4 (motif B) within the endogenous *IL1R1* promoter resulted in significant reduction of TRF2 binding and *IL1R1* expression (Supplementary Figure 2P).

TRF2-dependent recruitment of histone acetyl transferase p300 induces H3K27ac modification at the *IL1R1* promoter

Screening of activation (H3K4me3 and H3K27ac) and repressive (H3K27me3, H3K9me3) histone marks at the *IL1R1* promoter following TRF2 induction showed enhanced H3K27acetylation (Supplementary Figure 3A). In both HT1080 and MDAMB-231 cells, *IL1R1* promoter H3K27 acetylation increased/reduced on TRF2 induction/silencing, respectively (Figure 3A). We sought to find a potential histone acetyl transferase (HAT) and noted canonical HATs p300/CBP[36] at the *IL1R1* promoter in multiple cell lines in ENCODE (Supplementary Figure 3B). ChIP-qPCR confirmed p300 occupancy within upstream 200-400 bp promoter of *IL1R1* in TRF2-up conditions, that reduced significantly on TRF2 downregulation, in HT1080 and MDAMB-231 cells (Figure 3B). Furthermore, occupancy of CBP and acetylated-p300/CBP (activated HAT) was enriched at the *IL1R1* promoter on TRF2-induction in HT1080 cells (Figure 3C). Together these showed TRF2-mediated recruitment and acetylation of p300/CBP, resulting in H3K27 acetylation at the *IL1R1* promoter. *IL1R1* promoter occupancy of p300, CBP, ac-p300/CBP and H3K27ac was relatively low in HT1080-LT compared to HT1080 cells with shorter telomeres (Figure 3D) consistent with lower TRF2 occupancy at the *IL1R1* promoter in LT cells (Figure 2A).

To test direct function of TRF2 in p300 recruitment Flag-TRF2 mutants (K176R, K179R or K190R required for protein-protein interaction; K293R for acetylation[37,38]) were screened (Supplementary Figure 3C). TRF2-K293R gave notably compromised activation of *IL1R1* (Figure 3E and Supplementary Figure 3C) and significantly reduced p300 and ac-p300/CBP recruitment on the *IL1R1* promoter relative to TRF2-wildtype (WT)-induction (Figure 3F). However, binding of flag-TRF2-293R at the *IL1R1* promoter was similar to TRF2-WT (Figure 3F) suggesting loss in TRF2-mediated p300 recruitment and not due to promoter binding by TRF2-293R. This was further consistent with interaction of TRF2 with p300, and acetylated p300, evident from co-immunoprecipitation (Figure 3G). To ascertain direct TRF2-p300 interaction,

and consequent H3K27 acetylation, we did histone-acetyl-transfer assays using purified p300 and histone H3, and acetyl-coA (substrate for the acetyl group) with or without recombinant TRF2. Transfer of the acetyl group to histone H3 was significantly enhanced in presence of both TRF2 and p300, relative to p300 only; and, TRF2 without p300 gave marginal HAT activity (Figure 3H). These together demonstrate a direct function of TRF2 in recruitment and HAT activity of p300 in H3K27 acetylation at the *IL1R1* promoter.

Cancer cells with higher TRF2 are sensitive to IL1-mediated NFKappaB (p65) activation

Primarily ligands IL1A/B via receptors IL1R1/R2 activate IL1 signaling through NFKappaB (p65/RELA)-Ser536 phosphorylation[39]. This induces *IL1B* and other inflammatory genes including *IL6, IL8* and *TNF.* Here we checked NFKappaB-Ser536 phosphorylation following stimulation with IL1B in presence/absence of TRF2 in HT1080 and MDAMB-231 cells. TRF2-induction gave relatively enhanced NFKappaB-Ser536 phosphorylation that sustained for a longer duration compared to uninduced in both cell types; total NFKappaB levels remained unaltered (Figure 4 A-B). We reasoned, in cells with longer telomeres IL1 signaling would be affected due to reduced TRF2 binding at the *IL1R1* promoter resulting in attenuated activation of *IL1R1*. In case of HT1080-LT cells NFKappaB-Ser536 phosphorylation, following IL1B stimulation, was notably delayed (3 hr vs 30 min in HT10180-LT or HT1080, respectively; Supplementary Figure 4A). Accordingly on stimulation with either IL1A or IL1B in TRF2-silenced condition expression of the NFKappaB targets *IL6, IL8* and *TNF* were reduced (Figure 4C). Further, the ligand TNFα was reported to induce NFkappaB in IL1-independent fashion[40] suggesting this pathway would be unaffected by presence/absence of TRF2. Indeed, expression of NFkappaB targets (*IL6, IL8* and TNF) remained unaffected on stimulation by TNFα in absence of TRF2, supporting the role of TRF2 in IL1 signaling specifically (Figure 4C). Additionally, TRF2 induction gave enhanced expression of *IL6, IL8* and *TNF*α, that was rescued in presence of the receptor antagonist IL1RA, further confirming the specific role of TRF2-IL1R1 in NFKappaB activation (Figure 4D).

HT1080 cells with doxycycline-inducible-TRF2 were used to make tumor xenografts in NOD-SCID mice. TRF2-induced tumors had enhanced IL1R1 and NFKappaB-Ser536 phosphorylation indicating NFKappaB activation relative to the xenograft tumors where TRF2 was not induced (Figure 4E-F). To directly test the function of IL1R1 in TRF2-mediated NFKappaB activation, *IL1R1*-knockout (KO; CRISPR-mediated) was made in HT1080 cells

having doxycline-inducible-TRF2: NFkappaB activation (Ser536-phosphorylation), including upregulation of the NFkappaB-target genes *IL2, IL6* and *TNF*, was significantly reduced following TRF2 induction in the KO cells compared to HT1080 cells (Supplementary Figure 4B). Together, these demonstrate the direct role of TRF2 in induction of IL1 signaling through upregulation of *IL1R1*.

Enhanced IL1 signaling induces infiltration of M2-type macrophage in breast and other cancers[17,26]. Here, we asked whether TRF2 affected TAM infiltration. TAM ($CD11b^{+}CD206^{+}$) was enhanced from ~5% to ~10% in TRF2-induced xenografts relative to the un-induced tumors (Figure 4F). Accordingly, expression of TAM markers (CD163 and CD206; Supplementary Figure 4C) was found to be higher in TRF2 induced xenograft tumors.

The clinical significance of blocking IL1 signaling in cancers has been widely reported[41–43]. Based on our findings, we attempted TRF2-mediated single-gene-targeted epigenetic silencing of *IL1R1*. The TRF2 mutant K293R, devoid of H3K27 acetylation activity, gave loss of function (Figure 3E-F). Therefore, TRF2-K293R was fused to dead-Cas9 (dCas9-TRF2-K293R), and dCas9-TRF2 was used as control. On using sgRNA against the *IL1R1* promoter we found significant activation or downregulation of *IL1R1* in case of dCas9-TRF2 or dCas9-TRF2-K293R, respectively, in HT1080 and MDAMB231 cells; whereas other TRF2-target genes[31] remained unaffected indicating single-gene specificity (Figure 4H). dCas9-TRF2-K293R diminished IL1R1 levels and resulted in reduced NFkappaB-Ser536 phosphorylation indicating attenuated NFKappaB activation in HT1080 and MDAMB 231 cells; dCas9-TRF2 as expected showed activation of IL1R1 and NFkappaB (Figure 4I).

Finally, we analyzed larger datasets for any broad implications. First, IL1 signaling and TAM-specific markers positively correlated in transcriptomes of 817 TNBC patients: Low/high expression of *IL1R1* or *IL1B* correlated with low/high expression of TAM-specific markers *CD163* and *CD206* respectively (Supplementary Figure 4D). Second, we analyzed 2593 patients across 30 cancer types (including breast, lung, pancreatic, bladder, renal and glioma), and 257 breast cancer patients with high/low *IL1R1*. High *IL1R1* was significantly associated with poor prognosis consistent with reported outcomes from enhanced TAM (Figure 4J). Third, Barthel *et. al.* analyzed telomere-dependent transcriptome in 9065 tumors from 31 cancer types noting immune-response genes as predominantly telomere-sensitive genes; tumor TL was estimated from WGS data[44]. On closer analysis, we observed 'macrophage-inhibitory-factor' genes were significantly altered on telomere elongation across the 31 cancers (Supplementary

Figure 4E). Together with our experimental results these connect immunosuppressive TAM to telomere-sensitive, and TRF2-dependent, IL1 signaling (Figure 4K),consistent with aggressive proliferation reported in TRF2-high tumors[45].

Discussion

Recently we described TL-sensitive expression of genes distant from telomeres[31]. Cells with relatively long telomeres sequestered more TRF2 at the telomeres affecting non-telomeric binding, and vice-versa. Proposed as the telomere-sequestration-partition (TSP) model[46] this is independent from telomere-positioning-effect (TPE) on expression of sub-telomeric genes (up to 10 Mb from telomeres)[47]. TL-dependent *IL1R1* activation by non-telomeric TRF2 is in tune with the TSP model (Figure 4K). Altered transcription when telomere maintenance is affected or TL-sensitive expression observed in varied contexts[31,48], particularly across 31 cancer types[44], appear consistent with TSP, and support TL-dependent IL1 signaling.

Besides TRF2, non-telomeric function of the shelterin protein RAP1 was reported in complex with NFKappaB[49]. Although TRF2 was implicated in influencing Natural Killer (NK) cells and infiltration of Myeloid Derived immuno-Suppressive Cells (MDSC)[50,51] underlying mechanisms were unclear. We recently noted transcription repression of telomerase (*hTERT*) to be TRF2-mediated in a PRC2-repressor dependent fashion[52] .This, interestingly, suggests the emerging role of TRF2 as a transcriptional modulator with repressor/activator (as shown here) functions depending on cofactor engagement that is possibly contextual. The RNA template of telomerase (*TERC*), but not *hTERT*, was higher in TNBC-LT (Supplementary Figure 5A), and telomerase activity (from 64 TNBC samples) did not positively correlate with telomere length (Supplementary Figure 5B) possibly due to the complexity of telomerase/TME interdependence as also noted earlier[19,53,54].

For functional significance of TL in TME we focused on IL1-signalling and TAM. It is possible that TL affects tumor-immune signalling through other immune cell types (implied by altered immune-response genes in TL-dependent gene-expression analysis[44,48]) and/or influences the nature of TAM, which is known to vary contextually[55]. These, together with the well-established effect of IL1-targeting in improving cancer prognosis[24,29,41,43] underlines the need for further work to understand telomere-sensitive IL1 signalling.

Tumors largely maintain shorter telomeres than normal tissue[19], and M2-type TAMs aid immunosuppression[56]. Results here reveal causal links between tumor-cell TL and TME. In tumor cells with shorter TL activated IL1 signaling increases M2-type TAM infiltration. It is possible therefore that short-TL tumor cells compete better against anti-tumor immune cells due to TAM-induced immunosuppression, gaining selective advantage. Together these reveal new molecular connections between telomeres and tumor immunosuppression, presenting another conceptual framework for better understanding of patient-specific response to cancer immunotherapy.

Acknowledgements

We acknowledge Manish Rai (confocal imaging), Debojyoti Chakraborty Lab (DeltaVision Microscopy), Vivek Rao (THP1 cells) and Mohit Agarwal (ELISA experiments) from CSIR-IGIB. Fellowships from CSIR (AKM, AS, SSR, SS, ASG, SVM, SB and DS); DBT-Wellcome Trust India Alliance (AKM, AS, MC, MV and AP); UGC (SD) and DST (DK) are acknowledged. R.S and N.G acknowledges intramural funding support from NCBS-TIFR. This work was supported by the DBT/Wellcome Trust India Alliance Fellowship [grant number IA/S/18/2/504021] awarded to SC, and research funding from the Council of Scientific and Industrial Research (CSIR) and Department of Biotechnology (DBT).

Author Contributions

Experimental design and execution: Tel-PNA FISH –SD; Tel-qRT PCR- MC,MV and AKM; Tel-Flow- AKM;CD206 IHC-AS and AKM;CD206/CD11b Flow- AKM and MC; F4/80 Flow-AKM; TNBO-M2 infiltration flow-AKM; gene expression(TNBC)- AKM and MC, Telomerase activity-MC, gene expression(TNBO, xenograft, ex-vivo)-AKM,SS. IF-AKM,SVM; ChIP-AKM,SS,ASG,AS; Luciferase assays- AKM,SSR,ASG; WB- AKM,SVM,ASG,SSR,SD;IP-AKM;HAT Assay- AKM; IL1B ELISA- SS,AKM; gene expression(dCAS9 related)-SD; Immuno-Flow for IL1R1- AKM,SD; Immuno-Flow NFKB related- AKM,SD; Data Analysis-AB,SKB,IG,NG,RS,SD,AKM;

Resources: TNBC tissue collection- AS; TNBO generation- DK, AKM,SVM,AS,AP; THP1-Macrophage–AKM; NOD-SCID xenograft tumors-AKM,SD; Luciferase constructs-SSR, ASG; CCR5-insert cells-SSR,AKM; HEK IL1R1 G4 mutant cells- SSR,AS; IL1R1 gRNA- SSR; HT1080-TERT inducible- ASG,DS;HT1080-TRF2 inducible- ASG; HT1080 IL1R1 KO-SSR,AKM; HT1080 IL1R1 KO TRF2 inducible- AKM;MDAMB-231 LT cells-SS,AP; TRF2 PTM

mutant plasmids- SB; TRF2 protein extraction-SB and ASG; TNBC whole genome sequencing-AS;HT1080-HT1080-LT RNA seq- SS,VA,MF;

Data collation-AKM, SD, AS, SSR, ASG, SVM, SC; Figure preparation-AKM, SD, AS, SC; Manuscript writing and editing- AKM, SD, AS, SC; Conceptualization of idea and planning of experiments- AKM and SC; Overall supervision and funding-SC.

Conflict of Interest

The authors declare no conflict of interest.

References

1. Shay, J. W. Role of Telomeres and Telomerase in Aging and Cancer. *Cancer Discov.* **6**, 584–593 (2016).

2. Greider, C. W. Telomerase activity, cell proliferation, and cancer. *Proc. Natl. Acad. Sci. U. S. A.* **95**, 90–92 (1998).

3. Blackburn, E. H. Telomere states and cell fates. *Nature* **408**, 53–56 (2000).

4. Artandi, S. E. E. & DePinho, R. A. A. Telomeres and telomerase in cancer. *Carcinogenesis* **31**, 9–18 (2009).

5. Paeschke, K. *et al.* Telomeres: Structures in need of unwinding. *FEBS Lett.* **584**, 3760–3772 (2010).

6. F Balkwill, A. M. M., Balkwill, F. & Mantovani, A. Inflammation and cancer: back to Virchow? *Lancet* **357**, 539–545 (2001).

7. Gonzalez, H. *et al.* Roles of the immune system in cancer: from tumor initiation to metastatic progression. *Genes Dev.* **32**, 1267–1284 (2018).

8. Jochems, C. & Schlom, J. Tumor-infiltrating immune cells and prognosis: the potential link between conventional cancer therapy and immunity. *Exp. Biol. Med. (Maywood).* **236**, 567 (2011).

9. Salgado, R. & Gevaert, T. Quantity of Immune Cells Predict Response to Immunotherapy in Cancer. *eClinicalMedicine* **41**, 101170 (2021).

10. Binnewies, M. *et al.* Understanding the tumor immune microenvironment (TIME) for effective therapy. *Nat. Med.* **24**, 541–550 (2018).

11. Shay, J. W. & Wright, W. E. Hayflick, his limit, and cellular ageing. *Nat Rev Mol Cell Biol* **1**, 72–76 (2000).

12. Jacobs, J. J. L. Senescence: back to telomeres. *Nat. Rev. Mol. Cell Biol.* **14**, 196–196 (2013).

13. Karlseder, J. Senescence Induced by Altered Telomere State, Not Telomere Loss.

Science (80-.). **295**, 2446–2449 (2002).

14. Hanahan, D. & Weinberg, R. a. The hallmarks of cancer. *Cell* **100**, 57–70 (2000).

15. Maciejowski, J. & Lange, T. de. Telomeres in cancer: tumour suppression and genome instability. *Nat. Rev. Mol. Cell Biol. 2017 183* **18**, 175–186 (2017).

16. DeNardo, D. G. & Ruffell, B. Macrophages as regulators of tumour immunity and immunotherapy. *Nat. Rev. Immunol. 2019 196* **19**, 369–382 (2019).

17. Pittet, M. J., Michielin, O. & Migliorini, D. Clinical relevance of tumour-associated macrophages. *Nat. Rev. Clin. Oncol. 2022 196* **19**, 402–421 (2022).

18. Hu, W. *et al.* Tumor-associated macrophages in cancers. *Clin. Transl. Oncol. 2015 183* **18**, 251–258 (2015).

19. Aviv, A., Anderson, J. J. & Shay, J. W. Mutations, Cancer and the Telomere Length Paradox. *Trends in Cancer* **3**, 253–258 (2017).

20. O'Callaghan, N. J., Dhillon, V. S., Thomas, P. & Fenech, M. A quantitative real-time PCR method for absolute telomere length. **44**, 807–809.

21. Ding, Z., Mangino, M., Aviv, A., Spector, T. & Durbin, R. Estimating telomere length from whole genome sequence data. *Nucleic Acids Res.* **42**, e75 (2014).

22. Went, P. T. *et al.* Frequent EpCam protein expression in human carcinomas. *Hum. Pathol.* **35**, 122–128 (2004).

23. Carmi, Y. *et al.* The Role of Macrophage-Derived IL-1 in Induction and Maintenance of Angiogenesis. *J. Immunol.* **183**, 4705–4714 (2009).

24. Mantovani, A., Dinarello, C. A., Molgora, M. & Garlanda, C. Interleukin-1 and Related Cytokines in the Regulation of Inflammation and Immunity. *Immunity* **50**, 778–795 (2019).

25. Lappano, R. *et al.* The IL1β-IL1R signaling is involved in the stimulatory effects triggered by hypoxia in breast cancer cells and cancer-associated fibroblasts (CAFs). *J. Exp. Clin. Cancer Res. 2020 391* **39**, 1–22 (2020).

26. Chittezhath, M. *et al.* Molecular Profiling Reveals a Tumor-Promoting Phenotype of Monocytes and Macrophages in Human Cancer Progression. *Immunity* **41**, 815–829 (2014).

27. Cassetta, L. *et al.* Isolation of Mouse and Human Tumor-Associated Macrophages. *Adv. Exp. Med. Biol.* **899**, 211 (2016).

28. Jaynes, J. M. *et al.* Mannose receptor (CD206) activation in tumor-associated macrophages enhances adaptive and innate antitumor immune responses. *Sci. Transl. Med.* **12**, 6337 (2020).

29. Cristofari, G. & Lingner, J. Telomere length homeostasis requires that telomerase levels are limiting. *EMBO J.* **25**, 565–574 (2006).

30. Mukherjee, A. K. *et al. Telomere repeat-binding factor 2 binds extensively to extra-telomeric G-quadruplexes and regulates the epigenetic status of several gene promoters*.

Journal of Biological Chemistry vol. 294 17709–17722 (American Society for Biochemistry and Molecular Biology Inc., 2019).

31. Mukherjee, A. K. *et al.* Telomere length-dependent transcription and epigenetic modifications in promoters remote from telomere ends. *PLOS Genet.* **14**, e1007782 (2018).

32. Wright, W. E., Brasiskyte, D., Piatyszek, M. a & Shay, J. W. Experimental elongation of telomeres extends the lifespan of immortal x normal cell hybrids. *EMBO J.* **15**, 1734–1741 (1996).

33. Mukherjee, A. K., Sharma, S. & Chowdhury, S. *Non-duplex G-Quadruplex Structures Emerge as Mediators of Epigenetic Modifications*. *Trends in Genetics* vol. 35 129–144 (2019).

34. Biffi, G., Tannahill, D., McCafferty, J. & Balasubramanian, S. Quantitative visualization of DNA G-quadruplex structures in human cells. *Nat. Chem.* **5**, 182–6 (2013).

35. Granotier, C. *et al.* Preferential binding of a G-quadruplex ligand to human chromosome ends. *Nucleic Acids Res.* **33**, 4182–4190 (2005).

36. Roth, S. Y., Denu, J. M. & Allis, C. D. Histone Acetyltransferases. *http://dx.doi.org/10.1146/annurev.biochem.70.1.81* **70**, 81–120 (2003).

37. Rizzo, A. *et al.* SIRT6 interacts with TRF2 and promotes its degradation in response to DNA damage. *Nucleic Acids Res.* **45**, 1820–1834 (2017).

38. YR, H. & IK, C. p300-mediated acetylation of TRF2 is required for maintaining functional telomeres. *Nucleic Acids Res.* **41**, 2267–2283 (2013).

39. A, W., P, W. & M, K. Interleukin-1 (IL-1) pathway. *Sci. Signal.* **3**, (2010).

40. Liu, T., Zhang, L., Joo, D. & Sun, S.-C. C. NF-κB signaling in inflammation. *Signal Transduct. Target. Ther. 2017 21* **2**, 1–9 (2017).

41. Briukhovetska, D. *et al.* Interleukins in cancer: from biology to therapy. **21**, 481–499 (2021).

42. Kaplanov, I. *et al.* Blocking IL-1β reverses the immunosuppression in mouse breast cancer and synergizes with anti–PD-1 for tumor abrogation. *Proc. Natl. Acad. Sci.* **116**, 1361–1369 (2019).

43. Mantovani, A., Barajon, I. & Garlanda, C. IL-1 and IL-1 Regulatory Pathways in Cancer Progression and Therapy. *Immunol. Rev.* **281**, 57 (2018).

44. Barthel, F. P. P. *et al.* Systematic analysis of telomere length and somatic alterations in 31 cancer types. *Nat. Genet. 2017 493* **49**, 349–357 (2017).

45. Muñoz, P., Blanco, R. & Blasco, M. A. Role of the TRF2 telomeric protein in cancer and ageing. *Cell Cycle* **5**, 718–721 (2006).

46. Vinayagamurthy, S., Ganguly, A. & Chowdhury, S. Extra-telomeric impact of telomeres: Emerging molecular connections in pluripotency or stemness. *J. Biol. Chem.* **295**, 10245–10254 (2020).

47. Robin, J. D. *et al.* Telomere position effect: regulation of gene expression with progressive telomere shortening over long distances. *Genes Dev.* **28**, 2464–2476 (2014).

48. Hirashima, K. *et al.* Telomere Length Influences Cancer Cell Differentiation In Vivo. *Mol. Cell. Biol.* **33**, 2988–2995 (2013).

49. Teo, H. *et al.* Telomere-independent Rap1 is an IKK adaptor and regulates NF-kappaB-dependent gene expression. *Nat. Cell Biol.* **12**, 758–767 (2010).

50. Biroccio, A. *et al.* TRF2 inhibits a cell-extrinsic pathway through which natural killer cells eliminate cancer cells. *Nat. Cell Biol.* **15**, 818–28 (2013).

51. Cherfils-Vicini, J. *et al.* Cancer cells induce immune escape via glycocalyx changes controlled by the telomeric protein TRF2. *EMBO J.* **38**, e100012 (2019).

52. Shalu Sharma, A. *et al.* Human telomerase is directly regulated by non-telomeric TRF2-G-quadruplex interaction. *CellReports* **35**, 109154 (2021).

53. Blasco, M. a, Rizen, M., Greider, C. W. & Hanahan, D. Differential regulation of telomerase activity and telomerase RNA during multi-stage tumorigenesis. *Nat. Genet.* **12**, 200–204 (1996).

54. Ghosh, A. *et al.* Telomerase directly regulates NF-B-dependent transcription. *Nat. Cell Biol.* **14**, 1270–1281 (2012).

55. Mantovani, A. & Locati, M. Tumor-associated macrophages as a paradigm of macrophage plasticity, diversity, and polarization lessons and open questions. *Arterioscler. Thromb. Vasc. Biol.* **33**, 1478–1483 (2013).

56. Allavena, P., Sica, A., Solinas, G., Porta, C. & Mantovani, A. The inflammatory micro-environment in tumor progression: The role of tumor-associated macrophages. *Crit. Rev. Oncol. Hematol.* **66**, 1–9 (2008).

Methods:

Cell lines, media and culture conditions

HT1080 fibrosarcoma cell line was purchased from ATCC. HT1080-LT cells[1] were a kind gift from Dr. J.Ligner. HT1080 and MRC5 (purchased from ATCC) cells and corresponding telomere elongated cells were maintained in Modified Eagle's medium (MEM) (Sigma-Aldrich) supplemented with 10% Fetal Bovine Serum (FBS) (Gibco). MDAMB231 (gift from Mayo Clinic, Minnesota, USA) and HEK293T (purchased from NCCS, Pune) cells were maintained in DMEM-HG (Dulbecco's Modified Eagle's medium - High Glucose) (Sigma-Aldrich) with a supplement of 10% FBS. All THP1 cell line (gift from Dr Vivek Rao, IGIB, Delhi and subsequently purchased from NCCS, Pune) and derivative cell types were maintained in RPMI with 10% FBS and 1X Anti-Anti (anti-biotic and anti-mycotic from Thermo Fisher Scientific). All cultures were grown in incubators maintained at 37ºC with 5% CO_2. All stable line generated from these cell types were maintained in the same media with 1X Anti-Anti.

Processing of tumor/xenograft tissue:

Tissues collected for this study was stored in RNA later (Sigma-Aldrich) in -80 °C. Approximately 10 milligram of tumor tissue was weighed and washed thrice with ice-cold 1X PBS- 1 ml (filtered). About 300 microlitres of PBS was left to submerge the tissue after the final wash. Using a sanitized razor blade, the tumor was cut into small pieces (the efficiency of the digestion is dependent on how well the tumor is minced; large pieces will not digest properly and may need extra digestion time). The tumor soup was transferred into a 15 ml tube using a P1000 pipette (cut the top of the tip in order to be able to take all the tissue) and the volume was adjusted to 4 ml of 1X pre-chilled PBS. 80 µl of Liberase TL stock solution (Roche) was mixed using a vortex and incubate for 45 min at 37 °C under continuous rotation. The sample was checked visually; the cell suspension should look smooth (if the cell suspension still contains tissue fragments digest for an additional 15 min). To end the enzymatic digestion,10 ml PBS with 1 % w/v BSA (Sigma-Aldrich) was added. The cells were filtered using a 100 µm cell strainer in a 50 ml tube and the volume adjusted to 20 ml with 1X PBS (pre-chilled). Cells were centrifuged for 7 min at 500 g and 4 °C. The supernatant was discarded and the cells were re-suspended in 1 ml Serum-free media. Subsequently, cells were counted and volume made up to get a cell density of 1 million cells/ ml. Following this, cell suspension was used for ChIP, DNA/RNA isolation and flow-cytometry.

Organoid generation and culture:

TNBC tissue was used to make tumor organoids using the following protocol-

1. The fresh tissue was stored in 5 ml of Media 1 (Advanced DMEM F12 + 1X Glutamax + 10mM HEPES + 1X AA).

2. 1-3 mm^3 tissue piece was cut, washed and minced in 10ml (Media 1).

3. The minced tissue was digested overnight on shaker in Media 1 with 1-2mg/ml of collagenase.

4. After overnight incubation the digested tissue was sequentially sheared using 1 ml pipette.

5. After each shearing step, the suspension was strained using 100µm filter to retain tissue pieces. Thus entering in subsequent shearing step with approximately 10 ml Advanced DMEM F12.

6. To this was added 2% FCS and centrifuged at 400 rcf.

7. The pellet was resuspended in 10mg/ml cold cultrex growth factor reduced BME Type 2 and 40µl drops of BME suspension was allowed to solidify on pre-warmed 24 well culture plates at 37°C 5% CO_2 for 30 min.

8. Upon complete gelation 400 µl of BC organoid medium was added to each well and plates transferred to 37°C 5% CO_2.

Medium component	Supplier	Catalogue number	Final concentration
R-Spondin 3	R&D	3500-RS/CF	250 $ng \cdot ml^{-1}$
Neuregulin 1	Peprotech	100-03	5 nM
FGF 7	Peprotech	100-19	5 $ng \cdot ml^{-1}$
FGF 10	Peprotech	100-26	20 $ng \cdot ml^{-1}$
EGF	Peprotech	AF-100-15	5 $ng \cdot ml^{-1}$ [a]
Noggin	Peprotech	120-10C	100 $ng \cdot ml^{-1}$
A83-01	Tocris	2939	500 nM

Y-27632	Abmole	Y-27632	5 mM
SB202190	Sigma	S7067	500 nM [b]
B27 supplement	Gibco	17504-44	1x
N-Acetylcysteine	Sigma	A9165-5g	1.25 mM
Nicotinamide	Sigma	N0636	5 mM
GlutaMax 100x	Invitrogen	12634-034	1x
Hepes	Invitrogen	15630-056	10 mM
Penicillin/Streptomycin	Invitrogen	15140-122	100 $U \cdot ml^{-1}$ / 100 $mg \cdot ml^{-1}$
Primocin	Invivogen	Ant-pm-1	50 $mg \cdot ml^{-1}$
Advanced DMEM/F12	Invitrogen	12634-034	1x

9. The media was changed every fourth day.

10. The culture was grown for 10 days before passaging.

II. Passaging Organoid Cultures

1. Cultrex growth factor reduced BME Type 2 geltrex was thawed overnight on ice at 4 °C.

2. Media was removed from the organoid wells and washed twice with PBS-EDTA.

3. For each well of 24 well plate 300 µl of TrypLE was added and incubated at 37°C 5% CO_2 for 5 min.

4. 600 µl of washing media (DMEM F12) was added and organoids were dissociated vigorously by pipetting.

5.. Organoid solution was transferred to 15 ml falcon with 5 ml washing media and centrifuged at 1000rpm for 5 min to pellet organoids.

6. Supernatant was carefully aspirated leaving behind 200ul media and 500ul of fresh media, mixed well gently and transferred to 1.5ml tube for centrifugation at 650*g for 5min at 4 °C .

7. Supernatant was gently aspirated and resuspended in cold cultrex and 40ul drop/well was seed in a pre-warmed 24 well plate.

8. Incubated for 30 min and add 400 µl of BC organoid medium.

M2 macrophage generation from THP1 cells:

THP1 cells (0.5 million cells in 1ml) were seeded in a 35 mm dish and treated with PMA (10 ng/ml) (Sigma-Aldrich) for 24 hrs in RPMI complete media (+ 10% FBS) (Gibco). PMA was removed and cells were cultured for 48 hrs in RPMI to get semi-adherent M0 cells. Following this, cells were treated with IL4 (10 ng/ml) (Gibco) and IL13 (20 ng/ml) (Gibco) for 24 hrs in RPMI complete media. Cells were checked for expected morphological changes and trypsinized for use as M2 macrophages.

M2 macrophage infiltration assay in TNBC tumor organoids:

M2 macrophages were labelled with Cell Tracker red dye (Thermo Fisher Scientific) for 30 mins and the excess dye was washed off. 10000 labelled M2 macrophages in 20 ul 1X PBS were introduced in a 96 well with TNBC organoids in a dome with supplement enriched media (200 µl). 12 hrs. later, the media was washed off with 3 1X PBS washes and the organoid dome was extracted with 100 µl TrypLE (Gibco) and resuspended with 100 ul chilled 1X PBS. This cocktail was kept on ice for 5 mins and centrifuged at 1000g for 10 mins. The supernatant was removed and the process was repeated.

The cells were resuspended in 500 ul chilled 1X PBS and subjected to Flow-cytometric analysis for scoring percentage of labelled (red) M2 macrophages infiltrating the organoids.

Xenograft tumor generation in NOD-SCID mice:

The xenograft tumor generation in NOD SCID tumors was outsourced to a service provider (Vivo Bio TechLtd – Telangana, India). 2.5 million cells (HT1080, HT1080-LT or HT1080-TRF2 inducible) were subcutaneously injected in healthy male mice (4-6 weeks old) and tumor growth was allowed. In case of TRF2 inducible HT1080 cells, tumors were allowed to grow to 100 mm^3 before oral dosage of doxycycline (or placebo control) was started at 2 mg/kg of body weight of mice. Mice were sacrificed to obtain tumors when tumors reached an average volume of 600 mm^3(± 100).

Telomeric Fluorescent *in-situ* hybridization (FISH)

FFPE tissue sections on coated slides were procured from hospital. Telomere-specific PNA probe [TelC-FITC-F1009-(CCCTAA)n from PNABio] was used following the manufacturer protocol with minor modifications. Briefly, the tumor tissue sections were deparaffinized using Xelene (Sigma-Aldrich) followed by incubation for 2 min each in 100%, 90%, 70%, and 50% cold ethanol (Merck) to rehydrate the tissue. Treatment with RNase solution was given for 5-10 mins in PBS at room temperature. Slides were washed in chilled PBS twice followed by dehydration with an increasing concentration of ethanol gradient. Slides were briefly warmed at 80ºC and then 250 nM PNA was added with hybridization buffer (20 mM Tris, pH 7.4, 60% formamide (Sigma-Aldich), 0.5% of 10% Goat Serum). Slides were heated and covered with the buffer at 85ºC for 10 mins, kept at room temperature in a dark humid chamber for 4 hrs to overnight to facilitate slow cooling and hybridization. The unbound PNA was washed with wash buffer (2X SSC, 0.1% Tween-20(Thermo Fisher Scientific)) followed by PBS wash twice. DAPI solution (Sigma-Aldrich) was added for 5 mins and then the slides were washed in PBS. ProLong Gold Antifade Mountant (Thermo Fisher Scientific) was added and the section was covered with a cover glass. Imaging was done with a Leica SP8 confocal microscopy system. Images were analyzed using open source image analysis software Fiji (Image J, imagej.net/software/fiji/).

PNA-FISH image analysis: pixel-by-pixel normalization:

To rule out any bias in the telomeric signal (PNA) from cell density (DAPI) the PNA intensity was normalized against the DAPI signal. For pixel-by-pixel normalization we used OpenCV (OpenCV, 2015. *Open Source Computer Vision Library).* Briefly, the green (PNA) and blue (DAPI) channels were first individually extracted (image dimension following extraction: 1024x1024) and optimized (max normalization of pixels, i.e., each pixel normalized to the maximum intensity pixel in the image). Finally the difference in intensity of each pixel on subtraction of DAPI from PNA was plotted as shown below.

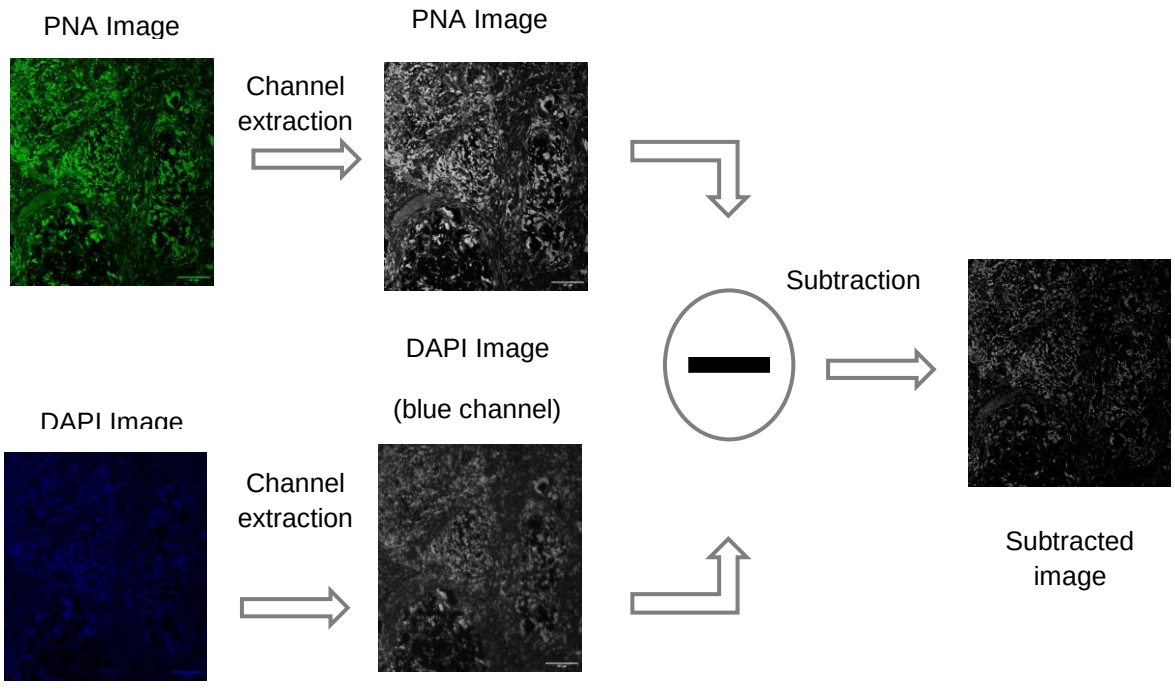

DNA and RNA extraction from TNBC/xenograft tissue:

Allprep DNA/RNA Universal kit (Qiagen) was used as per manufacturer's suggested protocol for extraction of DNA and RNA from single cell suspension prepared from tissues as described before.

Telo-qPCR:

For telomere length assessment by qRT PCR, telomere specific primers and single copy number gene 36B4 for normalization was used in PCR reactions with sample DNA using reported protocol[2].

The primers used are as follows:

Tel F CGGTTTGTTTGGGTTTGGGTTTGGGTTTGGGTTTGGGTT

Tel R GGCTTGCCTTACCCTTACCCTTACCCTTACCCTTACCCT

36B4F CAGCAAGTGGGAAGGTGTAATCC

36B4R CCCATTCTATCATCAACGGGTACAA

The relative telomere length of TNBC patient tissue samples were estimated by normalizing to telomere signal of HT1080 fibrosarcoma cells (reference cell type) as follows:

Telomere signal= $2^{-(Ct\ Tel - Ct\ 36B4)}$

Relative telomere length (RTL) = Telomere signal (sample) / Telomere signal (reference)

Flow-cytometry:

The procedure for Flow-cytometry was adapted from basic flow cytometry guidelines from CST and has been previously reported in Sharma *et al*,2021[3]. The cell suspension was fixed with 4% formaldehyde and permeabilizied with 0.1% triton X (in 1XPBS) for nuclear proteins. Incubation of primary antibody (1:500 v/v in 1% BSA in 1X PBS) for 1 µg/ml antibody concentration for 2 hours at RT or at 4ºCovernight, was followed by PBS wash (3 times) and fluorescently labelled secondary antibody (1:1000 v/v) for 2hours at RT. Following this, cells were washed with 1X PBS (3 times) and re-suspended in 1XPBS for flow-cytometric analysis using BD Accuri C6 or BD FACSAria III. Equal number of events (10000 for most of the analysis) were recorded for calculating percentage infiltration.

For single channel analysis, histogram prolife (log scale) was generated in ungated sample-SSC-FSC plots. For quadrant gating for double positive cells (two channels), biex- scale plots or log scale were used. All statistics like mean fluorescence intensity and standard deviation were estimated using built-in tools for analysis in the software FlowJo.

Relative Telomeres length (RTL) by Flow-cytometry:

The RTL value is calculated as the ratio between the telomere signal of each sample and the control cell. The Telomere PNA Kit/FITC kit from Dako (Agilent) was used to estimate Telomere length signal in samples. The process has been previously standardized and reported [4].

TelSeq- estimation of telomere length using sequencing data

We used TelSeq[5] to estimate the average telomere length (TL) for each tumor and normal sample in our dataset. TelSeq was run with default parameters using WGS(whole genome Sequencing) samples with coverage ≥ 30X, except the read length parameter (-r) which was set to 150 to match with our data. Briefly, the TL was calculated as the total number of reads containing seven or more telomeric repeats ("TTAGGG") divided by the total number of reads with GC content 48-52%. Further, the resultant value was multiplied with a constant value to account for genome size and the number of telomeric ends. This was done separately for each read group within a sample, and then the weighted average was calculated for each sample by taking into account the number of reads per group (as weights).

The estimated average TL [represented in Kilobase-pair (Kb) units] for tumor and normal samples has been provided in Supplementary Figure 1C. Overall, we found that the tumor samples have lower TL scores (Median: 3.20 Kb) as compared to the matched normal samples (Median: 4.67 Kb). Also, the TL estimates from our tumor samples (Median: 3.20 Kb, range:2.3 to 21.10 Kb) were comparable to the TCGA breast cancer cohort (WGS) (Median: 3.5 Kb, range: 1.4 to 29.7 Kb) analyzed by Barthel et al, 2017[6].

To check if the tumor samples with high TL estimates were confounded by the aneuploidy and tumor purity (which was not taken into account in the TelSeq analysis), we computed the purity and ploidy values for each tumor sample (where possible) using ASCAT[7] through Sarek pipeline[8]. However, we found no significant difference in the purity (Wilcoxon test two-sided P = 0.25) and ploidy (Wilcoxon test two-sided P = 0.52*)* values between tumor samples with high versus low TL scores, suggesting that the tumors with high TL estimates were not influenced by these parameters.

IL1B and IL1RA treatment:

Reconstituted IL1B (Sigma-Aldrich) was treated to appropriate cells at 10ng/ml concentration followed by assays. Similarly, IL1RA (Abcam) was treated to appropriate cell/TNBO at 20ng/ml concentration followed by assays at appropriate time points in specific experiments.

IL1B ELISA:

IL1B ELISA was performed using Human IL-1 beta/IL-1F2 DuoSet ELISA kit by R&D Biosystems. As per manufacturer's protocol 96 well microplate was coated with100ul per well of freshly prepared Capture Antibody diluted 100 times in PBS without carrier protein. Thereafter the plate was sealed and incubated overnight at room temperature. Following day the capture antibody was aspirated after which each well was washed three times with 1X Wash Buffer (PBST). After the last wash, the remaining wash buffer was removed carefully and completely by aspiration and blotting it against clean paper towels. The prepped, empty wells were blocked at room temperature for 1hr by adding 300 µL of Reagent Diluent (20% BSA in 1X PBST) to each well. Wash the wells as in the step above. Next we added the samples and standard protein of known increasing concentrations (100ul in volume) diluted in Reagent Diluent. The plates were then covered with an adhesive strip and incubated for 2 hours at room temperature. Post incubation, the wells were washed as above for plate preparation. Following the washes we added 100ul of freshly prepared Detection Antibody diluted 100 times in PBS. The plate was covered and incubated for 2hrs at room temperature. Post incubation the wells were washed thrice as in the previous step. Finally for generating detectable signal we added 100 µL of Streptavidin-HRP to each well, covered the plate and incubated it in dark at room temperature for 20mins. Next the wells were washed thrice as in steps above. After aspirating the wells clean of any buffer we added 100ul of Substrate Solution to each well and incubated the plates again in dark at room temperature for 20minutes. Finally, 50ul of stop solution was added to each well and mixed well by gentle tapping. The signal was measured using a microplate reader set to 450 nm, 570 and 540nm. Perform wavelength correction by subtracting readings at 540 nm or 570 nm from the readings at 450 nm.

Antibodies

Primary antibodies:

TRF2 rabbit polyclonal (Novus NB110-57130)- ChIP, IP, WB

TRF2 mouse monoclonal (Millipore 4A794)- Flow cytometry

TRF1 mouse monoclonal (Novus NB110-68281)-WB

IL1R1 rabbit polyclonal (abcam ab106278)- IF, Flow-Cytometry, WB

DDK/FLAG mouse monoclonal (Sigma-F1804)- ChIP, WB

BG4 recombinant antibody (Sigma Aldrich MABE917)- ChIP

P300 (CST D2X6N) rabbit monoclonal- ChIP, IF,WB

Ac-p300/CBP (CST 4771) rabbit monoclonal-ChIP,WB

CBP (CST 7389) rabbit monoclonal- ChIP,WB

P65(NFKB) (CST 8242) rabbit monoclonal- WB

Ser536 P p65 NFKB (CST 3033) rabbit monoclonal- WB

IKB (CST 4814) mouse monoclonal- WB

p-IKB (CST 2589) rabbit monoclonal- WB

CD44 (CST 3570) mouse monoclonal-IF

Histone H3 rabbit polyclonal (Abcam ab1791)-ChIP

H3K27ac rabbit polyclonal (Abcam ab4729)-ChIP

H3K4me3 rabbit polyclonal (Abcam ab8580)- ChIP

H3K27me3 rabbit monoclonal (abcam ab192985)- ChIP

H3K9me3 rabbit polyclonal (abcam ab8898)- ChIP

Beta-actin mouse monoclonal (Santacruz C4)-WB

GAPDH mouse monoclonal (Santacruz 6C5)-WB

CD11b Monoclonal Antibody (ICRF44), eBioscience™- Flow cytometry

F4/80 Monoclonal Antibody (BM8), eBioscience™- Flow cytometry

CD206 Monoclonal Antibody (MR5D3) Invitrogen- Flow cytometry

APC anti-human CD326 (EpCAM) (9C4) BioLegend- Flow cytometry

Anti-Rabbit IgG/Anti-mouse IgG (Millipore) was used for isotype control.

Secondary antibodies:

anti-Rabbit-HRP(CST), anti-Mouse-HRP(CST),mouse-ALP (sigma),rabbit-ALP(sigma) anti-rabbit Alexa Fluor 488, anti-mouse Alexa Fluor 594 (Molecular Probes, Life Technologies).

Real time PCR

Total RNA was isolated from cells using TRIzol Reagent (Invitrogen, Life Technologies) according to manufacturer's instructions. For TNBC tissue and xenograft, Allprep DNA/RNA Universal kit from Qiagen was used. The cDNA was prepared using High-Capacity cDNA Reverse Transcription Kit (Applied Biosystems) using manufacturer provided protocol. A relative transcript expression level for genes was measured by quantitative real-time PCR using a SYBR Green (Takara) based method. Average fold changes were calculated by the difference in threshold cycles (Ct) between test and control samples. *GAPDH* / 18S gene was used as internal control for normalizing the cDNA concentration of each sample.

RT PCR primers used have been enlisted as follows:

mRNA expression primers:

IL1R1FP	GGCTGAAAAGCATAGAGGGAAC
IL1R1 RP	CTGGGCTCACAATCACAGG
TRF2 FP	CAGTGTCTGTCGCGGATTGAA
TRF2 RP	CATTGATAGCTGATTCCAGTGGT
IL1B FP	ATGATGGCTTATTACAGTGGCAA
IL1B RP	GTCGGAGATTCGTAGCTGGA
IL1A FP	AGATGCCTGAGATACCCAAAACC
IL1A RP	CCAAGCACACCCAGTAGTCT
IL2 FP	CATTTGTGGTTGGGTCAGG
IL2 RP	AGTGAGGAACAAGCCAGAGC
IL6 FP	AGCACTCCTTGGCAAAACTG
IL6 RP	CGGAAGGAACCATCTCACTG
TNF FP	GCCAGAGGGCTGATTAGAGA
TNF RP	TCAGCCTCTTCTCCTTCCTG
IL8 FP	GAATGGGTTTGCTAGAATGTGATA
IL8 RP	CAGACTAGGGTTGCCAGATTTAAC

IL10 FP	GACTTTAAGGGTTACCTGGGTTG
IL10 RP	TCACATGCGCCTTGATGTCTG
IL4 FP	CCAACTGCTTCCCCCTCTG
IL4 RP	TCTGTTACGGTCAACTCGGTG
IL13 FP	GAAGGCTCCGCTCTGCAAT
IL13 RP	TCCAGGGCTGCACAGTACA
CD206 FP	GGGTTGCTATCACTCTCTATGC
CD206 RP	TTTCTTGTCTGTTGCCGTAGTT
CD163 FP	TTTGTCAACTTGAGTCCCTTCAC
CD163 RP	TCCCGCTACACTTGTTTTCAC
GAPDH FP	TGCACCACCAACTGCTTAGC
GAPDH RP	GGCATGGACTGTGGTCATGAG
18S FP	TTCGGAACTGAGGCCATGAT
18S RP	TTTCGCTCTGGTCCGTCTTG

TRF2 target gene expression primers from Mukherjee *et al,* 2018[4].

RNA-seq analysis:

RNA was extracted using TRIzol TruSeq RNA Library Prep Kit v2 was used from preparation of libraries for sequencing. Raw Illumina sequencing reads were checked for quality using FastQC (version 0.11.9) followed by adapter clipping and trimming using Trimmomatic (version 0.39)~~23~~ with default parameters. Trimmed reads were then aligned to the human reference genome (GRCh38, GENCODE v36) using STAR aligner (version 2.7.8a)~~26~~. FeatureCounts (subread package version 2.0.1) was used to quantify gene expression. Quality checks were performed at each step using the MultiQC tool (version 1.10.1)~~28~~. Differential gene expression analysis was performed using the DESseq2 package (version 1.30.0)~~29~~ in R (version 4.0.3). The analysis was performed by removing the effects of confounding variables such as batch and replicate using the appropriate design formula. Gene expression was normalized using variant stabilizing transformation (vst) for visualization purposes. Genes with BH-adjusted p value < 0.05 and absolute Log2 fold change greater than 1 (at least 100% fold change in either direction) were taken as significantly differentially expressed.

ChIP (Chromatin Immunoprecipitation)

ChIP assays were performed as as previously reported by Mukherjee *et al.*,2018,2019[4,9]. Briefly, 3-5 million cells were fixed with ~1% formaldehyde (Sigma-Aldrich) for 10 min and lysed. Chromatin was sheared to an average size of ~300-400 bp using Biorupter (Diagenode). 10% of the sonicated fraction was processed as input using phenol–chloroform and ethanol precipitation. ChIP was performed for endogenous/ectopically expressed protein using 1:100 dilution (v/v) of the respective ChIP grade antibody incubated overnight at 4°C. Immune complexes were collected using Salmon sperm DNA-saturated Magnetic Dynabeads (-50 µg per sample) and washed extensively. Phenol-chloroform-isoamylalcohol was used to extract DNA from the immunoprecipitated fraction. ChIP DNA was quantified by Qubit HS ds DNA kit (Thermo Fisher Scientific). Quantified ChIP samples were validated by qRT-PCR.

The ChIP-qRT PCR primers are as follows:

ChIP- qRT PCR primers:	
IL1R1-1000 FP	CCCCTTCCACAGAAGAAACCTGG
IL1R1-1000 RP	CGCAGAAGCCAGTGGGAGG
IL1R1-800 FP	AGCCCAGGTGGGTGCCA
IL1R1-800 RP	ATGACAGAATGATTCTTTGCTCTGTGG
IL1R1-600 FP	TATTTGTCAGGCGCCCCTGG
IL1R1-600 RP	CATACATCTGTGTGTGCCTGGG
IL1R1-400 FP	CAGGAAGCCATACATCTGTGTAGC
IL1R1-400 RP	GAATGTTATACACACACTCATACACACACACA
IL1R1-200 FP	GAGTGTGTGTATAACATTCATTACTGCAAAC
IL1R1-200 RP	ATGAAAAGATACAAGTGAAGAGCTGCC
IL1R1+200 FP	TGGGAGGTGACACCCAGTTTAAG
IL1R1+200 RP	CCAACTCTGGGCCTTCCCAC
IL1R1 3' UTR FP	TCCTTTGACTTATTGTCCCCACT
IL1R1 3' UTR RP	TCTTCAACACTTAGGGCATCTT
IL1R1 -20 KB FP	TTGTCCTGAATAGCCGCAGG
IL1R1 -20 KB RP	CCCTCGAGAAAACAGCCCAT

Immunofluorescence microscopy:

Adherent cells were seeded on coverslips and allowed to reach a confluency of ~ 70%. Cells were fixed using freshly prepared 4% Paraformaldehyde by incubating for 10 min at RT. Cells were permeabilized with 0.25% Triton™ X-100 (10 min at RT) and treated with blocking solution (5% BSA in PBS) for 2 hrs at RT. All the above stated were followed by three washes with ice cold PBS for 5 mins each. Post-blocking, cells treated with relevant antibodies (1:500 for TRF2, 1:500 for IL1R1 and 1:1000 for CD44/p300) and incubated overnight at 4ºC in a humid chamber. Post-incubation, cells were washed alternately with PBS and PBST three times and probed with secondary Ab (rabbit Alexa Fluor 488(1:1000) / mouse Alexa Fluor 594 (1:1000)) for 2 hrs at RT. Cells were washed again alternately with PBS and PBST three times and mounted with Prolong Gold anti-fade reagent with DAPI. Images were taken on Leica TCS-SP8 confocal microscope/ Cytiva Deltavision microscope. Lasers of emission wavelength 405nm, 488nm and 532 nm were used imaging for DAPI, Alexa Fluor 488 secondary Ab and Alexa Fluor 594 Ab respectively. Laser intensity was kept 20% for DAPI and 40-60% for Alexa Fluor secondary antibodies. ImageJ (FIJI) software was used to calculate signal intensity (a.u.).

Western blotting:

For western blot analysis, protein lysates were prepared by suspending cell pellets in 1X RIPA (with 1x mammalian protease inhibitor cocktail). Protein was separated using 10%/12% SDS-PAGE and transferred to polyvinylidenedifluoride membranes (Immobilon FL, Millipore). After blocking, the membrane was incubated with primary antibodies. Post incubation with primary antibodies (1:1000 v/v), the membrane was washed with 1X PBS and then incubated with appropriate secondary antibodies (1:2000 v/v). Following secondary antibody incubation, the membrane was washed with 1XPBS. The blot was finally developed using HRP substrate/BCP NBT and reagents from Millipore.

HT1080 TRF2 and TERT inducible cells:

TRF2 cDNA sequence was inserted into pENTR11 vector and the cassette was transferred into lentiviral plasmid pCW57.1 by gateway cloning. Following this viral particles were generated from HEK293T cells and the viral soup with polybrene (Sigma-Aldrich) was used for transduction. Cells with insert were selected with 1µg/ml of puromycin and tested for TRF2 induction using varying doxycycline concentrations.

Similarly TERT cDNA was amplified from a mammalian expression vector and inserted into pENTR11 vector. Subsequently, the same strategy was used to generate and test TERT inducible HT1080 cells.

Vector constructs

The pCMV6-myc-DDK(FLAG)-TRF2 vector (TRF2 WT) was procured from Origene (RC223601). The mutants delB and delM constructs used in the study have been previously reported[10] and made through mutagenesis of the TRF2 WT construct. TRF2 shRNA was procured from Origene (TL308880). Side-directed Mutagenesis was performed on the TRF2 WT plasmid to generate the PTM mutants.

For customizing dCas9-TRF2 fusion plasmids, the backbone of dCAS9-VP64-GFP (Addgene 61422) was used. IL1R1 sgRNA was custom designed against IL1R1 promoter G-quadruplex (G4-motif B) and cloned in pX333 (Addgene 64073) backbone after replacing Cas9 with mCherry.

Transfections

TRF2 wildtype (myc/DDK tag) or mutant mammalian expression vector pCMV6 was transfected into HT1080 /MDAMB231 cells that were 60 % confluent using Lipofectamine 2000 transfection reagent (following the manufacturers' protocol). 2-4µg of plasmid was used for transfection in a 35 mm well for each case.

In case of TRF2 shRNA (Origene)/TERC shRNA (Santa Cruz Biotechnology), 4µg of plasmid was used for transfection in a 35 mm well for each case and Fugene HD transfection reagent was used as per manufacturer's protocol. Cells were then maintained in 1µg/ml of puromycin for stable shRNA maintenance. For dCAS9-TRF2 fusion constructs, co-transfected with IL1R1 sgRNA plasmid, FugeneHD was used at recommended concentrations.

TRF2 silencing by siRNA:

HT1080 cells were transfected with TRF2 siRNA oligonucleotides (synthesized from Eurogenetics Pvt. Limited)[3] using lipofectamine 2000 (Invitrogen) transfection reagent according to manufacturer's instructions. Silencing was checked after 48 hr of transfection. Pooled scrambled siRNA was used as control.

Luciferase assay:

IL1R1 promoter (upto 1500 bp upstream of transcription start site) was cloned in PGL3 basic vector upstream of firefly luciferase construct. G4 motif disrupting mutations were introduced in the promoter construct by site directed mutagenesis.

Plasmid (pGL4.73) containing a CMV promoter driving Renilla luciferase was co-transfected as transfection control for normalization. After 48h, cells were harvested and luciferase activities of cell lysate were recorded by using a dual-luciferase reporter assay system (Promega).

Circular Dichroism

Circular Dichroism profiles (220 nm to 300 nm) were obtained for representative G4 motifs identified within IL1R1 promoter and an overlap with TRF2 high confidence ChIP seqpeak. Circular Dichroism showed the formation of G4-motif with the unaltered sequence while mutated G4 sequence gave partial/complete disruption of the G4-motif under similar conditions (buffer used for G- quadruplex formation -10mM Na cacodylate and 100 mM KCl). The circular dichroism (CD) spectra were recorded on a Jasco-89spectropolarimeter equipped with a Peltier temperature controller. Experiments were carried out using a 1mm path-length cuvette over a wavelength range of 200-320 nm. Oligonucleotides were synthesized commercially from Sigma-Aldrich. 2.5uMoligonucleotides were diluted in sodium cacodylate buffer (10 mM sodium cacodylate and 100 mM KCl, pH 7.4) and denatured by heating to 95ºC for 5 min and slowly cooled to 15ºC for several hours. The CD spectra reported here are representations of three averaged scans taken at 20ºC and are baseline corrected for signal contributions due to the buffer.

CCR5-IL1R1 promoter insert cells:

IL1R1 promoter and downstream firefly luciferase (and G4 mutant variant) was inserted in HEK293T cells by using strategy previously standardized and reported for TERT promoter-gaussia insertion in the same locus[3].

IL1R1 promoter G4 mutant HEK cells:

Custom designed gRNA pair was used to insert mutant G4 template sequence (G4 mutantB) into the IL1R1 endogenous promoter by co-transfecting Cas9and gRNA pair with doner template SSODN sequence. Following this, single cell screen was done for positive mutant colony. Once identified an appropriate mutant colony was used for experiments.

sgRNA and SSODN details are as follows:

sgRNA1- 5'- GCTGCCAATGGGT**G**GAGTCTTG**G**G -3' (efficiency score (Doench et al)- 35)

-ve strand, ssODN: 91bp (PAM proximal)- 36bp (PAM distal)

Target strand is +ve strand. Non-target stand is –ve strand. ssODN shud be +ve strand.

ssODN (mutated): chr2:102070276-102070402

GGGACACTGCAGCCCTGGCCTGGCCTACTTTTCTCTTCTCCCATATCTGGAAAATGAAAGT
AGCCTGACGTATCCGGGGAC**A**CGGC**A**CAAGACTC**A**ACCCATTGGCAGCTCTTCACTTGTA
TCTTTT

sgRNA2- 5'- GCAATGGGT**G**GAGTCTTG**G**GCCG**G** -3' (efficiency score (Doench et al)- 40)

-ve strand, ssODN: 85bp (PAM proximal)- 42bp (PAM distal)

Immunoprecipitation:

Immunoprecipitation of proteins was performed using modified version of suggested IP protocol from CST. Cells were lysed using cell lysis buffer ((1X) 20 mM Tris (pH 7.5), 150 mM NaCl (Sigma-Aldrich), 1 mM EDTA (Sigma-Aldrich), 1 mM EGTA (Sigma-Aldrich), 1% Triton X-100 (Sigma-Aldrich), 2X mPIC (Thermo Fisher Scientific)) and treated with relevant primary antibody (1: 100 v/v) overnight at 4ºC or mock IgG on rotor. 50 µg of Dyanbeads (blocked with BSA-5% for 60 mins at RT) was added to the lysis soup and kept for 2 hrs in mild agitation. Dynabeads were magnetically separated and washed thrice (with 1X PBS with 0.1% Tween-20). The beads were resuspended with 1X RIPA (50 µl) and 1X Laemmli buffer. This was followed by denaturation at 95ºCfor 10 mins and followed by western blot for specific proteins.

HAT assay:

Histone acetyl transferase (HAT) assay was performed as per manufacturers' protocol from Active motif. Mammalian TRF2 and p300 full length were commercially procured from origene and abcam respectively and used for the assay.

IL1R1 knockout HT1080 cells:

Two sets of gRNAs (sequences?) targeting either exon 3 or exon3-7 of *IL1R1* coding region were cloned in PX459 (Addgene 62988) and co-transfected in HT1080 cells, followed by puromycin selection and single cell screening for IL1R1 knockout cells. A knockout clone was selected (based on IL1R1 depletion) and used for further experiments.

Gene ontology and cBIO PORTAL ANALYSIS:

Gene ontology analysis was done using gene list [6] using publicly available resource –The Gene Ontology Resource database (http://geneontology.org/). Fold enrichment, FDR values and p-values were calculated using PANTHER. Ontology plot was made using MS Excel multivariate plot. Immune related gene expression correlation was done using cBioPortal (https://www.cbioportal.org/) in the TCGA Breast Invasive carcinoma dataset.

For survival analysis, custom cutoffs were implemented on TCGA data set using cBIOPORTAL 'gene query' function to segregate IL1R1 high/low expression samples and then respective patient survival data was fetched and plotted. Details of datasets are as follows:

pan-cancer: N=2593 (IL1R1 high- 187, rest IL1R1 low) -Pan-cancer analysis of whole genomes (ICGC/TCGA, Nature 2020)

breast cancer N= 257 (IL1R1 high- 37, rest IL1R1 low)-Breast Invasive Carcinoma (TCGA, Firehose Legacy)

TRAP (Telomere Repeat Amplification protocol) for telomerase activity

Protein lysate was prepared in 1X CHAPS Lysis Buffer and the assay was performed using TRAPeze™ RT Telomerase Detection Kit (Merck) per manufacturer's instructions.

Statistical Analysis:

For all datasets with N> 5, Mann Whitney U test/Wilxocin's test was performed using interface provided within GRAPHPAD PRISM software. For paired datasets, paired T Test with Welch's correction was performed for significance. Median values and correlations were calculated using MS excel functions.

Ethics statement:

The authors declare that relevant ethical approvals were taken to procure and use human clinical patient tissue and mouse xenograft tissue for experiments whose results have been shared in the manuscript.

Data availability:

The authors declare that all data necessary to support the inferences are included in the manuscript and supplementary information. Additionally, raw data for TNBC whole genome sequencing and RNA sequencing (HT1080-HT1080-LT cells) will be made public before publication. The data will, in the meanwhile, will be made available by the corresponding author upon reasonable request.

References (Methods):

1. Cristofari, G. & Lingner, J. Telomere length homeostasis requires that telomerase levels are limiting. *EMBO J.* **25**, 565–574 (2006).

2. O'Callaghan, N. J., Dhillon, V. S., Thomas, P. & Fenech, M. A quantitative real-time PCR method for absolute telomere length. **44**, 807–809.

3. Shalu Sharma, A. *et al.* Human telomerase is directly regulated by non-telomeric TRF2-G-quadruplex interaction. *CellReports* **35**, 109154 (2021).

4. Mukherjee, A. K. *et al.* Telomere length-dependent transcription and epigenetic modifications in promoters remote from telomere ends. *PLOS Genet.* **14**, e1007782 (2018).

5. Ding, Z., Mangino, M., Aviv, A., Spector, T. & Durbin, R. Estimating telomere length from whole genome sequence data. *Nucleic Acids Res.* **42**, e75 (2014).

6. Barthel, F. P. *et al.* Systematic analysis of telomere length and somatic alterations in 31 cancer types. *Nat. Genet. 2017 493* **49**, 349–357 (2017).

7. Raine, K. M. *et al.* ascatNgs: Identifying Somatically Acquired Copy-Number Alterations from Whole-Genome Sequencing Data. *Curr. Protoc. Bioinforma.* **56**, 15.9.1-15.9.17 (2016).

8. Garcia, M. *et al.* Sarek: A portable workflow for whole-genome sequencing analysis of

germline and somatic variants. *F1000Research* **9**, 63 (2020).

9. Mukherjee, A. K. *et al. Telomere repeat-binding factor 2 binds extensively to extra-telomeric G-quadruplexes and regulates the epigenetic status of several gene promoters*. *Journal of Biological Chemistry* vol. 294 17709–17722 (American Society for Biochemistry and Molecular Biology Inc., 2019).

10. Hussain, T. *et al.* Transcription regulation of CDKN1A (p21/CIP1/WAF1) by TRF2 is epigenetically controlled through the REST repressor complex. *Sci. Rep.* **7**, 11541 (2017).

Main Figures

Figure 1

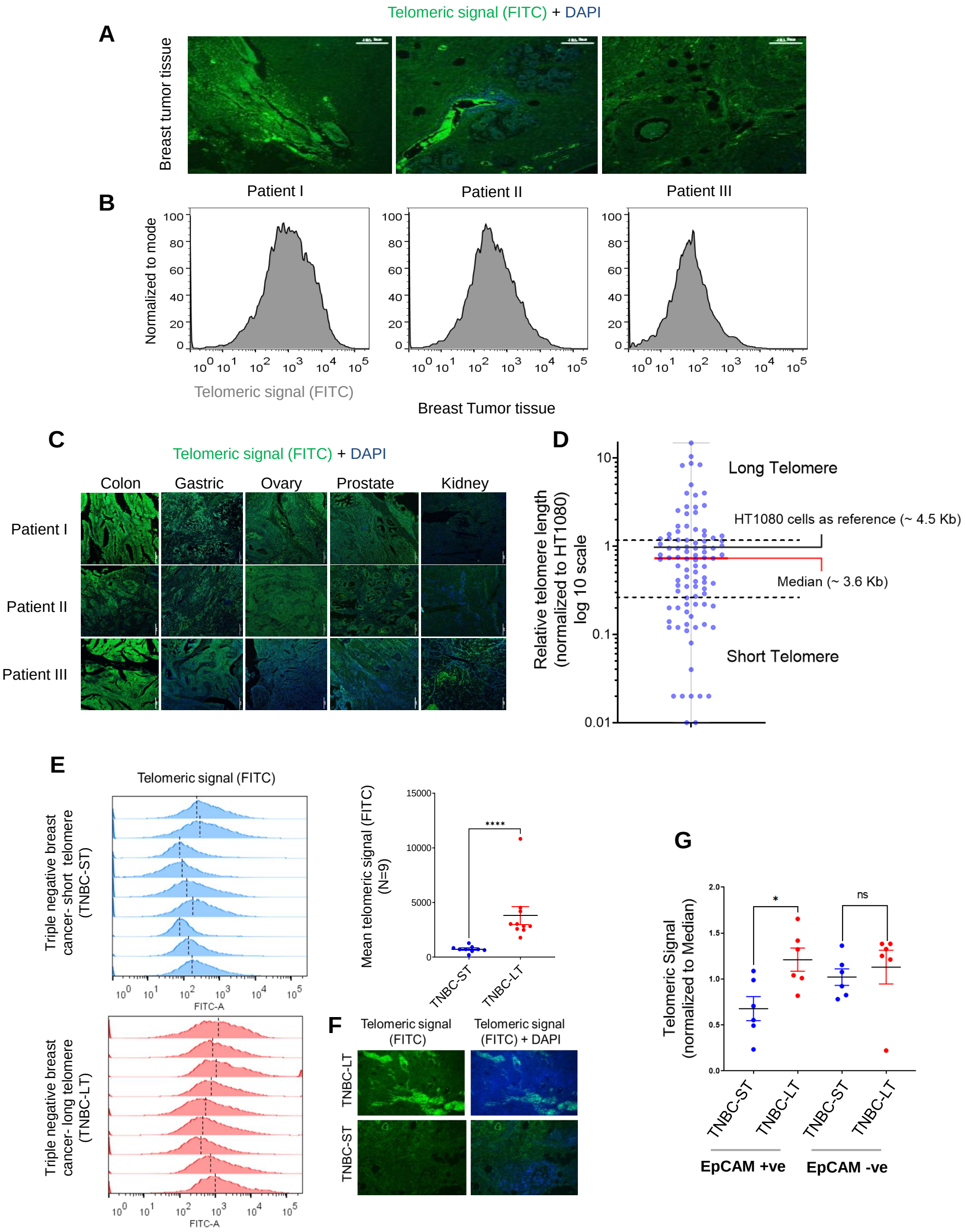
A
Telomeric signal (FITC) + DAPI
Breast tumor tissue
B
Patient I
Patient II
Patient III
Normalized to mode
Telomeric signal (FITC)
Breast Tumor tissue
C
Telomeric signal (FITC) + DAPI
Colon
Gastric
Ovary
Prostate
Kidney
Patient I
Patient II
Patient III
D
Relative telomere length (normalized to HT1080) log 10 scale
Long Telomere
HT1080 cells as reference (~ 4.5 Kb)
Median (~ 3.6 Kb)
Short Telomere
E
Telomeric signal (FITC)
Triple negative breast cancer- short telomere (TNBC-ST)
Triple negative breast cancer- long telomere (TNBC-LT)
FITC-A
Mean telomeric signal (FITC) (N=9)
****
TNBC-ST
TNBC-LT
F
Telomeric signal (FITC)
Telomeric signal (FITC) + DAPI
TNBC-LT
TNBC-ST
G
Telomeric Signal (normalized to Median)
*
ns
TNBC-ST
TNBC-LT
TNBC-ST
TNBC-LT
EpCAM +ve
EpCAM -ve

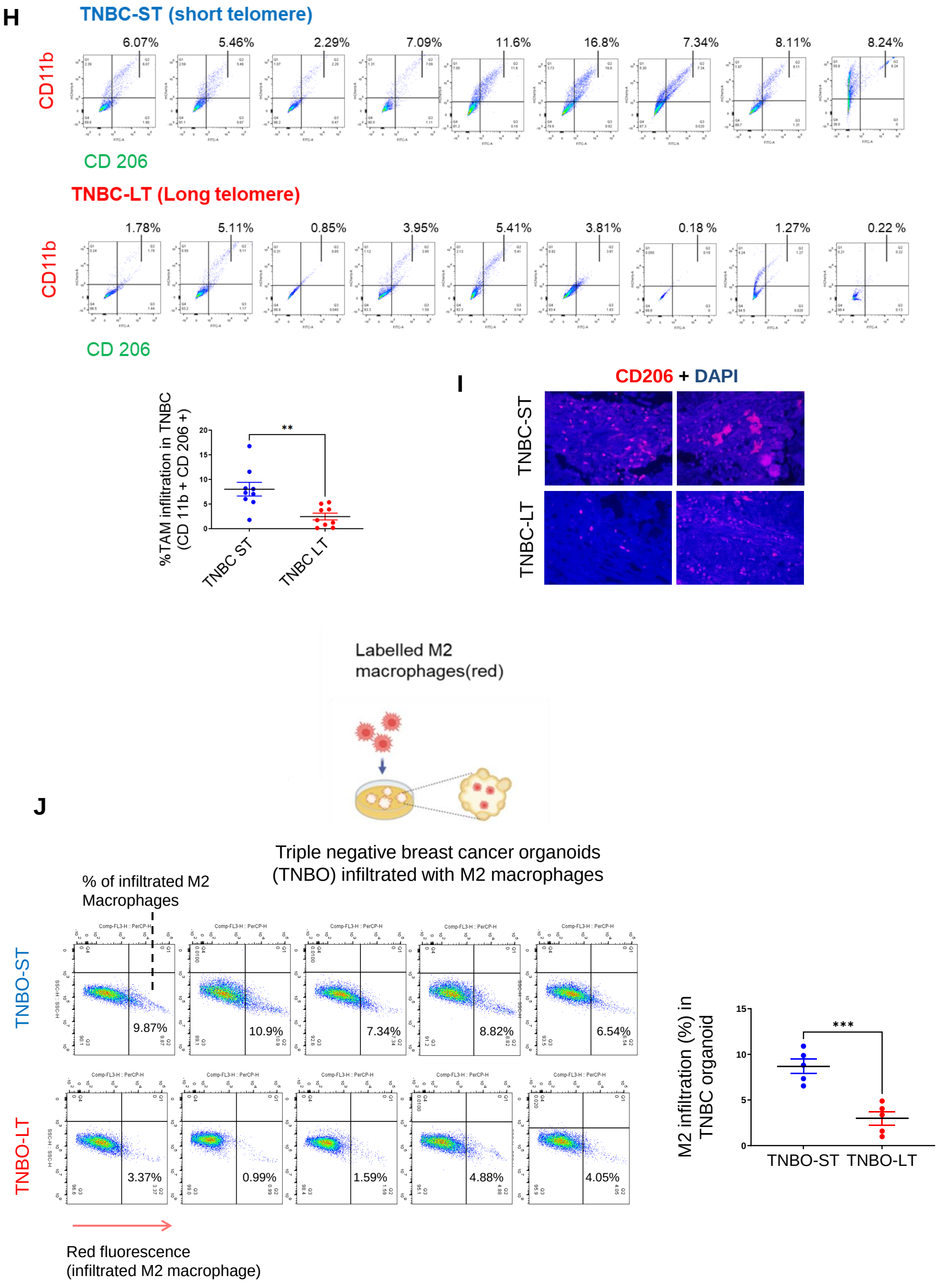
H
TNBC-ST (short telomere)
CD11b
6.07%
5.46%
2.29%
7.09%
11.6%
16.8%
7.34%
8.11%
8.24%
CD 206
TNBC-LT (Long telomere)
CD11b
1.78%
5.11%
0.85%
3.95%
5.41%
3.81%
0.18 %
1.27%
0.22 %
CD 206
%TAM inflitration in TNBC
(CD 11b + CD 206 +)
**
TNBC ST
TNBC LT
I
CD206 + DAPI
TNBC-ST
TNBC-LT
Labelled M2
macrophages(red)
J
Triple negative breast cancer organoids
(TNBO) infiltrated with M2 macrophages
% of infiltrated M2
Macrophages
TNBO-ST
9.87%
10.9%
7.34%
8.82%
6.54%
TNBO-LT
3.37%
0.99%
1.59%
4.88%
4.05%
Red fluorescence
(infiltrated M2 macrophage)
M2 infiltration (%) in
TNBC organoid
***
TNBO-ST
TNBO-LT

Mouse- xenograft tumors

K

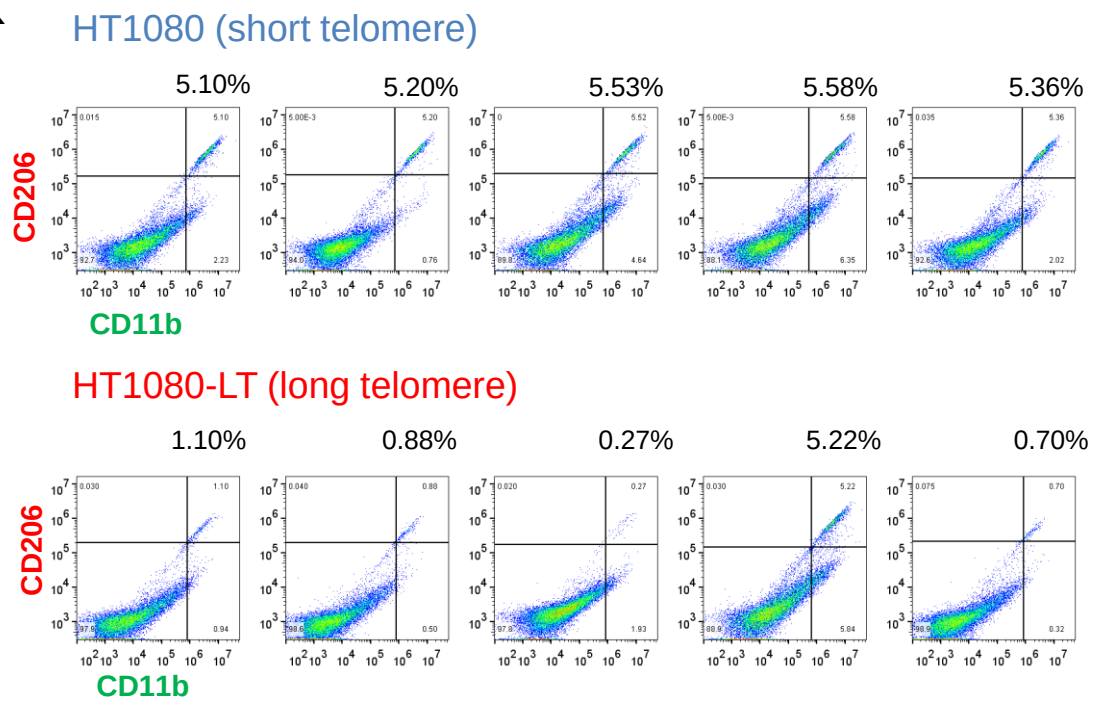

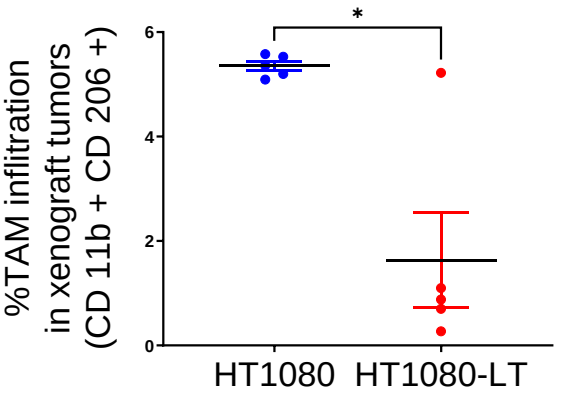

L

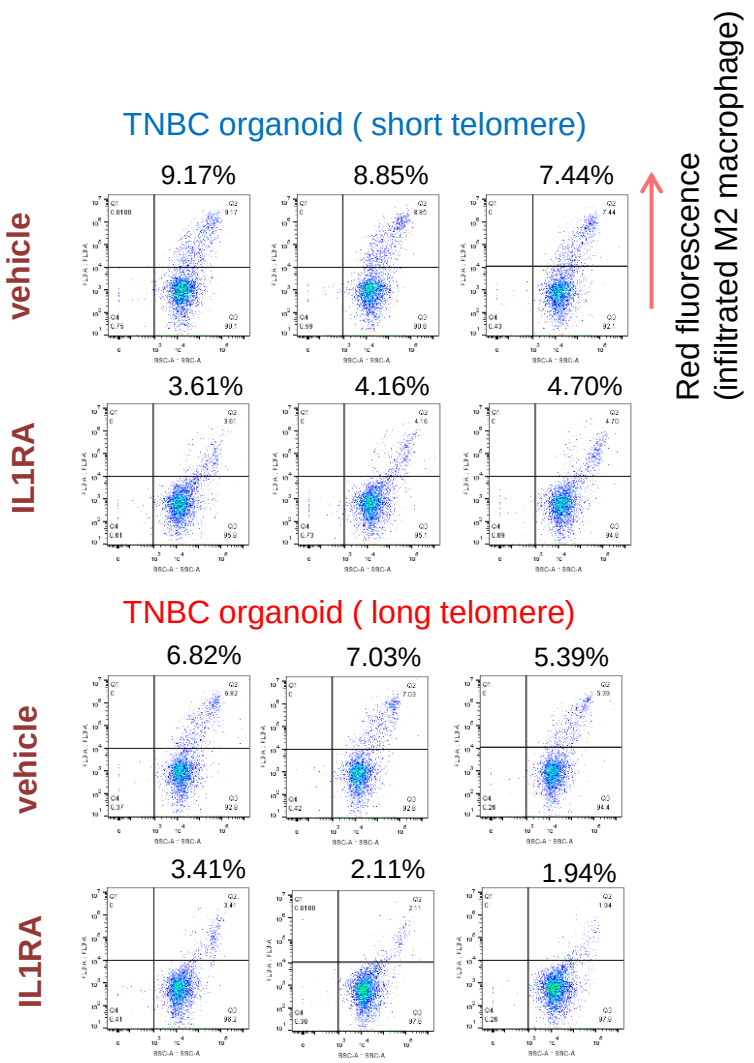

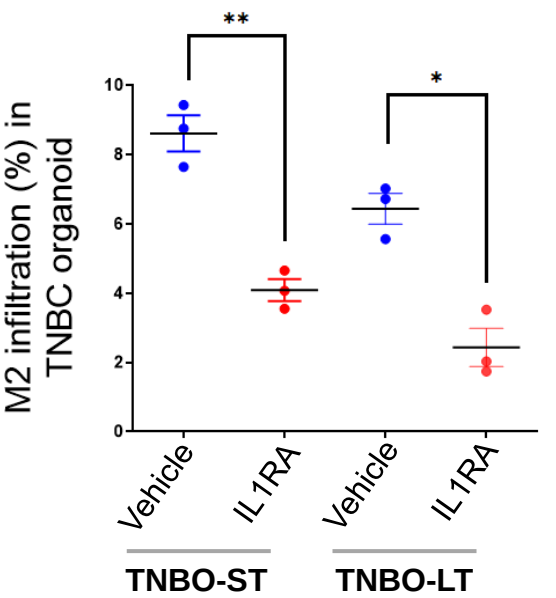

Figure 1: Tumor macrophage infiltration is telomere sensitive

A-B: Breast cancer tissue sections from three independent patients stained using telomere-specific FITC probes and counterstained with DAPI (A) and telomeric signal from the same tissues by flow cytometry using telomere-specific FITC labeled probes (B).

C. Tissue sections from colon, gastric, ovarian, prostate and kidney cancer patients (three patients in each case) stained with telomere-specific probe and counterstained with DAPI.

D. Relative telomere length of Triple Negative Breast Cancer (TNBC) samples (94 patients) by Telo-qPCR as reported earlier; signal from telomere-specific primers was normalized to single copy number gene 36B4 for individual samples. All samples were run with HT1080 DNA as control and telomeric signal from HT1080 cells (telomere length ~4.5 Kb) was used as reference for relative measurement; median telomere length (3.6 Kb) shown by red bar; samples >50% or <50% of median (dotted lines) were designated as long or short telomere samples respectively.

E. Flow cytometry analysis of telomere length of TNBC tissues from telomeric signal using telomere–specific FITC-labeled PNA probe; quantification of mean telomeric signal for nine TNBC-ST (short telomere, top left panel) and nine TNBC-LT (long telomere bottom left panel) shown in top right panel.

F. TNBC tissue slides hybridized with telomere-specific PNA probes and counter stained with DAPI. Representative images for long/short telomere TNBC tissue shown.

G. TNBC tissue (N=6 each for long or short telomere samples) stained with EpCAM (far red) and hybridized with telomere-specific PNA probe (FITC). Mean telomeric signal was plotted in total $EpCAM^{+ve}$ or $EpCAM^{-ve}$ cells.

H. Percentage tumor-associated-macrophage (TAM) infiltration in TNBC tissue with short (TNBC-ST) or long (TNBC-LT) telomeres using markers CD11b and CD206 ($CD11b^{+}CD206^{+}$ cells shown in top right quadrant); quantification of TAM infiltration from individual TNBC-ST or TNBC-LT plotted below.

I. TNBC tissue slides stained with TAM-specific marker CD206 for macrophage infiltration within tissue (counterstained with DAPI); representative images for two independent long or short telomere TNBC tissues shown.

J. Labelled (red) M2 macrophages derived from THP1 cells incubated with triple negative breast tissue-derived organoids (TNBO) for 12 hours (scheme in top panel). Infiltration of M2 macrophages in organoids shown as percentage of labelled (red) M2 macrophages in individual flow-cytometry plots (florescence signal (FL3) in x-axis in log scale; left panels); percentage infiltration from five TNBO-ST or five TNBO-LT samples shown in right panel.

K. Percentage of TAM in xenograft tumors (developed in mouse from HT1080 or HT1080-LT cells) using markers CD11b and CD206; values for HT1080 and HT1080-LT tumors shown in plot (right panel).

L. Labelled (red) M2 macrophage infiltration in presence/absence of receptor antagonist IL1RA (20 ng/ml) for tumor organoids with short (TNBO-ST) or long telomeres (TNBO-LT) in three replicates; percentage values for M2 infiltration plotted in right panel. Red florescence (FL3; y-axis in log scale) and respective percentage M2 infiltration values marked on top of individual flow cytometry plots.

Statistical significance was calculated using Mann-Whitney's non-parametric test for individual graphs (p values: * ≤ 0.05, ** ≤ 0.01, *** ≤ 0.001, **** ≤ 0.0001).

Figure 2

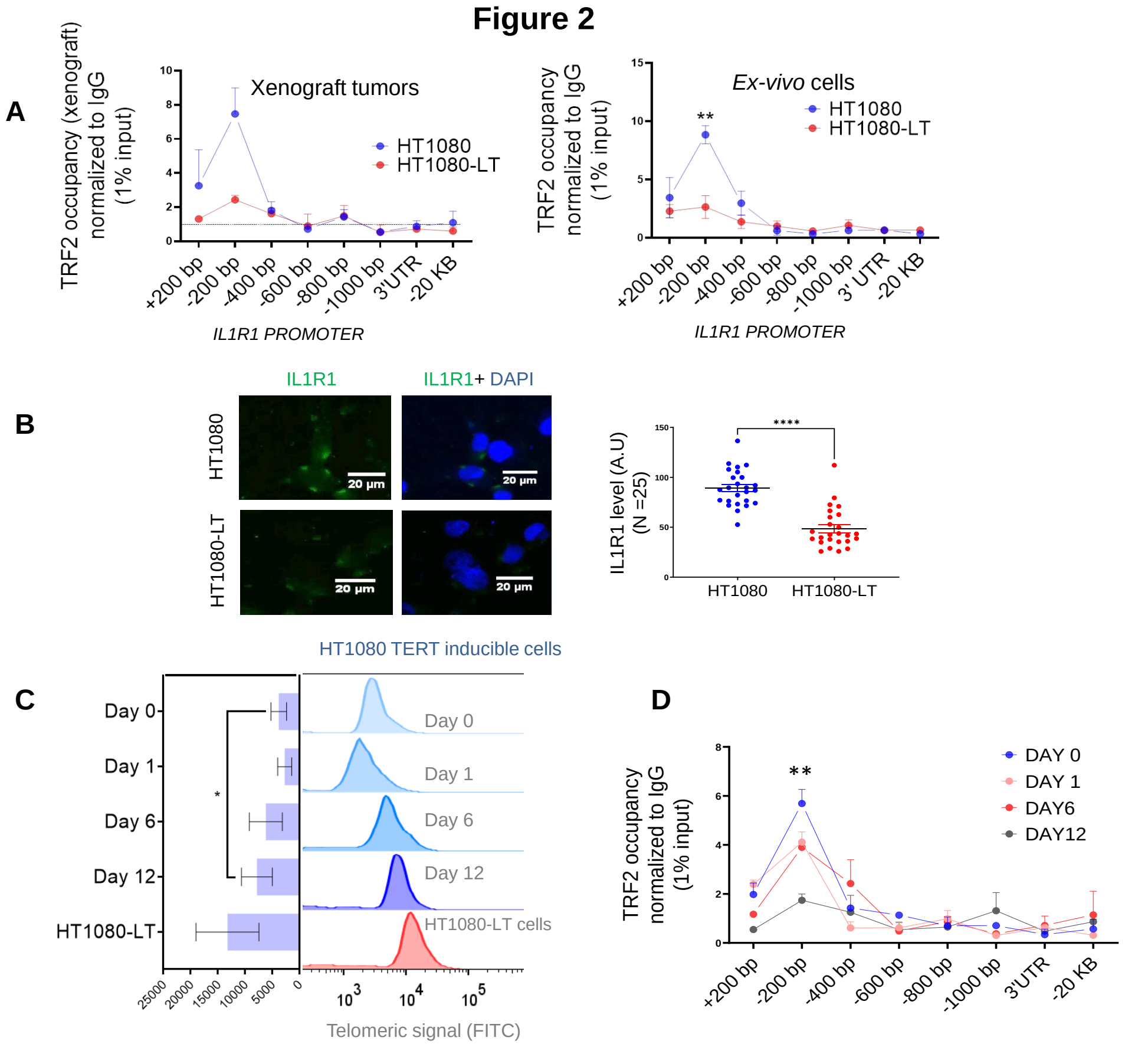
A
Xenograft tumors
HT1080
HT1080-LT
TRF2 occupancy (xenograft) normalized to IgG (1% input)
+200 bp
-200 bp
-400 bp
-600 bp
-800 bp
-1000 bp
3'UTR
-20 KB
IL1R1 PROMOTER
Ex-vivo cells
TRF2 occupancy normalized to IgG (1% input)
**
3' UTR
B
IL1R1
IL1R1+ DAPI
HT1080
HT1080-LT
20 µm
IL1R1 level (A.U) (N =25)
****
C
HT1080 TERT inducible cells
Day 0
Day 1
Day 6
Day 12
HT1080-LT
HT1080-LT cells
Telomeric signal (FITC)
D
DAY 0
DAY 1
DAY6
DAY12
E
CD 44 + DAPI
IL1R1 (green)
merge
Single stack
HT1080 control
HT1080 TRF2
HT1080 cells
IL1R1 Level (A.U) N=25
control
TRF2
Dox (µg/ml) 0 2 4
TRF2
GAPDH
IL1R1
Normalized to Mode
control
TRF2 induced

F

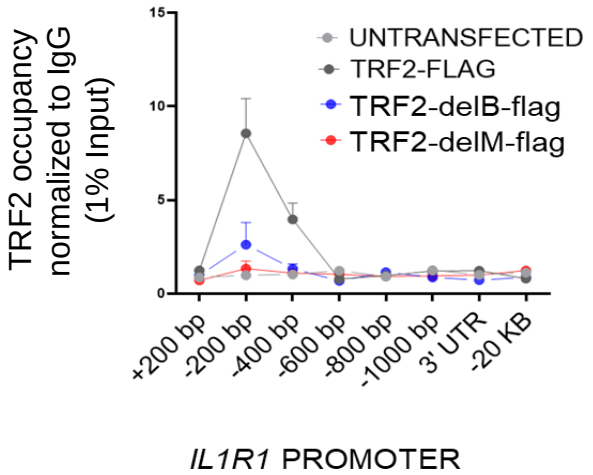
TRF2 occupancy normalized to IgG (1% Input)
UNTRANSFECTED
TRF2-FLAG
TRF2-delB-flag
TRF2-delM-flag
+200 bp
-200 bp
-400 bp
-600 bp
-800 bp
-1000 bp
3' UTR
-20 KB
IL1R1 PROMOTER

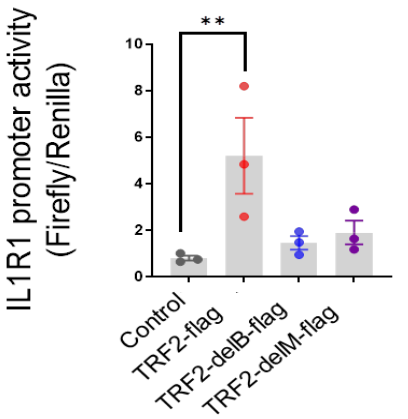
IL1R1 promoter activity (Firefly/Renilla)
**
Control
TRF2-flag
TRF2-delB-flag
TRF2-delM-flag

G

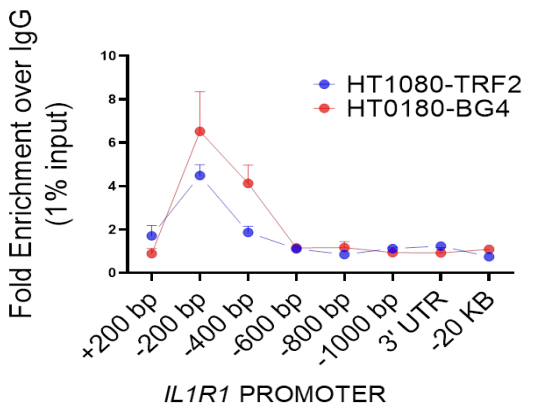
Fold Enrichment over IgG (1% input)
HT1080-TRF2
HT0180-BG4
+200 bp
-200 bp
-400 bp
-600 bp
-800 bp
-1000 bp
3' UTR
-20 KB
IL1R1 PROMOTER

H

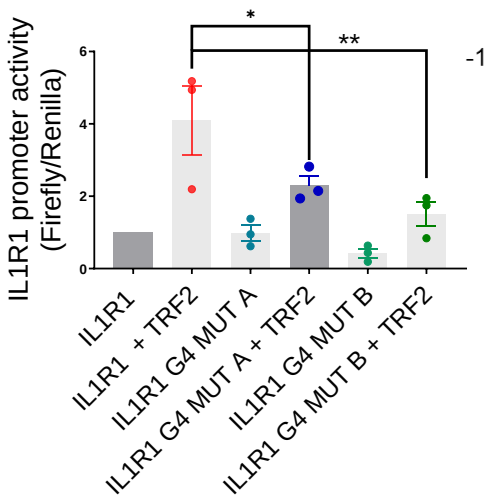
IL1R1 promoter activity (Firefly/Renilla)
*
**
IL1R1
IL1R1 + TRF2
IL1R1 G4 MUT A
IL1R1 G4 MUT A + TRF2
IL1R1 G4 MUT B
IL1R1 G4 MUT B + TRF2

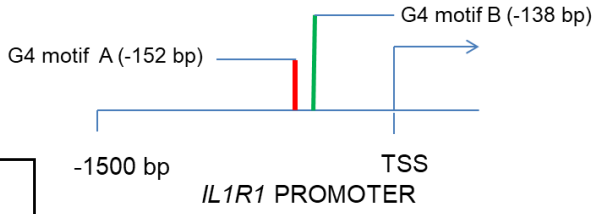
G4 motif B (-138 bp)
G4 motif A (-152 bp)
-1500 bp
TSS
IL1R1 PROMOTER

I

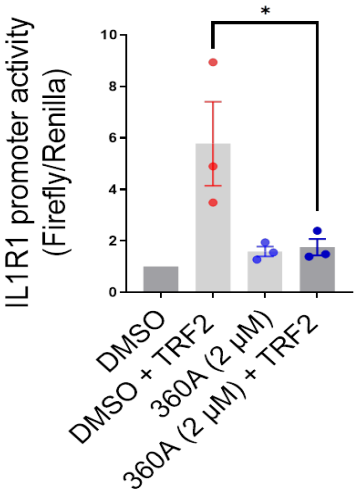
IL1R1 promoter activity (Firefly/Renilla)
*
DMSO
DMSO + TRF2
360A (2 μM)
360A (2 μM) + TRF2

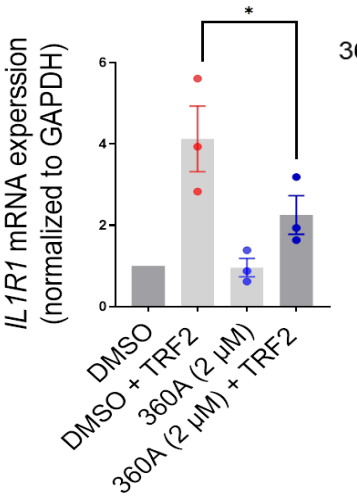
IL1R1 mRNA experssion (normalized to GAPDH)
*
DMSO
DMSO + TRF2
360A (2 μM)
360A (2 μM) + TRF2

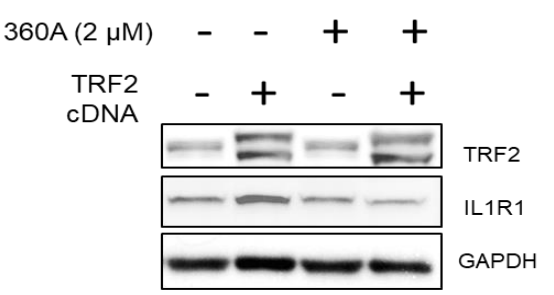
360A (2 μM) - - + +
TRF2 cDNA - + - +
TRF2
IL1R1
GAPDH

J

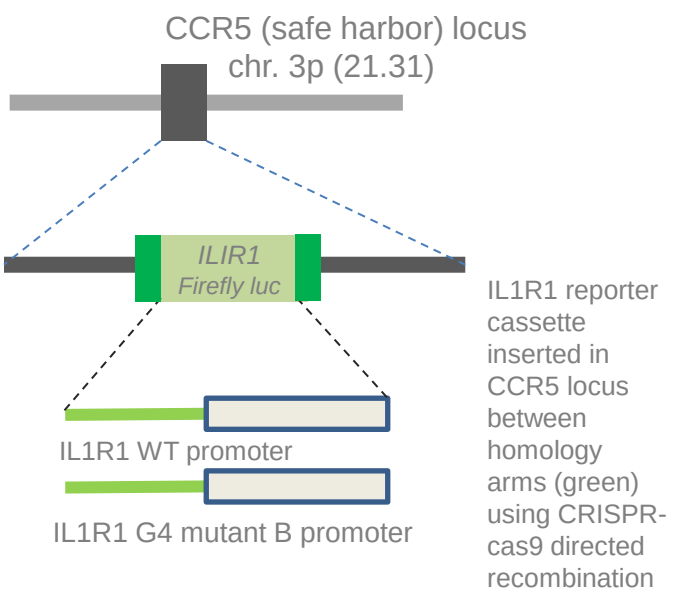
CCR5 (safe harbor) locus
chr. 3p (21.31)
ILIR1
Firefly luc
IL1R1 WT promoter
IL1R1 G4 mutant B promoter
IL1R1 reporter cassette inserted in CCR5 locus between homology arms (green) using CRISPR-cas9 directed recombination

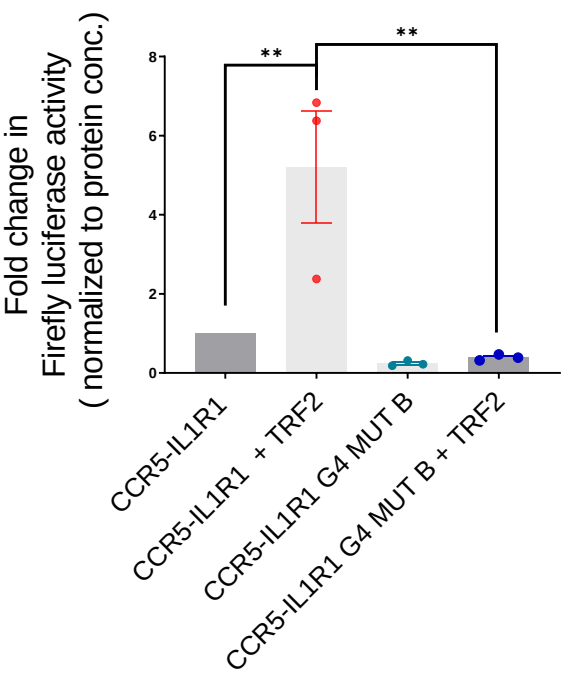
Fold change in Firefly luciferase activity (normalized to protein conc.)
**
**
CCR5-IL1R1
CCR5-IL1R1 + TRF2
CCR5-IL1R1 G4 MUT B
CCR5-IL1R1 G4 MUT B + TRF2

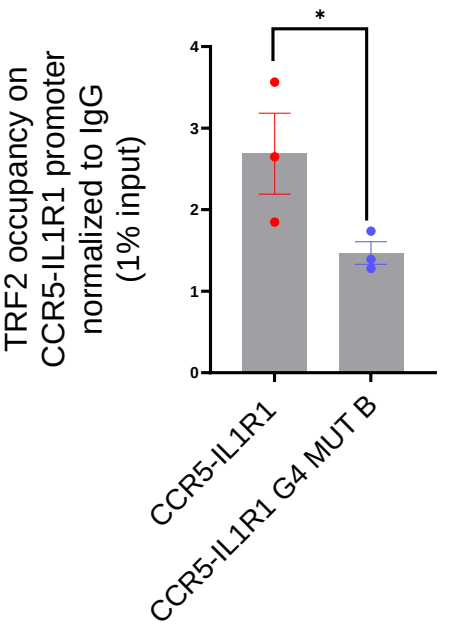
TRF2 occupancy on CCR5-IL1R1 promoter normalized to IgG (1% input)
*
CCR5-IL1R1
CCR5-IL1R1 G4 MUT B

Figure 2: Non-telomeric TRF2 induced activation of IL1R1 is telomere-dependent

A. Occupancy of TRF2 by ChIP-qPCR at the *IL1R1* promoter spanning +200 to -1000 bp of TSS was reduced in xenograft tumors made from HT1080 cells with long telomeres (HL1080-LT) relative to ones with short telomeres (HT1080) cells (N=3 in each case; left panel) and in ex-vivo cultured HT1080-LT compared to HT1080 cells (right panel); IL1R1-3'UTR or a region 20 kb upstream were used as negative controls for TRF2 binding.

B. IL1R1 levels by immunofluorescence microscopy in HT1080 or HT1080-LT cells; cells were stained with DAPI for marking the cell nucleus; IL1R1 levels from 25 individual cells shown in graph (right panel).

C. Telomere length by flow-cytometry of telomeric signal in HT1080 cells (hTERT-inducible stable line) following 0, 1, 6, 12 or 20 days of hTERT induction; HT1080-LT shown as positive control for enhanced telomere length; mean telomeric signal (FITC) plotted bar graph (left).

D. TRF2 occupancy ChIP-qPCR on the *IL1R1* promoter spanning +200 to -1000 bp of TSS in HT1080 cells following 0, 1, 6 or 12 days of hTERT induction in ex-vivo culture; primers and normalization as in Figure 2A; IL1R1-3'UTR or a region 20 kb upstream used as negative controls.

E. IL1R1 levels in control or TRF2-induced HT1080 cells. CD44 used for cell-surface marker and nuclei were stained with DAPI; 25 cells in each condition were scored and plotted in the summary graph (top right panel). TRF2 and IL1R1 levels by western blots following TRF2 induction with 2 or 4 µg/ml doxycycline (Dox) in HT1080 cells (stably transformed for Dox-inducible TRF2); GAPDH as loading (lower left panels). TRF2 and IL1R1 in control or TRF2-induced HT1080 cells by flow-cytometry; TRF2/IL1R1 in x-axis in log scale for 20 thousand cells (lower right panels).

F. TRF2 ChIP-qPCR spanning +200 to -1000 bp of *IL1R1* TSS for TRF2 occupancy (left panel) and promoter activity (luciferase reporter including -1500 bp TSS; right panel) following expression of flag-tag TRF2 full-length, or the mutants TRF2-delB or TRF2-delM; anti-flag antibody used for ChIP; IL1R1-3'UTR or a region 20 kb upstream were used as negative controls.

G. ChIP-qPCR following BG4 ChIP at the IL1R1 promoter (fold enrichment over mock) overlaid with TRF2 occupancy (fold enrichment over IgG) in HT1080 cells.

H. IL1R1 promoter activity in HT1080 cells from luciferase-reporter without or with G4-deforming substitutions against G4 motif A (IL1R1G4-MUT-A) or G4 motif B (IL1R1-G4 MUT-B) in presence or absence of TRF2 induction; G4 motifs A and B as shown in schematic; specific base substitutions shown in Supplementary Figure 2O.

I. *IL1R1* promoter activity, mRNA and protein levels in presence/absence of the G4 binding ligand 360A with or without TRF2 induction.

J. IL1R1 promoter-firefly luciferase reporter cassette, with or without substitutions deforming the G4 motif B, was artificially inserted at the CCR5 locus using CRISPR-cas9 gene editing in HEK293T cells (scheme in left panel). Promoter activity from (center panel); and TRF2 occupancy by ChIP-qPCR (right panel) at the artificially inserted IL1R1 promoter without or with G4-deforming substitutions (IL1R1G4 MUT-B); specific base changes as shown in Supplementary Figure 2O; ChIP-qPCR primers designed specific to the inserted promoter using the homology arms.

Statistical significance was calculated using Mann-Whitney's non-parametric test for individual graphs where N≥5. In case of independent repetitions of the same experiment, unpaired T test with Welsh's correction was performed for significance (p values: * ≤ 0.05, ** ≤ 0.01, *** ≤ 0.001, **** ≤ 0.0001). Error bars correspond to standard error of mean from three independent experiments unless N is stated otherwise.

Figure 3

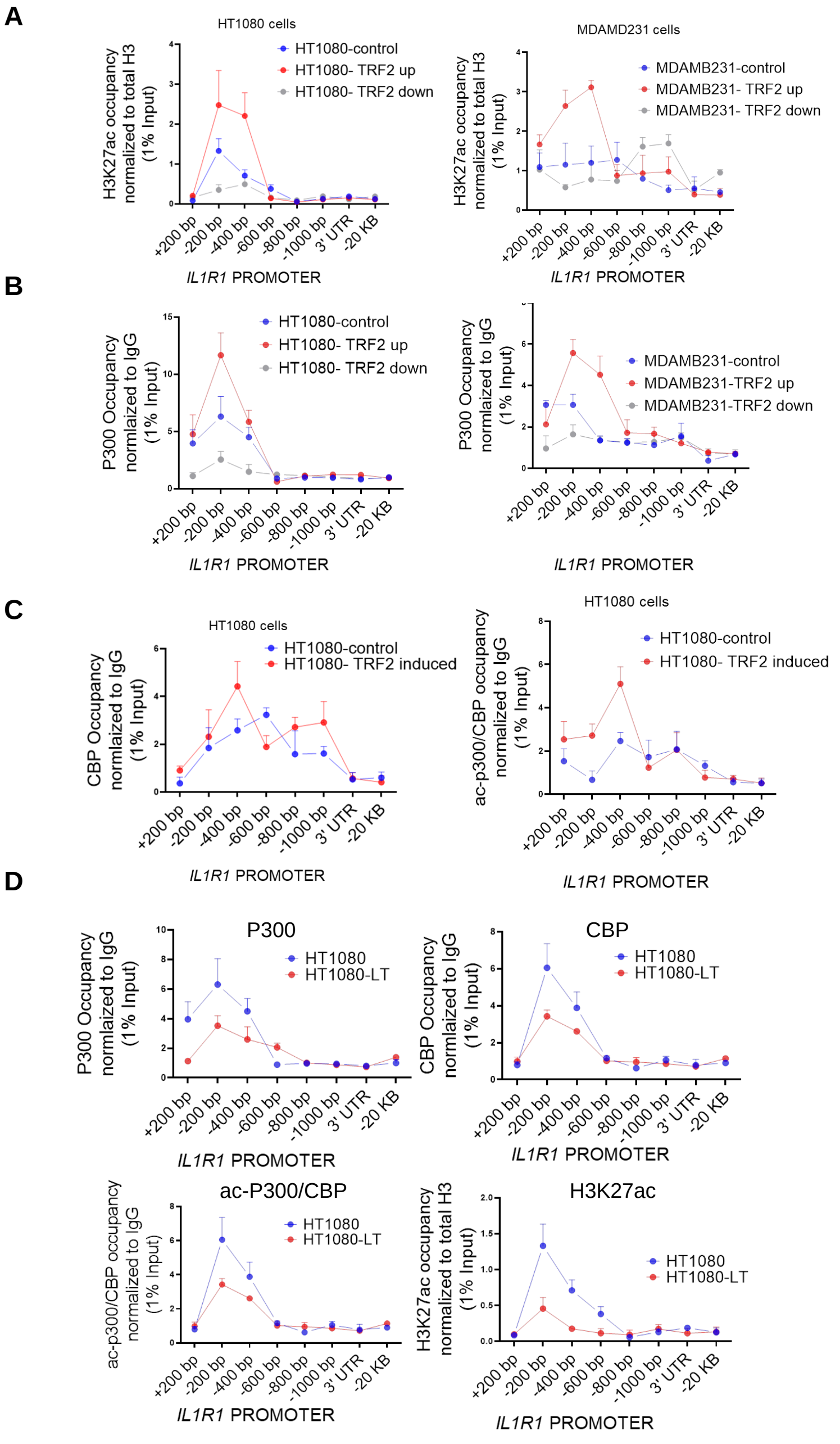
A
HT1080 cells
H3K27ac occupancy normalized to total H3 (1% Input)
HT1080-control
HT1080- TRF2 up
HT1080- TRF2 down
+200 bp
-200 bp
-400 bp
-600 bp
-800 bp
-1000 bp
3' UTR
-20 KB
IL1R1 PROMOTER
MDAMD231 cells
MDAMB231-control
MDAMB231- TRF2 up
MDAMB231- TRF2 down
B
P300 Occupancy normlaized to IgG (1% Input)
P300 Occupancy normlaized to IgG (1% Input)
MDAMB231-TRF2 up
MDAMB231-TRF2 down
C
CBP Occupancy normlaized to IgG (1% Input)
HT1080- TRF2 induced
ac-p300/CBP occupancy normalized to IgG (1% Input)
D
P300
HT1080
HT1080-LT
CBP
ac-P300/CBP
H3K27ac

E

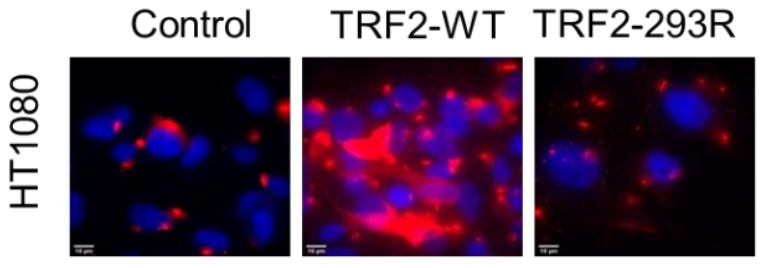

IL1R1 (red) + DAPI

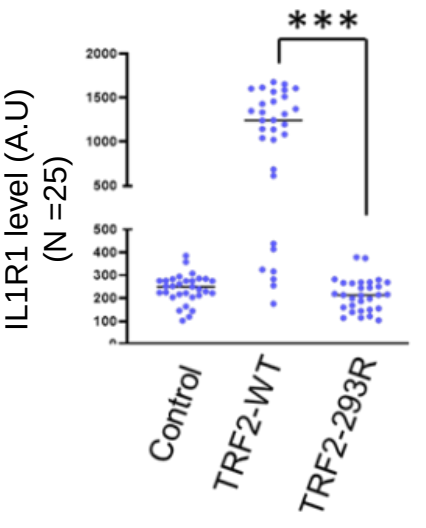

F

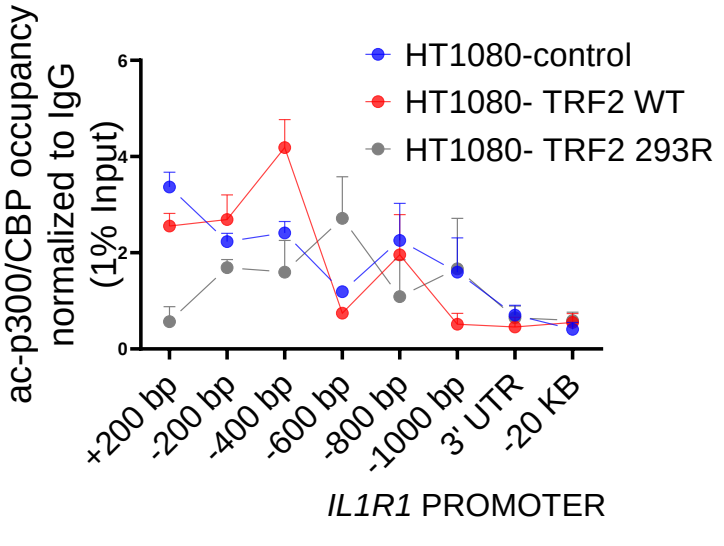

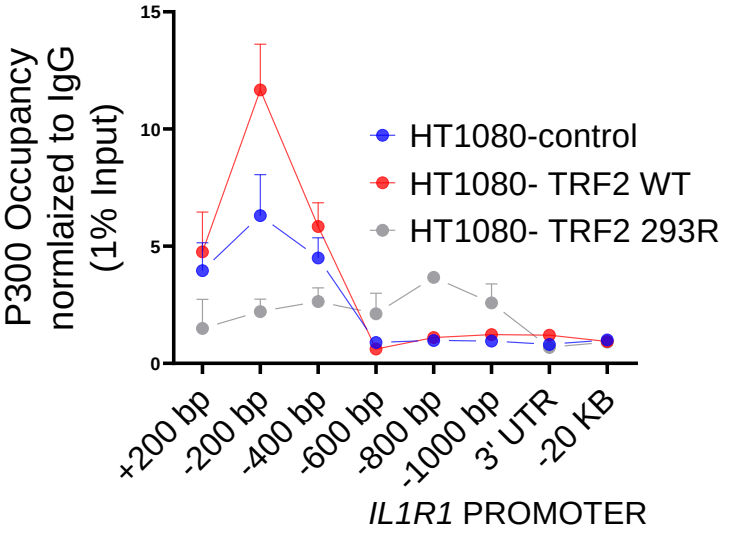

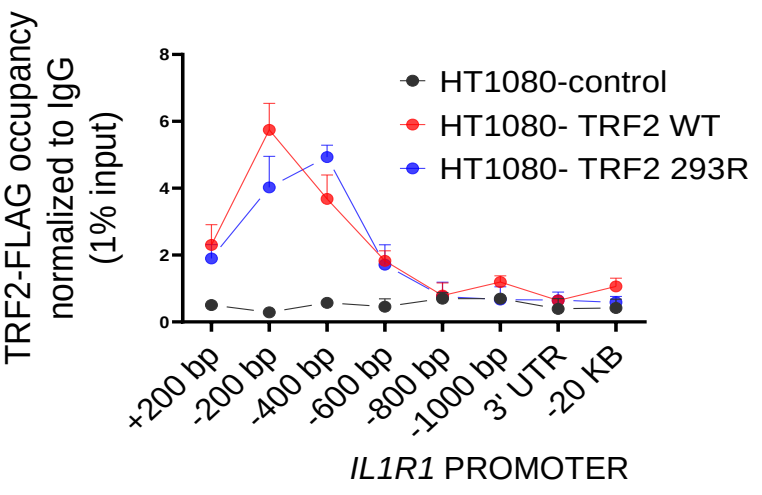

G

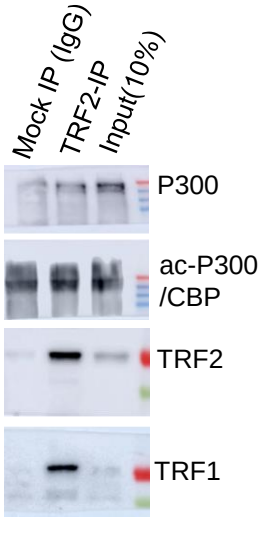

H

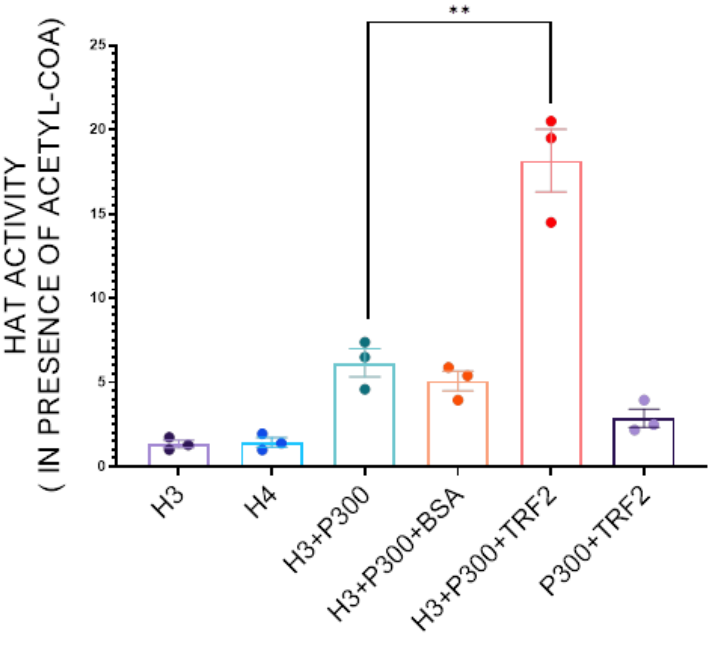

Figure 3: TRF2 recruits the histone acetyl transferase p300 to the IL1R1 promoter

A. H3K27ac occupancy at the *IL1R1* promoter spanning +200 to -1000 bp of TSS by ChIP-qPCR in HT1080 (left panel) and MDAMB231 cells (right panel) in control (uninduced), TRF2-induced (up) or TRF2-down conditions; IL1R1-3'UTR or a region 20 kb upstream were used as negative controls.

B. p300 occupancy on the *IL1R1* promoter in HT1080 (left panel) and MDAMB231 cells (right panel) in control (uninduced), TRF2-induced or TRF2-down conditions; IL1R1-3'UTR or a region 20 kb upstream were used as negative controls.

C. CBP (left panel) and ac-p300/CBP (right panel) occupancy on the *IL1R1* promoter in HT1080 cells in control (uninduced) or TRF2-induced conditions; IL1R1-3'UTR or a region 20 kb upstream were used as negative controls.

D. p300, CBP, acp300/CBP and H3K27Ac occupancy on the *IL1R1* promoter in HT1080 and HT1080-LT cells; IL1R1-3'UTR or a region 20 kb upstream were used as negative controls.

E. Immunofluorescence for IL1R1 in HT1080 cells without (control) or with induction of flag-tag TRF2 WT or mutant TRF2-293R; quantification from 25 cells in each case shown in graph.

F. Occupancy by ChIP-qPCR of acp300/CBP (left panel) or p300 (right panel) without (control) or with induction of TRF2-WT or TRF2-293R; and occupancy of flag-tag TRF2-WT or TRF2-293R on the IL1R1 promoter in HT1080 cells (bottom panel); IL1R1-3'UTR or a region 20 kb upstream were used as negative controls.

G. Immunoprecipitation using TRF2 antibody probed for p300, acp300/CBP, TRF2 or TRF1 (positive control) in input, TRF2 IP fraction or mock IP fraction in HT1080 cells.

H. Histone acetyl transferase (HAT) assay using purified histone H3/H4 and full-length p300 as substrate in presence/absence of recombinant TRF2; BSA (bovine serum albumin) was used as a non-specific mock protein.

All protein ChIP, other than histones, were normalized to 1% input and fold-change shown over respective IgG. Statistical significance was calculated using Mann-Whitney's non-parametric test for individual graphs where N≥5. In case of independent repetitions of the same experiment, unpaired T test with Welsh's correction was performed for significance (p values: * ≤ 0.05, ** ≤ 0.01, *** ≤ 0.001, **** ≤ 0.0001). Error bar correspond to standard error of mean from three independent experiments unless N is stated otherwise.

Figure 4

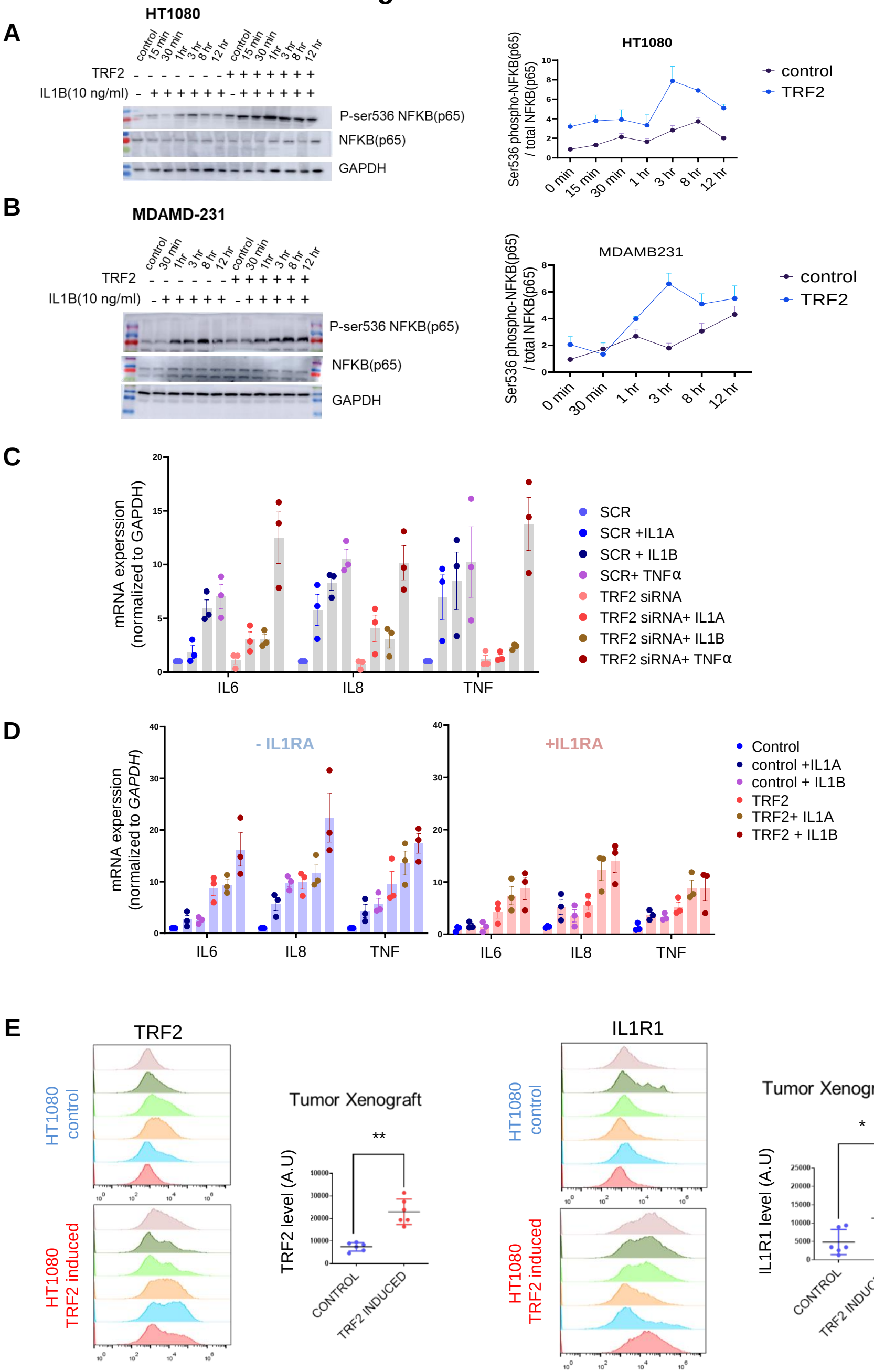
A
HT1080
control
15 min
30 min
1hr
3 hr
8 hr
12 hr
TRF2
IL1B(10 ng/ml)
P-ser536 NFKB(p65)
NFKB(p65)
GAPDH
Ser536 phospho-NFKB(p65) / total NFKB(p65)
0 min
1 hr
control
TRF2
B
MDAMD-231
30 min
MDAMB231
C
mRNA experssion (normalized to GAPDH)
IL6
IL8
TNF
SCR
SCR +IL1A
SCR + IL1B
SCR+ TNFα
TRF2 siRNA
TRF2 siRNA+ IL1A
TRF2 siRNA+ IL1B
TRF2 siRNA+ TNFα
D
- IL1RA
+IL1RA
Control
control +IL1A
control + IL1B
TRF2
TRF2+ IL1A
TRF2 + IL1B
E
TRF2
IL1R1
HT1080 control
HT1080 TRF2 induced
Tumor Xenograft
TRF2 level (A.U)
IL1R1 level (A.U)
CONTROL
TRF2 INDUCED
**
*

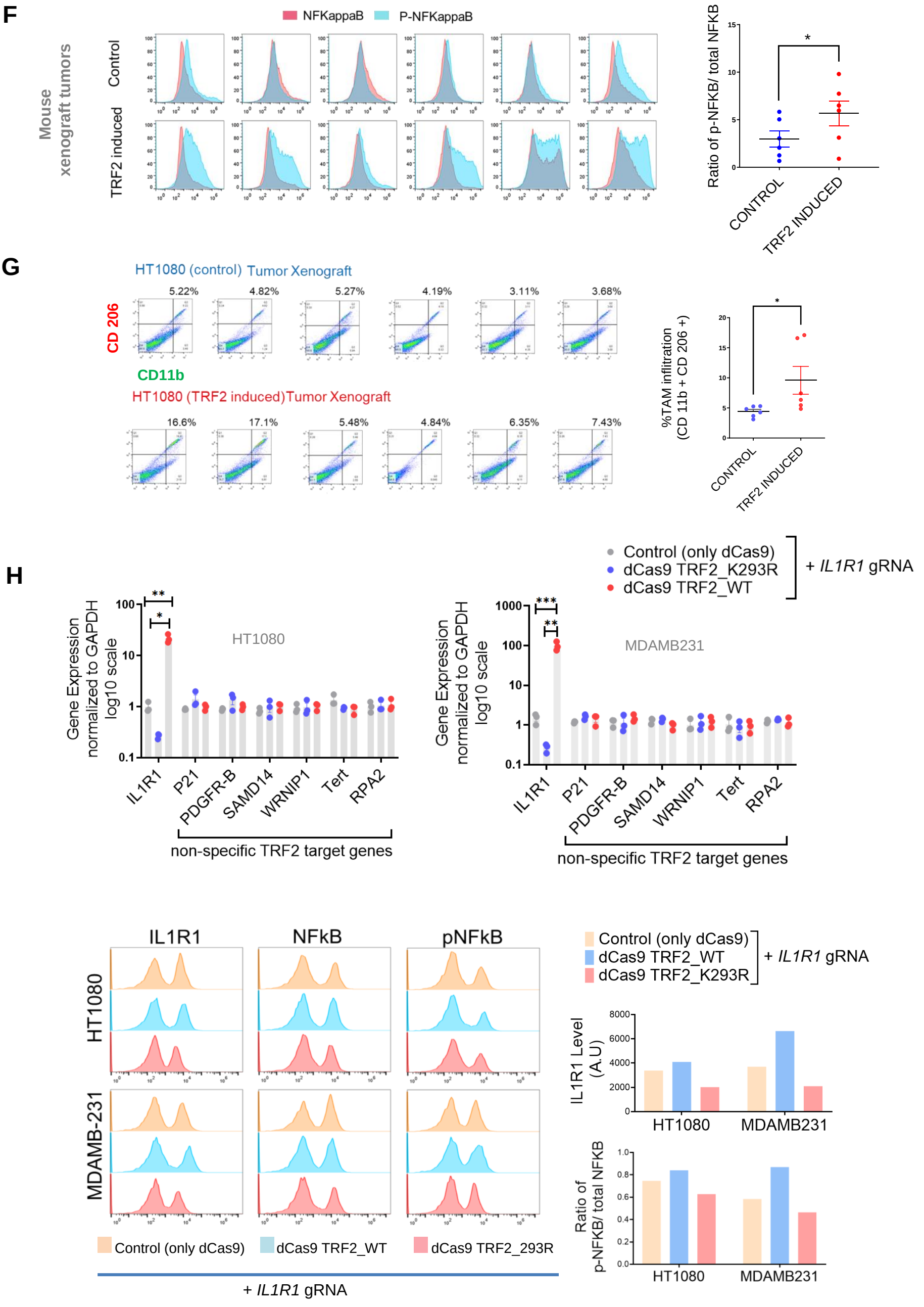
F
NFKappaB
P-NFKappaB
Mouse xenograft tumors
Control
TRF2 induced
Ratio of p-NFKB/ total NFKB
CONTROL
TRF2 INDUCED
G
HT1080 (control) Tumor Xenograft
5.22%
4.82%
5.27%
4.19%
3.11%
3.68%
CD 206
CD11b
HT1080 (TRF2 induced)Tumor Xenograft
16.6%
17.1%
5.48%
4.84%
6.35%
7.43%
%TAM infiltration (CD 11b + CD 206 +)
CONTROL
TRF2 INDUCED
H
Control (only dCas9)
dCas9 TRF2_K293R
dCas9 TRF2_WT
+ IL1R1 gRNA
Gene Expression normalized to GAPDH log10 scale
HT1080
MDAMB231
IL1R1
P21
PDGFR-B
SAMD14
WRNIP1
Tert
RPA2
non-specific TRF2 target genes
IL1R1
NFkB
pNFkB
HT1080
MDAMB-231
Control (only dCas9)
dCas9 TRF2_WT
dCas9 TRF2_293R
+ IL1R1 gRNA
Control (only dCas9)
dCas9 TRF2_WT
dCas9 TRF2_K293R
+ IL1R1 gRNA
IL1R1 Level (A.U)
HT1080
MDAMB231
Ratio of p-NFKB/ total NFKB
HT1080
MDAMB231

J

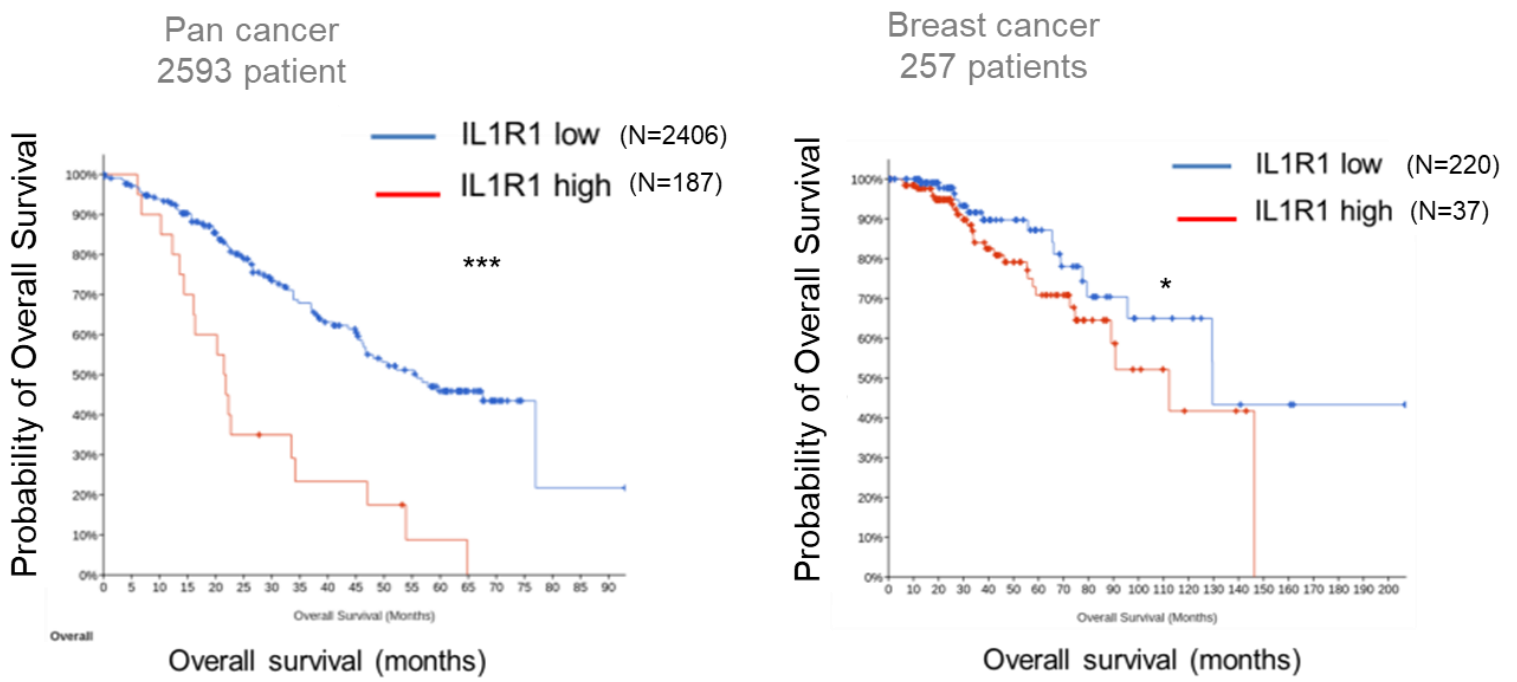
Pan cancer
2593 patient
IL1R1 low (N=2406)
IL1R1 high (N=187)
***
Probability of Overall Survival
Overall survival (months)
Breast cancer
257 patients
IL1R1 low (N=220)
IL1R1 high (N=37)
*
Probability of Overall Survival
Overall survival (months)

K

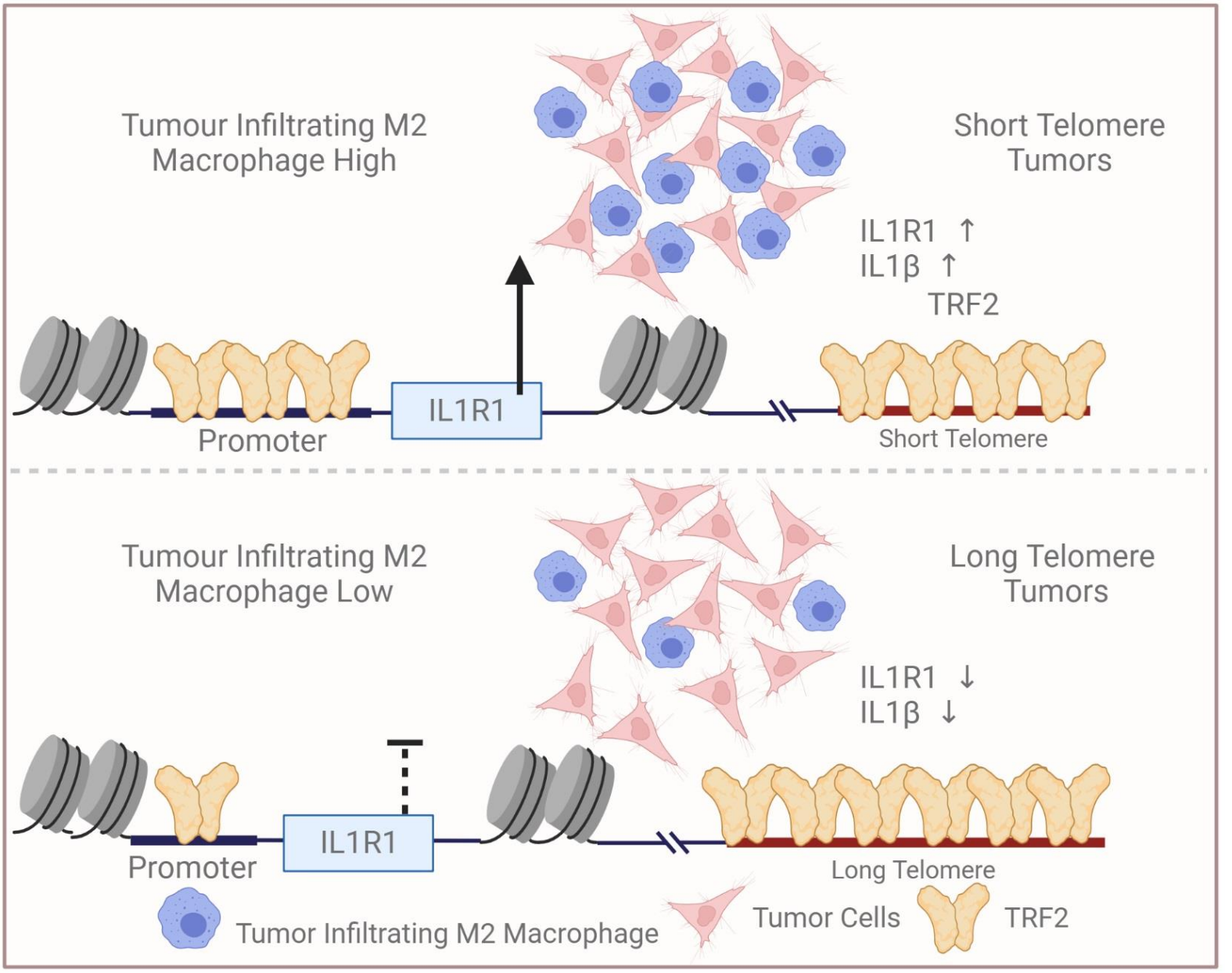
Tumour Infiltrating M2
Macrophage High
Short Telomere
Tumors
IL1R1 ↑
IL1β ↑
TRF2
IL1R1
Promoter
Short Telomere
Tumour Infiltrating M2
Macrophage Low
Long Telomere
Tumors
IL1R1 ↓
IL1β ↓
IL1R1
Promoter
Long Telomere
Tumor Infiltrating M2 Macrophage
Tumor Cells
TRF2

Figure 4: TRF2-dependent IL1 pathway activates NFkappa B (p65) in cancer cells and promotes TAM infiltration

A-B. NFKappaB activation in presence of IL1B (10 ng/ml) in HT1080 (A) or MDAMB231 (B) cells with or without TRF2 induction; activation signaling was confirmed through NFKappaB-Ser536 phosphorylation (normalized to total NFKappaB); ratio of Ser566-p/total NFKappaB plotted for respective blots from three independent replicates (right panels).

C. Expression of NFKappaB targets *IL6, IL8* or *TNF* in presence/absence IL1A, IL1B or TNF-α (10 ng/ml) for 24 hr in control (scrambled siRNA) or TRF2-low (TRF2 siRNA) conditions in HT1080 cells.

D. Expression of *IL6, IL8* or *TNF* in control or TRF2-induced conditions on treatment with either IL1A or IL1B (10 ng/ml) for 24 hr in absence (left panel) or presence (right panel) of the IL1-receptor-antagonist IL1RA (20 ng/ml) in HT1080 cells.

E. TRF2 (left panel), IL1R1 (right panel) levels from xenograft tumors in NOD-SCID mice (control or doxycycline-induced TRF2 in HT1080 cells; N=6 mice in each group) by immuno-flow cytometry; mean fluorescence signal from individual tumors in control or TRF2-induced tumors plotted in adjacent graphs.

F. NFkappaB/phosphor-Ser536-NFKappaB levels in xenograft tumors developed in NOD-SCID mice (control or doxycycline-induced TRF2 in HT1080 cells; N=6 mice in each group) by immuno-flow cytometry; mean fluorescence signal from individual tumors in control or TRF2-induced tumors plotted in adjacent graph; activation shown as ratio of pSer536-p-NFkappaB over total NFkappaB; significance was calculated using Wilcoxon's non-parametric test.

G. TAM infiltration within xenograft tumors (HT1080 control or HT1080-TRF2-induced; N=6 mice in each group) analyzed using markers CD11b and CD206; percentage $CD11b^{+}CD206^{+}$ from each tumor plotted in adjacent graph.

H-I. TRF2-wild type (WT) and TRF2-2293R mutant proteins fused with dCAS9 expressed and targeted to the IL1R1 promoter using *IL1R1*-specific gRNA in HT1080 (left) or MDAMB231 cells (right). Following this, expression of *IL1R1* or other TRF2 target genes (non-specific with respect to the IL1R1-gRNA) in HT1080 (left) or MDMB231 cells (right) shown in (H); and, IL1R1, NFKB and p-NFKB (Ser536-phosphorylation) levels by flow-cytometry in HT1080 or MDAM231 cells (I); mean fluorescence signal for IL1R1 and ratio of p-NFKB/total NFKB plotted in graphs on right panels.

J. Patient survival in either high or low IL1R1-expressing cancers analyzed from 2593 patients across 30 cancer types including breast, lung, pancreatic, bladder, renal and glioma (pan-cancer; left panel) and 257 breast cancer patients (right panel); publicly available TCGA data analyzed from cBIOPORTAL.

K. Scheme depicting relatively low infiltration of TAM in tumors with relatively long telomeres vis-à-vis tumors with short telomeres. Reduced non-telomeric TRF2 binding at the IL1R1 promoter in tumors with long telomeres, and consequent low IL1R1 activation, attenuated p65-mediated IL1-beta and macrophage infiltration. Figure created with BioRender.com.

Statistical significance has been calculated using Mann-Whitney's non-parametric test for individual graphs (p values: * ≤ 0.05, ** ≤ 0.01, *** ≤ 0.001, **** ≤ 0.0001) unless otherwise mentioned.

Supplementary Information

Supplementary table 1

Relative telomere length (RTL) of Triple Negative Breast Cancer (TNBC) patient samples

Key: Blue- TNBC-ST (short telomere); Red- TNBC-LT (long telomere)

TNBC (Triple negative breast cancer) -Sample ID	**RTL(relative telomere length)** normalized to reference cell line – HT1080 (~4.5 Kb)
4H I	0.01
5L X	0.01
4K VIII	0.02
6D I	0.02
2C III	0.02
5I V	0.02
5G VII	0.02
3G III	0.04
2G III	0.08
14G I	0.11
21J X	0.12
14I X	0.12
11K X	0.12
6J IX	0.12
23C VI	0.13
5E X	0.13
10H VII	0.14
4L I	0.16
4G IX	0.18
2K VIII	0.20
10K IV	0.20
5F III	0.21
6J VI	0.22
6E II	0.22
6D II	0.22
11M IV	0.26
22F II	0.27

12G VII	0.29
16H V	0.31
10H VI	0.33
8D II	0.35
23A VI	0.35
11M VII	0.36
14D VI	0.38
23A IV	0.39
4C VI	0.40
7D VII	0.41
18H I	0.44
1H VI	0.45
13D VI	0.51
2G VI	0.54
382 T	0.59
23A V	0.60
5G VIII	0.60
7J IX	0.70
9H X	0.71
12D I	0.72
21F IV	0.73
19L VI	0.74
13K II	0.74
11F III	0.75
7J VIII	0.79
12G VIII	0.80
5L II	0.80
7L IV	0.86
4F I	0.87
19I VI	0.95
7A VI	0.95
11M III	0.95
11M VII	0.95
10F VIII	0.98
8K II	0.98
20L III	1.01
17L IV	1.06
15H VII	1.09
7B VIII	1.14
10B VIII	1.15

18C V	1.17
16H X	1.18
7C II	1.22
15H IV	1.22
21B VIII	1.24
11F IV	1.31
18C V	1.33
3L III	1.37
21B III	1.47
17F X	1.50
17F II	1.55
13H VII	1.69
13H VII	1.69
15K IX	2.34
17L VI	2.42
17L I	2.54
18C I	2.78
10B V	2.81
15K V	2.90
12D VI	3.80
15K VI	3.99
12B IX	4.01
22B X	4.98
4C VI	8.25
8C III	8.40
17F IV	8.70
6J V	10.39
9G VIII	14.83

Supplementary Figures

Supplementary Figure 1

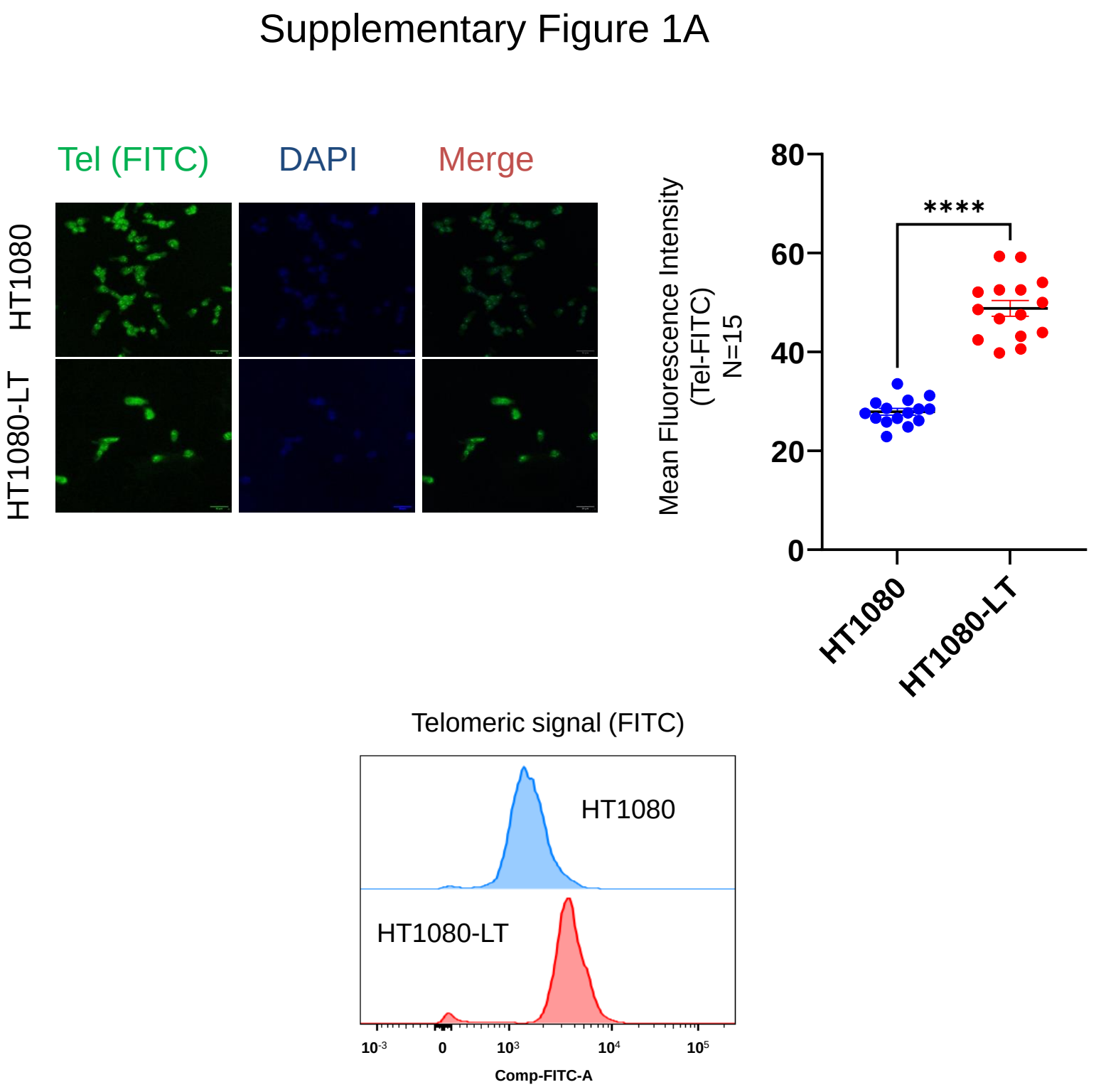

Supplementary Figure 1A:
Immuno-histochemical (IHC) staining of previously reported and well-characterized cells with short/long telomeres (fibrosarcoma HT1080 or the long-telomere version HT1080-LT cells in cell-isogenic background) hybridized with telomere-specific FITC-labelled PNA probe, counterstained with DAPI (top left panel); telomeric signal was enhanced in HT1080-LT cells (quantified in top right panel). This protocol was adapted for staining patient tumor samples (below). Flow-FISH using telomeric PNA probe showing increased telomeric signal in HT1080-LT compared to HT1080 cells (bottom panel).

Supplementary Figure 1B

Immuno-histochemical (IHC) sections from patient tumors in breast, colon, gastric, ovarian, prostate and kidney cancers (N=3 patients for each cancer type) hybridized with telomere-specific FITC labelled PNA probe, counterstained with DAPI. To rule out any bias in the telomeric signal (PNA) from cell density (DAPI) within the tumor microenvironment the PNA intensity was normalized pixel-by-pixel against the DAPI signal. For pixel-by-pixel normalization we used OpenCV (OpenCV, 2015. *Open Source Computer Vision Library).*

Breast

Tel (FITC) DAPI Merge Tel - DAPI

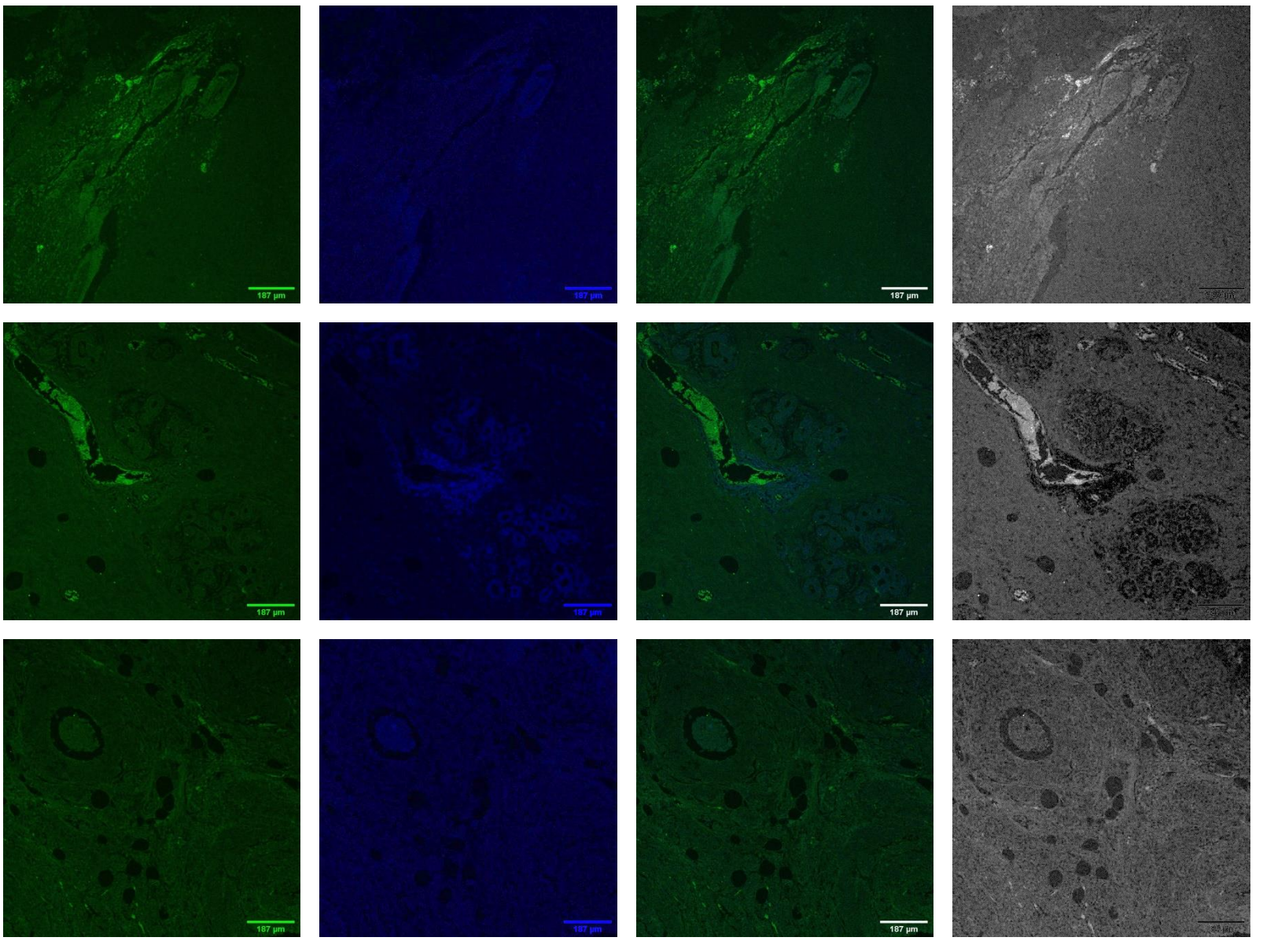

Colon

Tel (FITC) | DAPI | Merge | Tel - DAPI

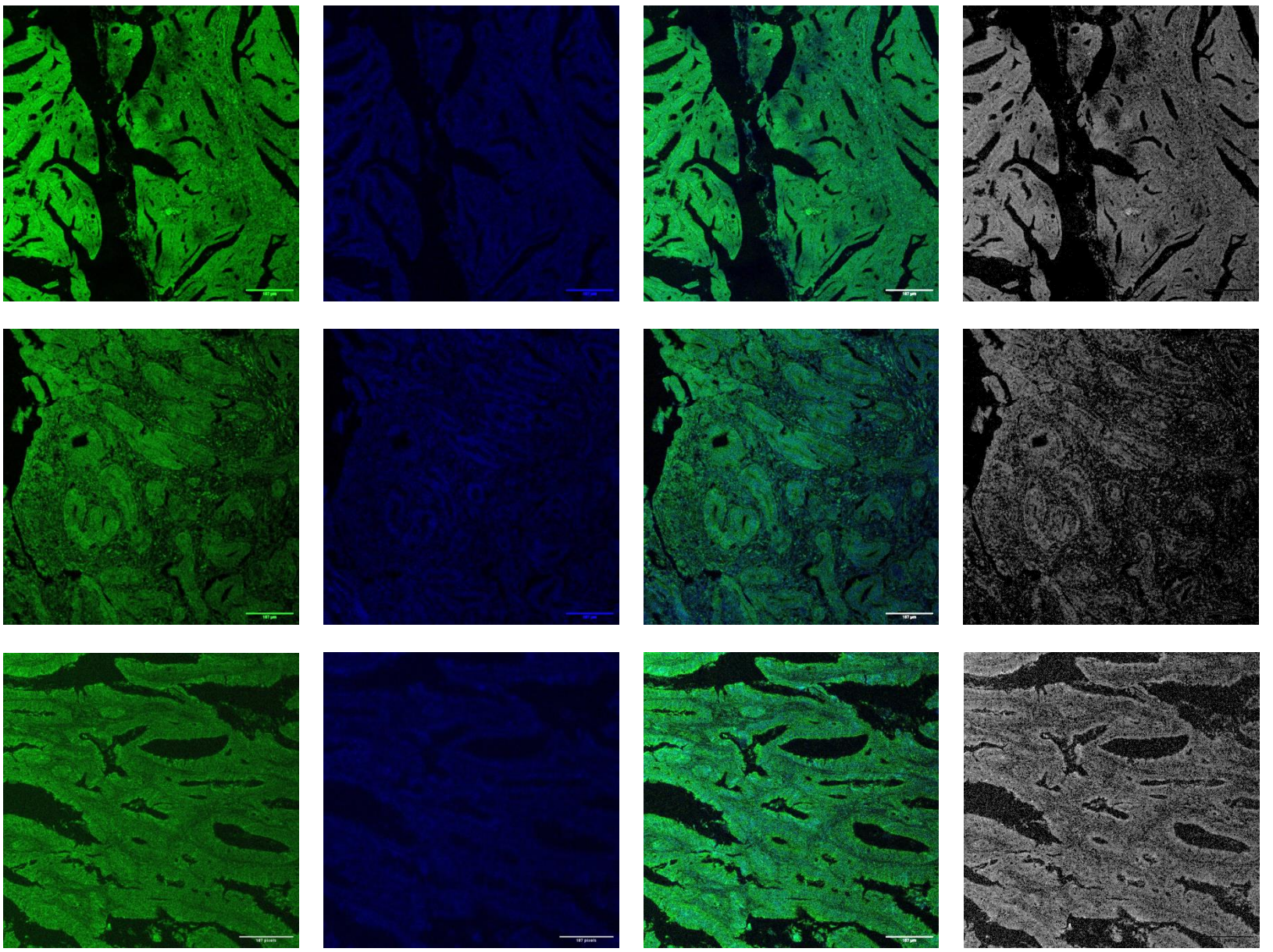

Gastric

Tel (FITC) | DAPI | Merge | Tel - DAPI

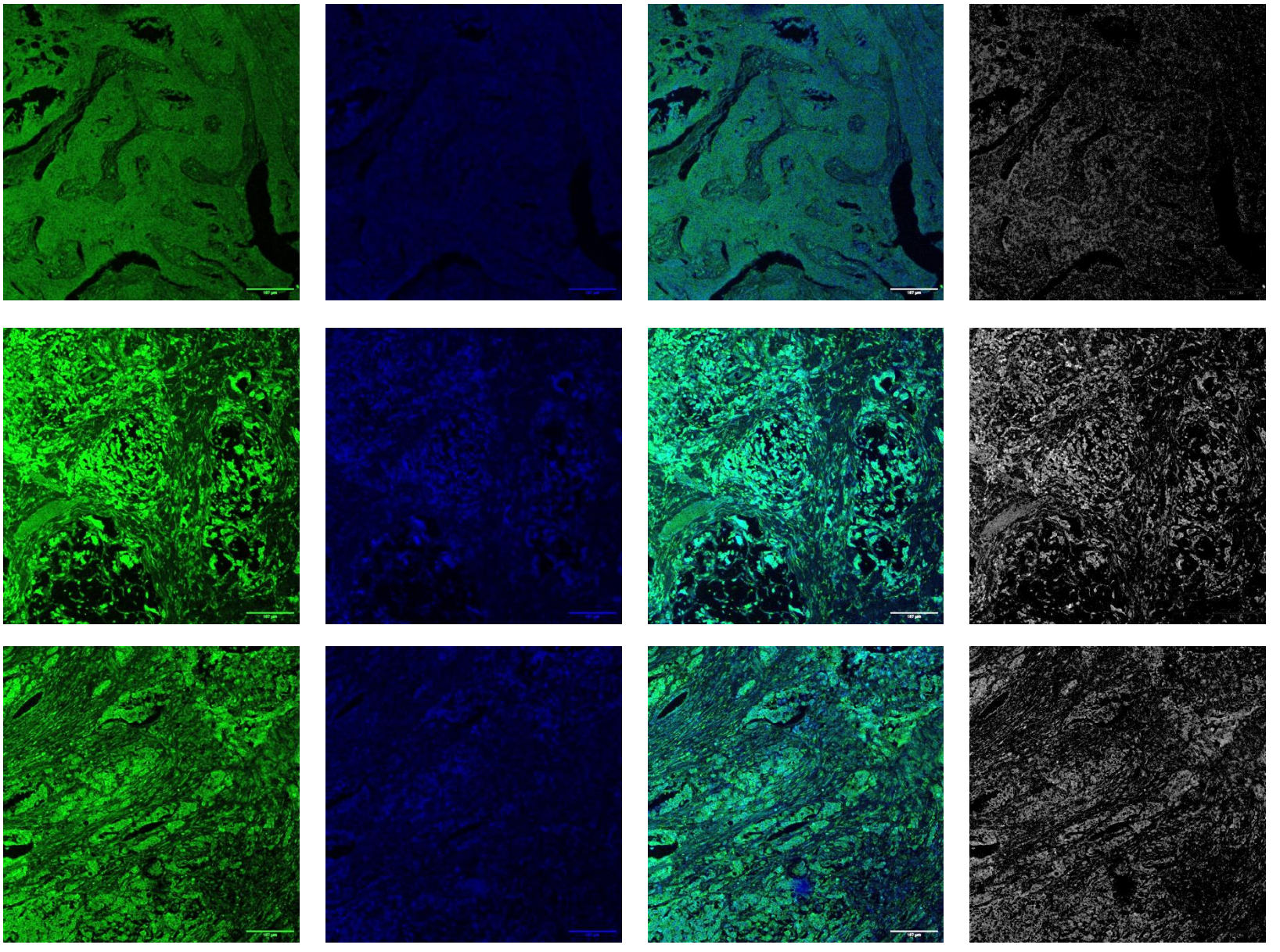

Ovary

Tel (FITC) | DAPI | Merge | Tel - DAPI

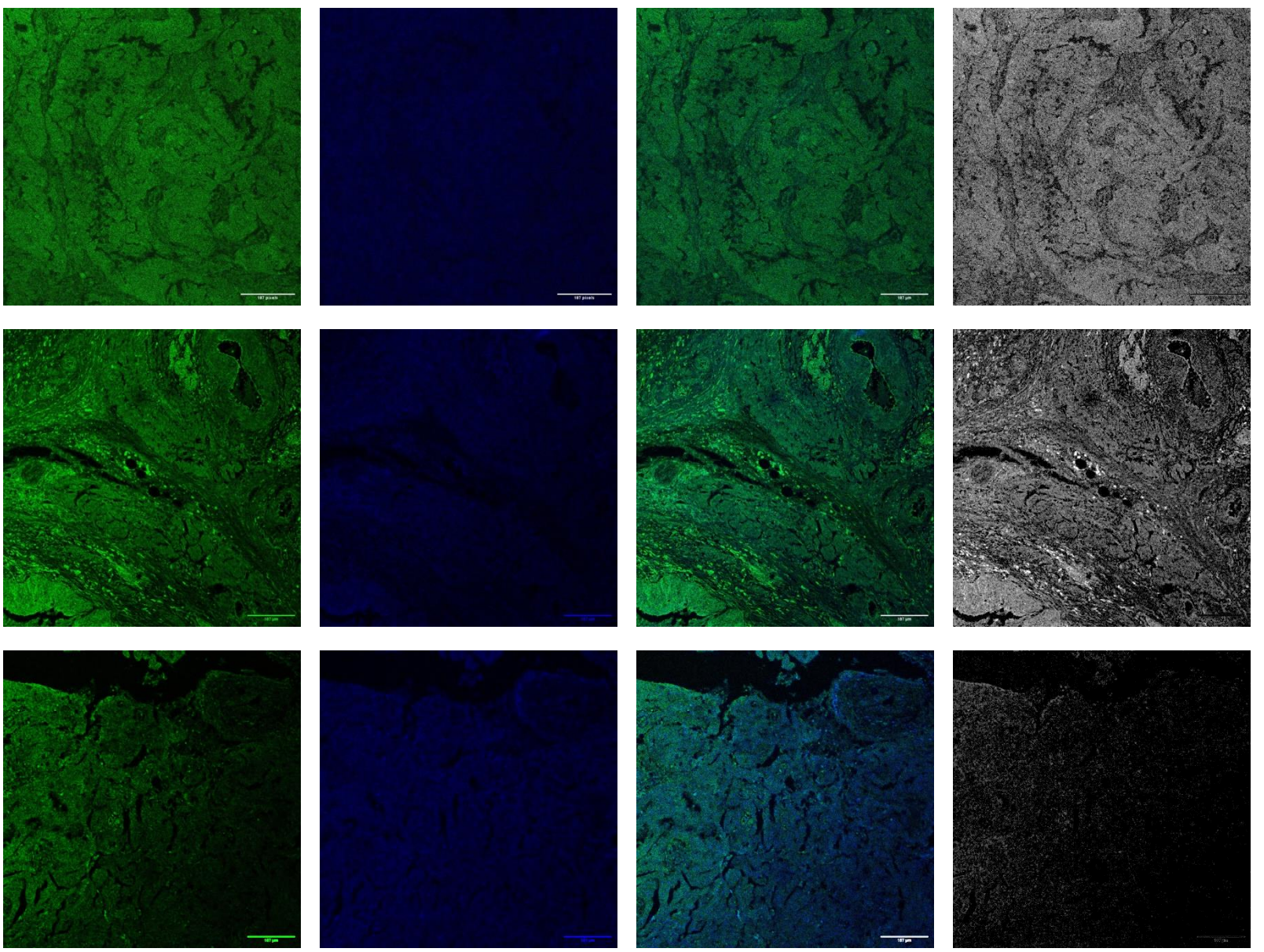

Prostate

Tel (FITC) | DAPI | Merge | Tel-DAPI

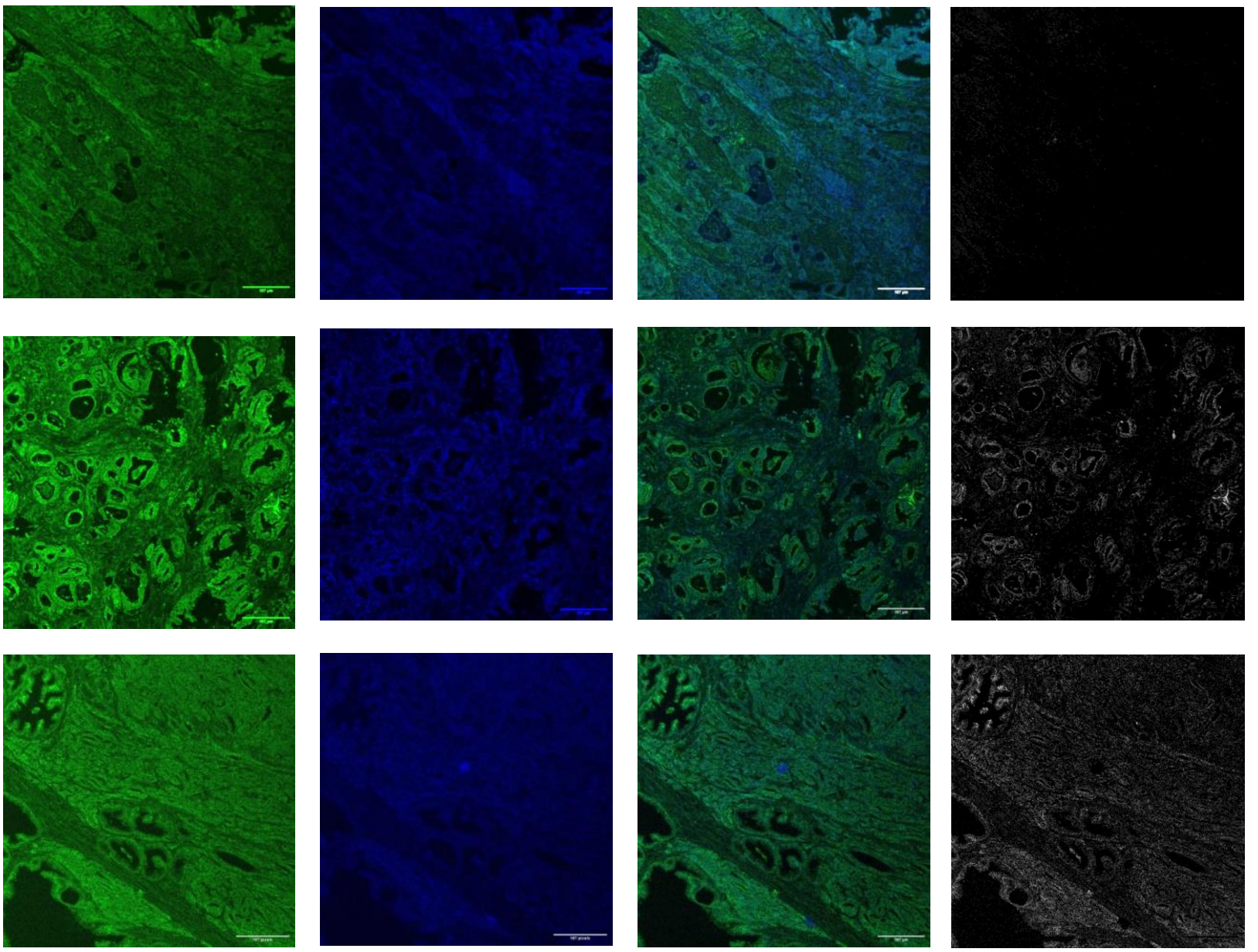

Kidney

Tel (FITC) | DAPI | Merge | Tel-DAPI

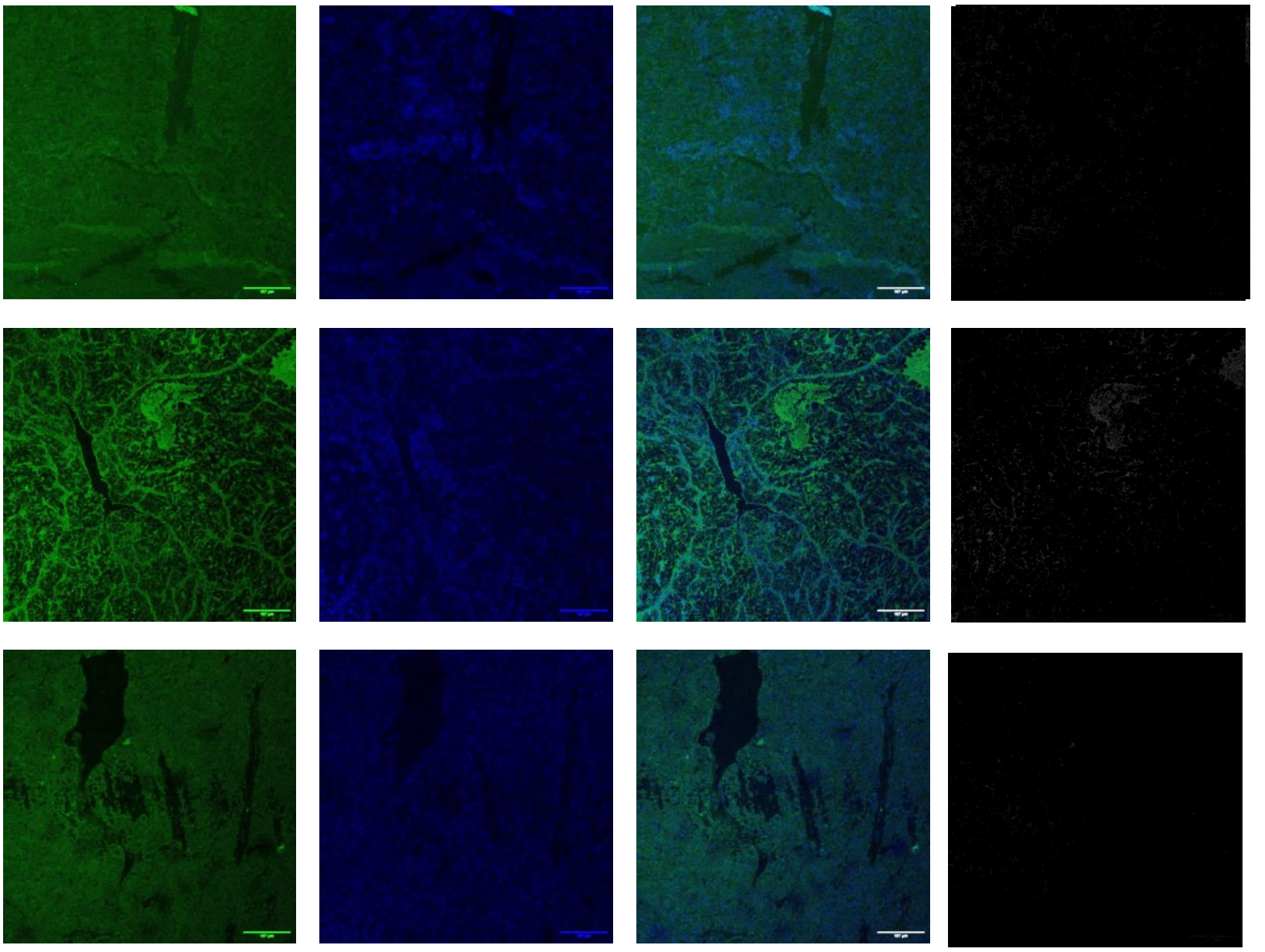

Supplementary Figure 1C

Telseq analysis

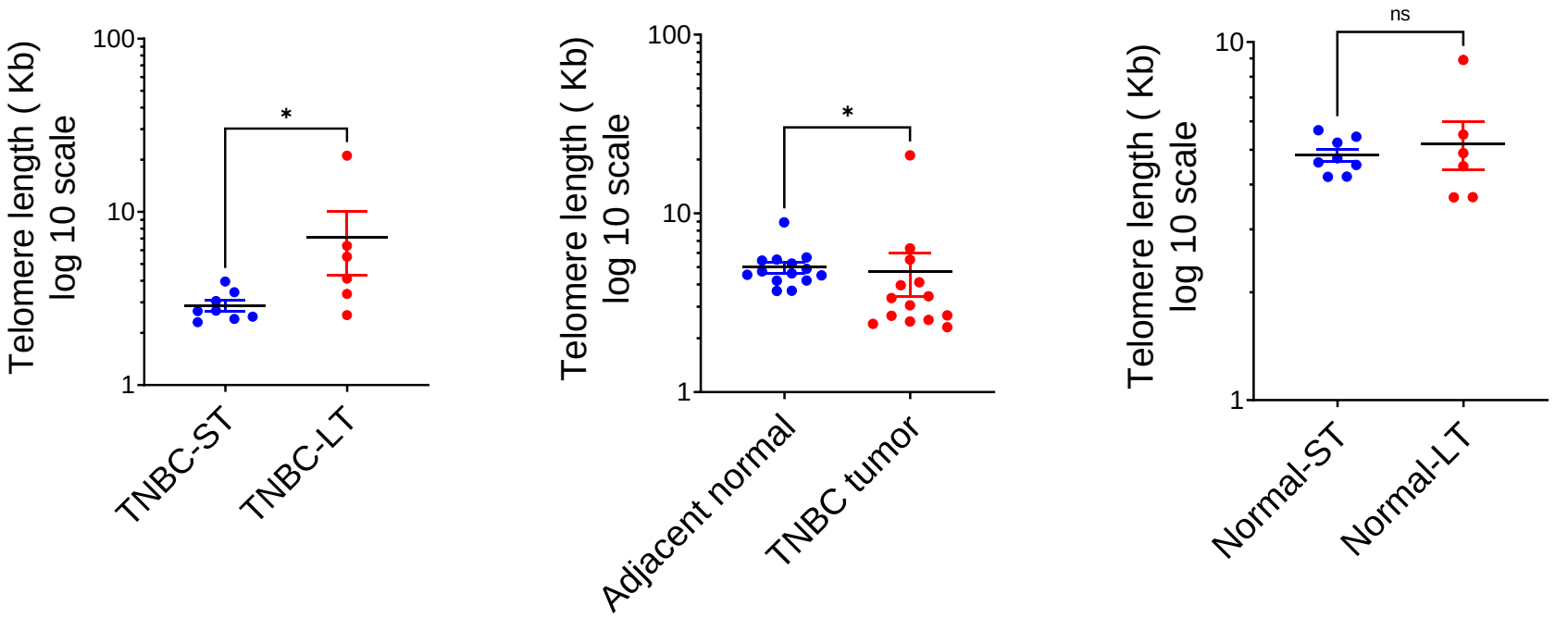

Patient ID	Total_reads_Normal	TL-Normal from Tel-Seq (Kb)	Total_reads_Tumor	TL-Tumor from Tel-Seq (Kb)	Annotation by telo-qPCR
15HIV	793841640	5.52	684690974	2.54	Long
17FII	821874738	3.69	798212363	6.37	Long
17FIV	1018357170	3.69	2217147041	3.36	Long
21BIII	857074906	4.50	1939381027	5.52	Long
22BX	937589074	8.92	2039824553	21.11	Long
8CIII	1205476805	4.89	3048252295	4.12	Long
10HVI	1964615991	5.68	2499660737	2.69	Short
11KX	1618874093	5.24	2060088701	2.41	Short
11MIV	1578986029	5.44	1624283175	2.31	Short
12GVII	1142304223	4.21	1399187739	3.06	Short
21CVIII	1253875224	4.74	1460333173	3.96	Short
23AIV	1352144501	4.21	2733959635	2.48	Short
23AVI	1632115660	4.54	2734342597	3.44	Short
4HI	873273625	4.61	1692643267	2.67	Short

Supplementary Figure 1C:
Telomere length was determined using the previously published algorithm Tel-Seq from sequenced genomes of TNBC samples (N=8 for TNBC-ST (short telomere) and N=6 for TNBC-LT (long telomere); and adjacent normal tissue from same patient). Samples identified as long-telomere (TNBC-LT) or short-telomere (TNBC-ST) using telo-qPCR were significantly different in TL, and consistent with telo-qPCR annotation (top right panel); TL of tumor samples was lower that adjacent normal tissue (top center); and TL from adjacent normal tissues in LT or ST samples did not vary significantly (top right). Table below with sequencing related details of the normal/tumor samples. Statistical significance was calculated using Mann-Whitney's non-parametric test.

Supplementary Figure 1D

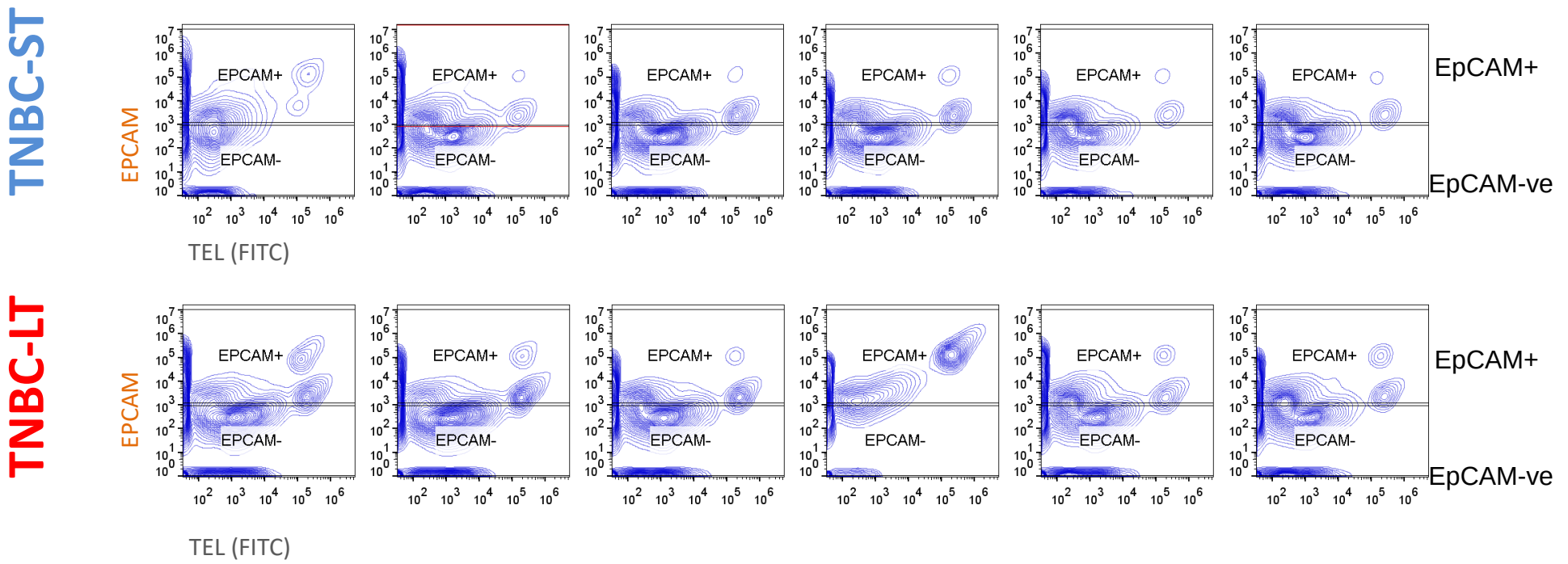

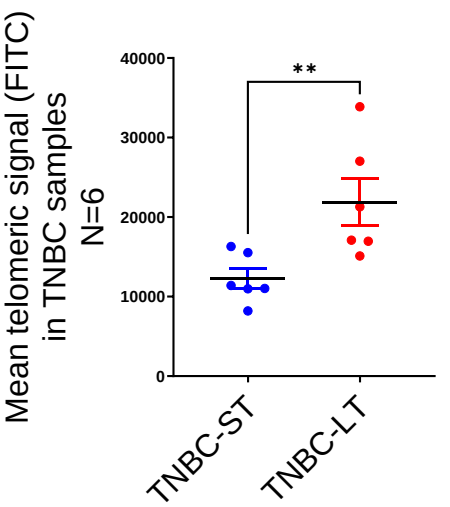

Supplementary Figure 1D:
TNBC samples (N= 6 each for long or short telomere samples) stained with EpCAM (far red) and then hybridized with telomere specific PNA probe (FITC). Mean telomeric signal was plotted in total cells. Statistical significance was calculated using Mann-Whitney's non-parametric test.

Supplementary Figure 1E

TNBC – CLINICAL TISSUE

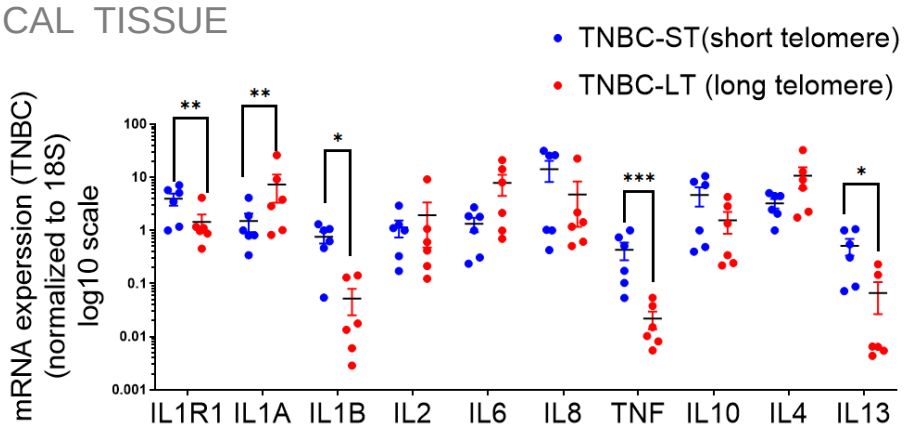

TNBC – ORGANOID (TNBO)

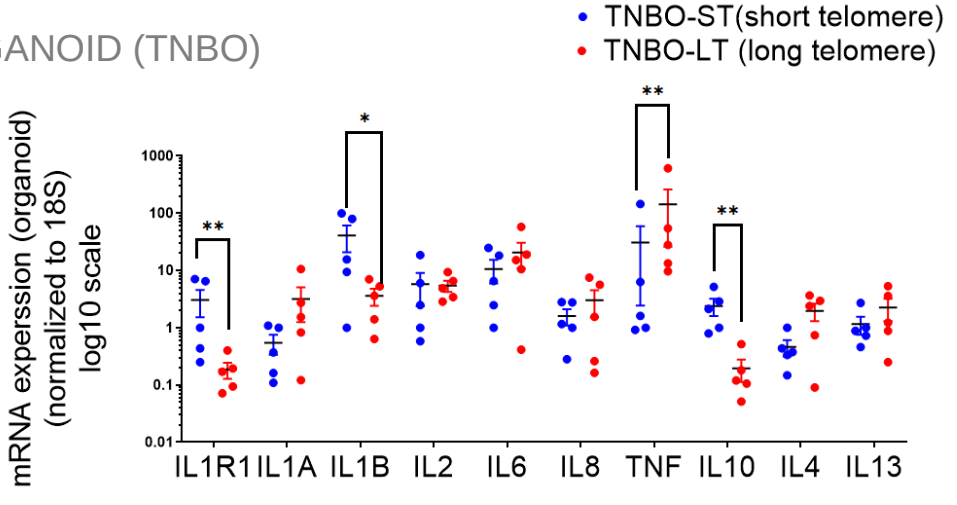

Mouse XENOGRAFT

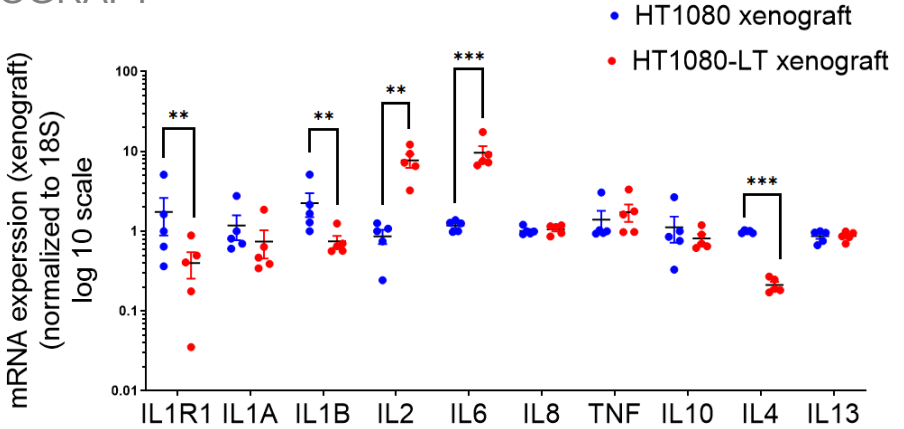

Ex-vivo CELLS

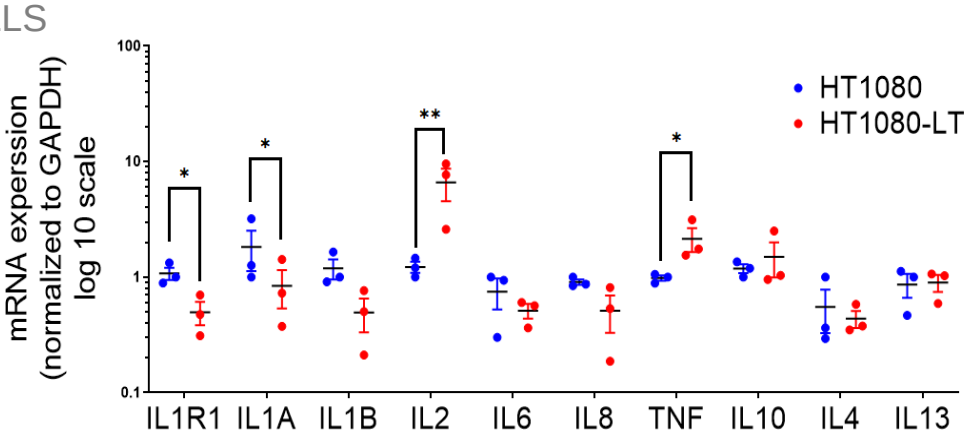

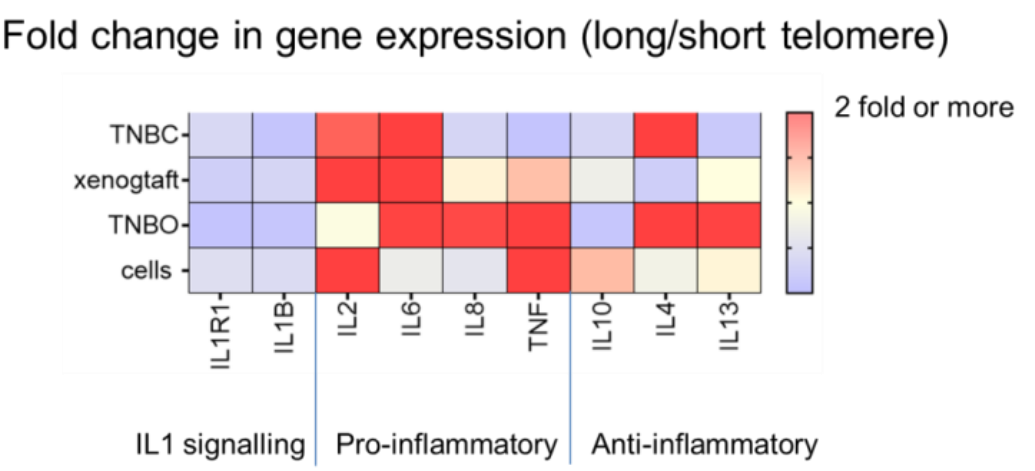

Supplementary Figure 1E:

mRNA expression of *IL1R1* and other key cytokines: *IL1A, IL1B, IL2, IL6, IL8*, *TNF, IL10, IL4* and *IL13* in long or short telomere TNBC tissue, TNBC-derived organoids with long/short telomeres (TNBO-ST or TNBO-LT), xenograft tumors (made from either short (HT1080) or long telomere (HT1080-LT) fibrosarcoma cells, and *ex-vivo* HT1080 or HT1080-LT cells; the *18S* gene was used for normalization in respective cases except for ex-vivo cells where *GAPDH* was used for normalization. Statistical significance was calculated using Mann-Whitney's non-parametric test (p values: * ≤ 0.05, ** ≤ 0.01, *** ≤ 0.001, **** ≤ 0.0001).
Bottom panel: Heat map summarizing the mRNA expression of key cytokines across the models shown above: TNBC tissue, TNBC derived organoids (TNBO), xenograft tumors or ex-vivo cells in long or short telomere cases. Fold change of gene expression (long with respect to short telomeres) color coded as per the reference legend along y-axis.

Supplementary Figure 1F

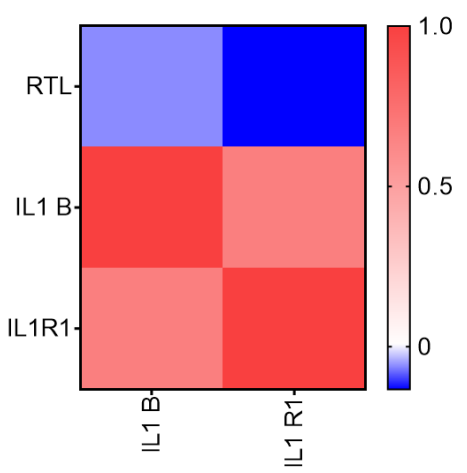

Supplementary Figure 1F:

Spearman correlation of *IL1R1*, *IL1B* expression and RTL (Relative telomere length*)* in 34 TNBC tissue samples with each other and RTL represented as heat map; gene expression was normalized to the18S gene; for telomere length the 36B4 single-copy gene was used for normalization (as in Figure 1D); fold change of TL was calculated with respect to TL in HT1080 cells.

Supplementary Figure 1G

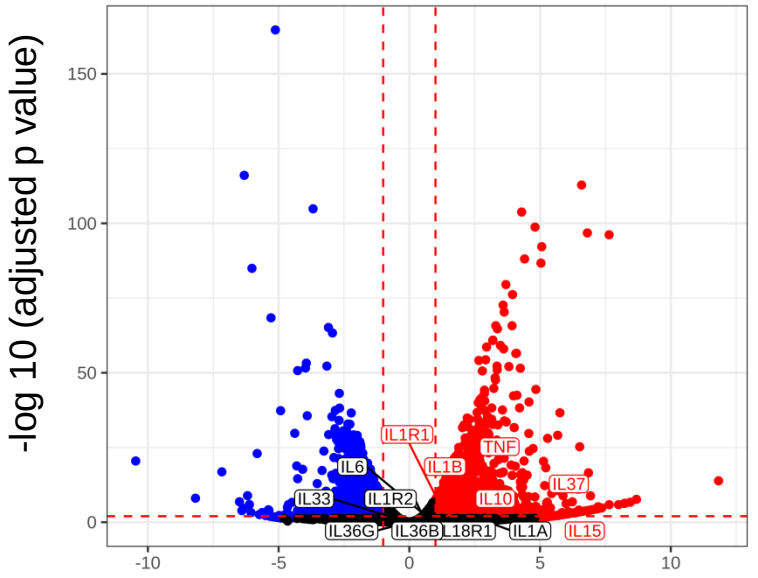

Log 2 Fold change of gene expression
(HT1080 relative to HT1080-LT)

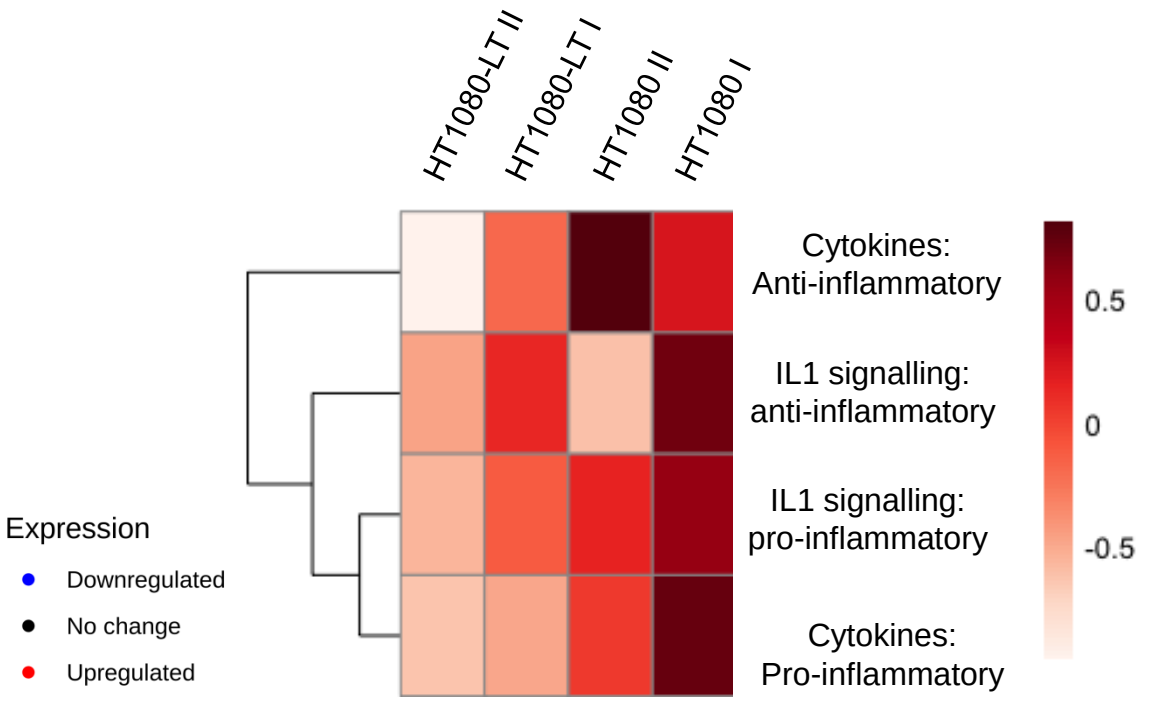

Supplementary Figure 1G:

Volcano plot of expressed genes in RNA-seq in HT1080 or HT1080-LT cells; x-axis has log-2 fold change for genes and the y-axis represents adjusted p values in log-10 scale. Out of the 4315 differentially expressed genes, 2079 were upregulated in HT1080-LT cells specific Key inflammation-related genes that have been marked in figure – most differentially expressed genes like *IL1R1*,*IL1B* and *IL10* were found to have higher expression in HT1080 cells compared to HT1080-LT cells (left panel);

Gene set enrichment analysis of key IL1 signalling related (pro- and anti-inflammatory) genes and key pro- and anti-inflammatory cytokines (right); color key represents fold enrichment.

Supplementary Figure 1H

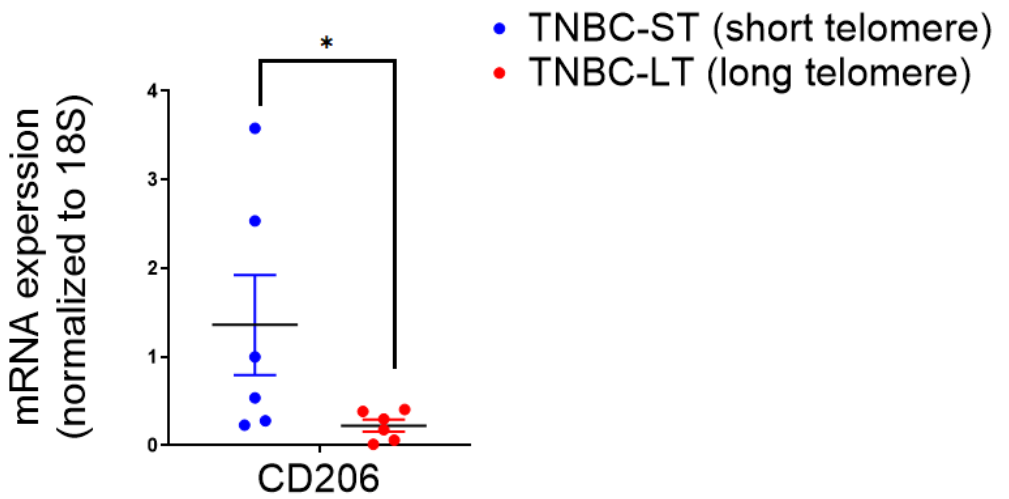

Supplementary Figure 1H:

mRNA expression of the M2 macrophage marker *CD206* in TNBC samples (six long or six short telomere cases) normalized to the *18S* gene in respective cases. Statistical significance was calculated using Mann-Whitney's non-parametric test (p values: * ≤ 0.05).

Supplementary Figure 1I

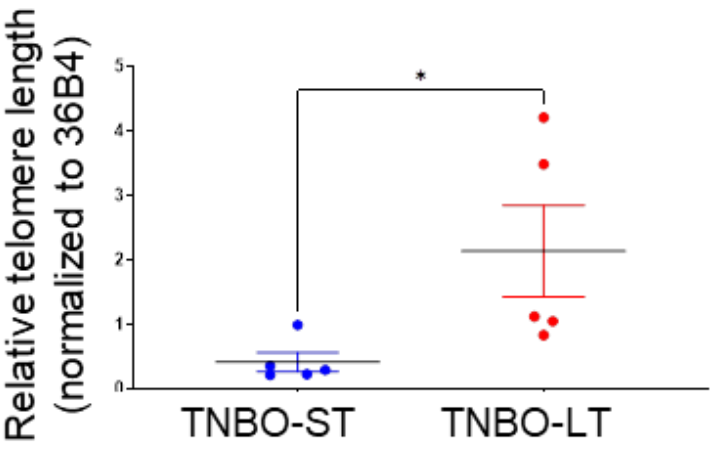

Supplementary Figure 1I:

Relative telomere length of triple negative breast tumor organoids (TNBO) derived from TNBC samples: five TNBO-ST (short telomere) and five TNBO-LT (long telomere) was estimated by telo-qRTPCR .

Supplementary Figure 1J

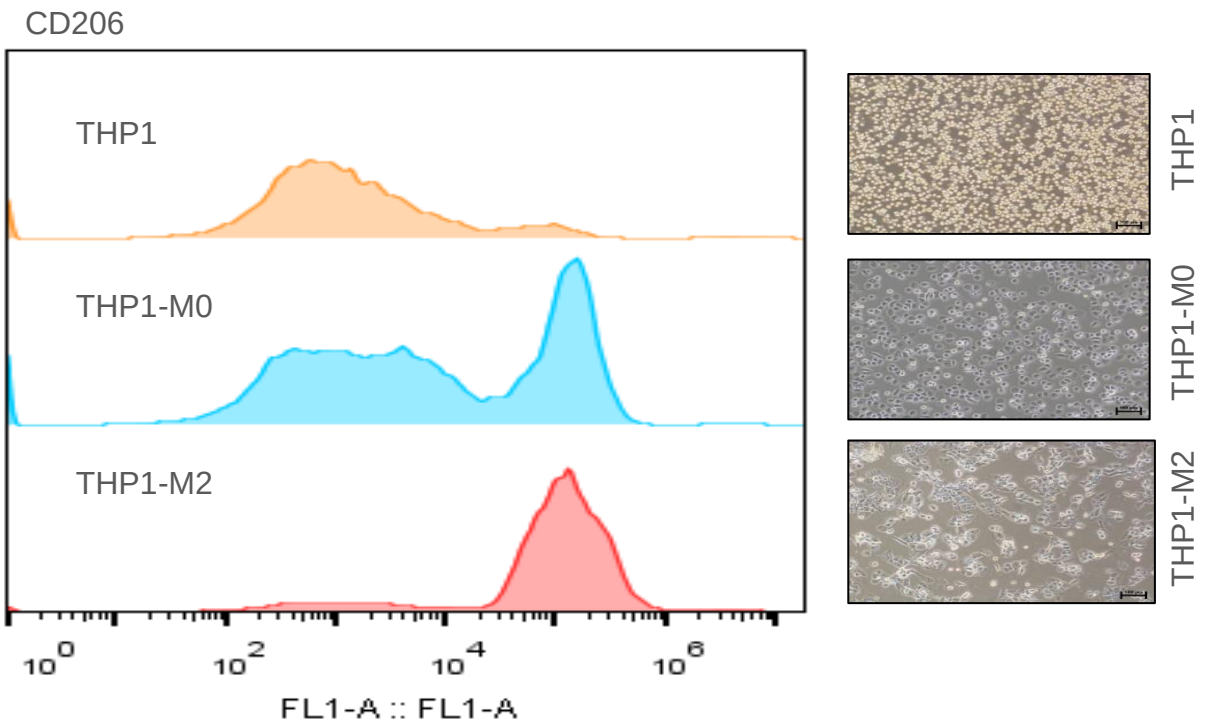

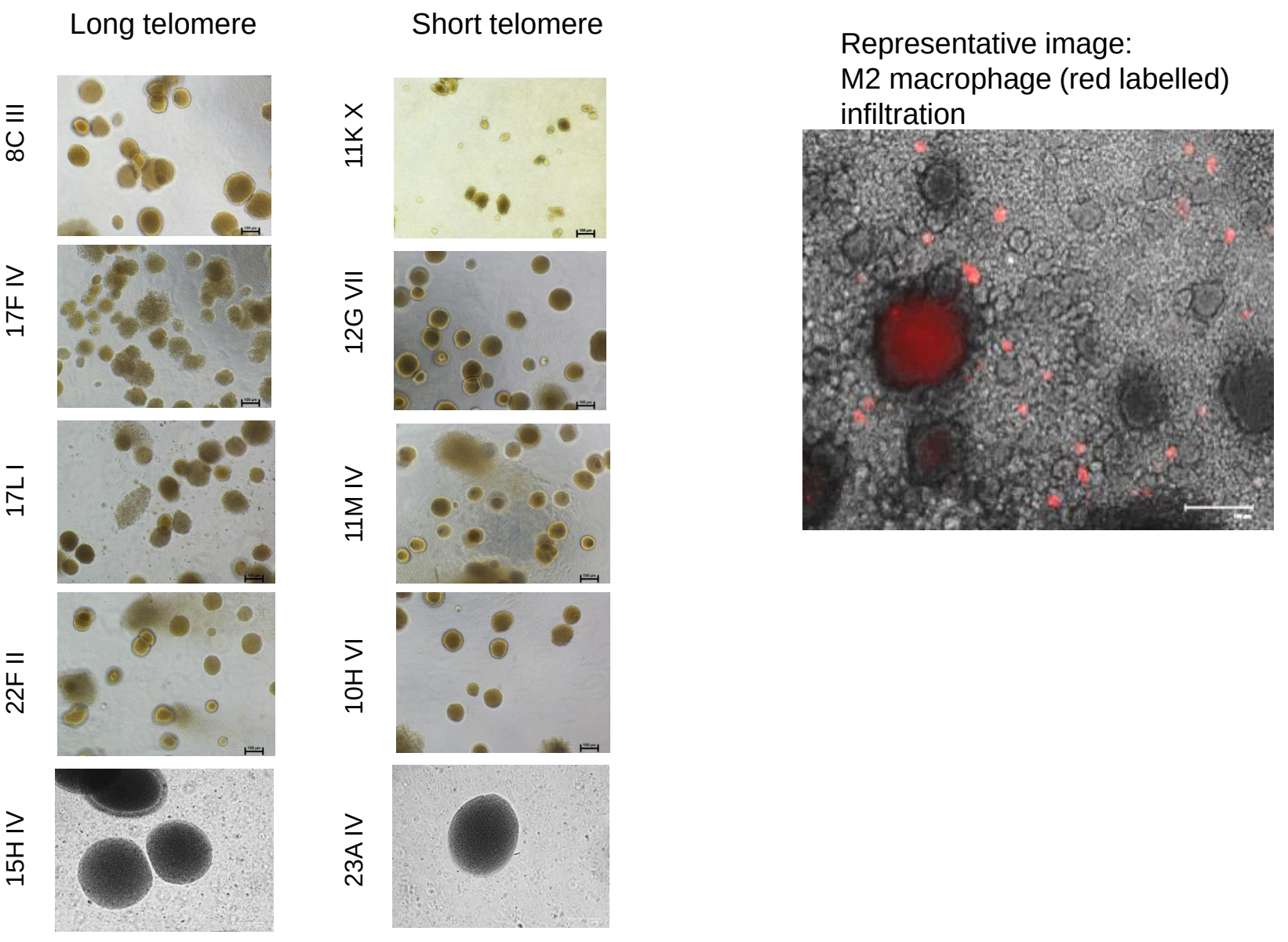

Supplementary Figure 1J:
CD206 levels by immuno-flow cytometry in THP1 cells and macrophages differentiated from THP1 cells into M0 or M2 types (described in Methods) and plotted along X-axis in log scale (top panel). Bright-field images at 10X magnification for each cell stage shown in top right panel. TNBC organoids (TNBO) formed from TNBO-ST (short telomere) and TNBO-LT (long telomere) samples (bottom left panels). Labelled M2 macrophages (red) introduced in the TNBO cultures and allowed to infiltrate. A representative image showing infiltration of M2 macrophages in the organoids (bottom right panel).

Supplementary Figure 1K

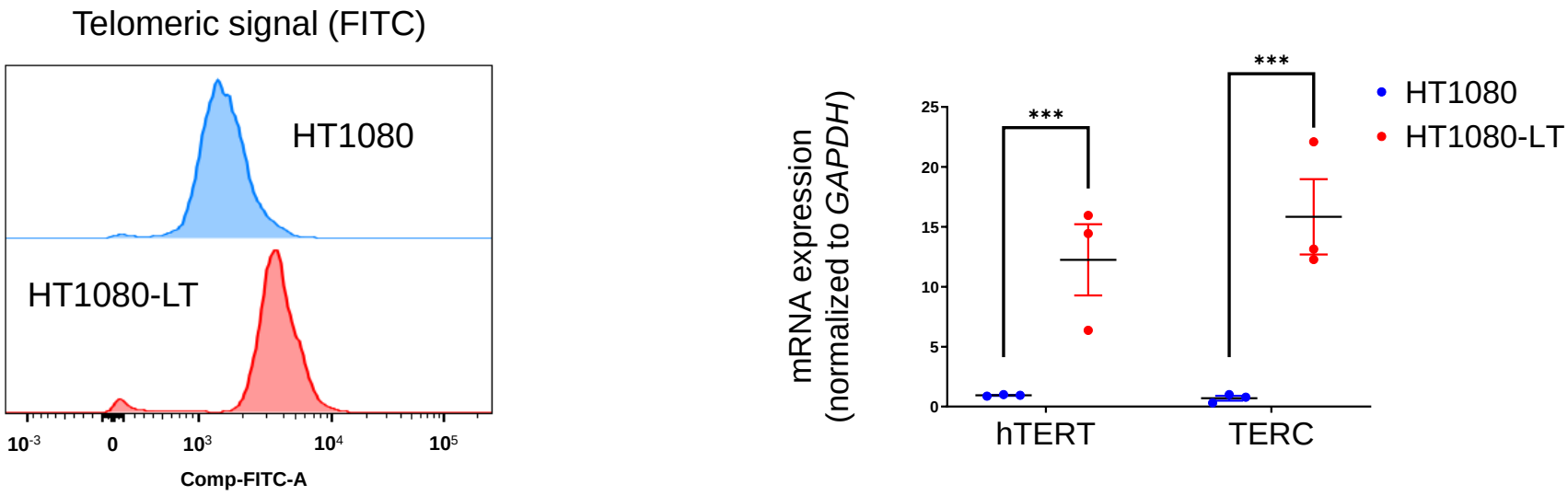

Supplementary Figure 1K:

Telomer length (TL) by flow-cytometry analysis of telomeric signal (FITC labeled PNA probe) showing increase in TL in HT1080-LT cells relative to HT1080 cells; plotted along x-axis in log scale (left panel). *hTERT* and *TERC* expression as expected was enhanced in HT1080-LT relative to HT1080 cells (normalized to GAPDH) (right panel); statistical significance was calculated using t-Test with Welch's correction (p values : * ≤ 0.05, ** ≤ 0.01, *** ≤ 0.001, **** ≤ 0.0001)

Supplementary Figure 1L-M

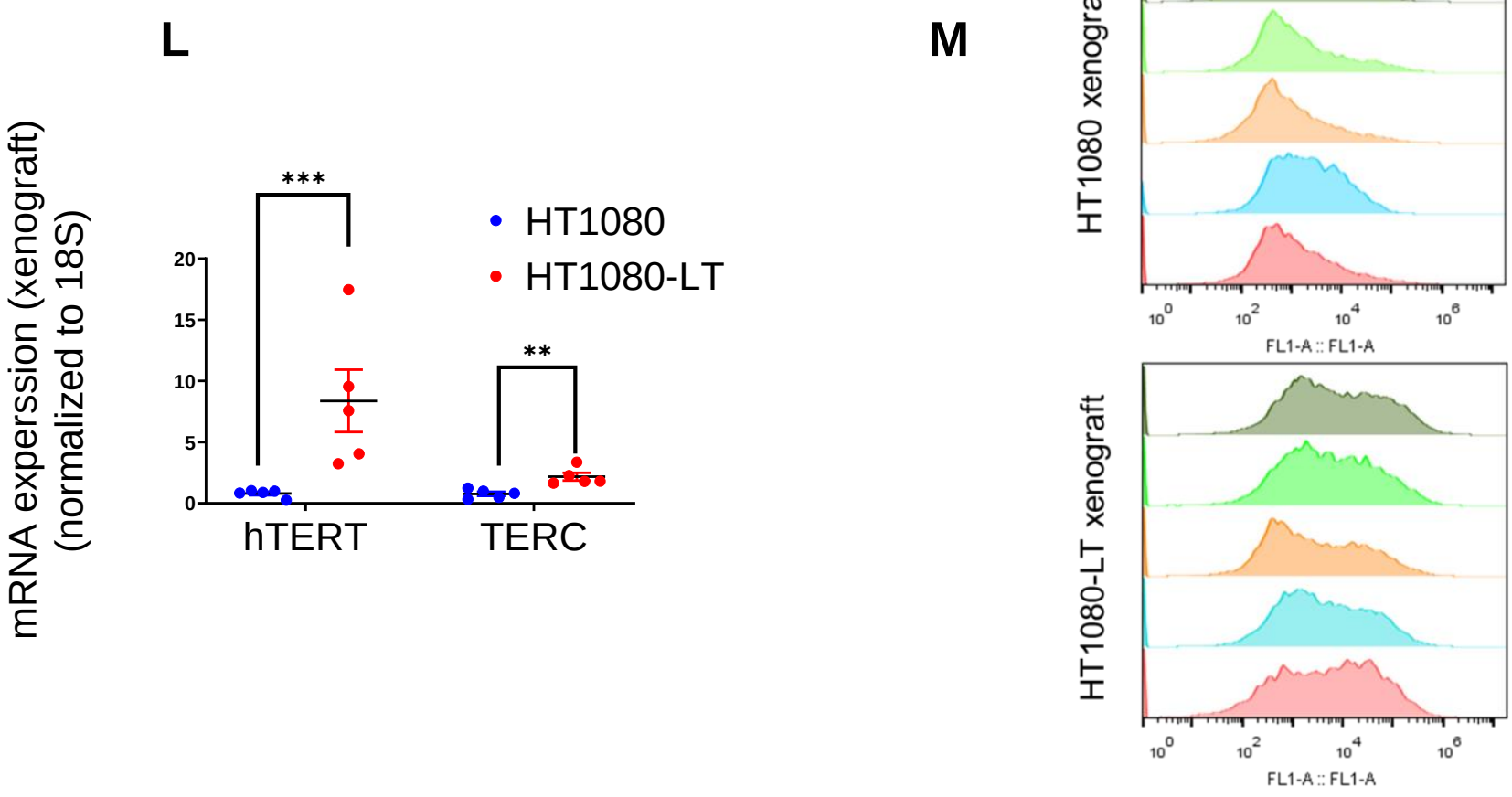

Supplementary Figure 1L-M:

mRNA expression of *hTERT* and *TERC* (normalized to 18S) in xenograft tumors in NOD-SCID mice injected with HT1080 or HT1080-LT cells (L). Statistical significance was calculated using Mann-Whitney's non-parametric test (p values : * ≤ 0.05, ** ≤ 0.01, *** ≤ 0.001, **** ≤ 0.0001). Telomere length of the xenograft tumors (following extraction of tumors) were checked by flow-cytometry and was higher in HT1080-LT xenograft tumors (M).

Supplementary Figure 1N

xenograft tumors

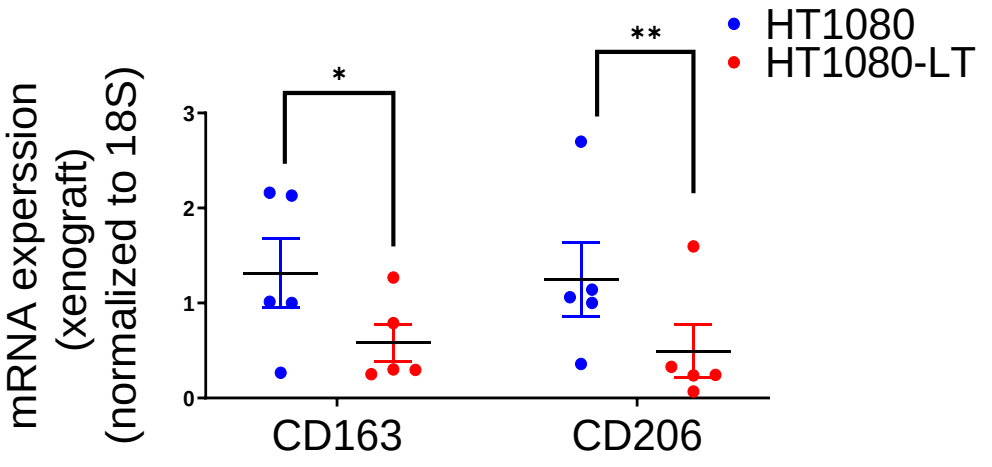

Supplementary Figure 1N:
Mouse M2 markers CD163 and CD206 were checked in the xenograft tumors using human 18S for normalization. Statistical significance was calculated using Mann-Whitney's non-parametric test (p values : * ≤ 0.05, ** ≤ 0.01, *** ≤ 0.001, **** ≤ 0.0001).

Supplementary Figure 1O

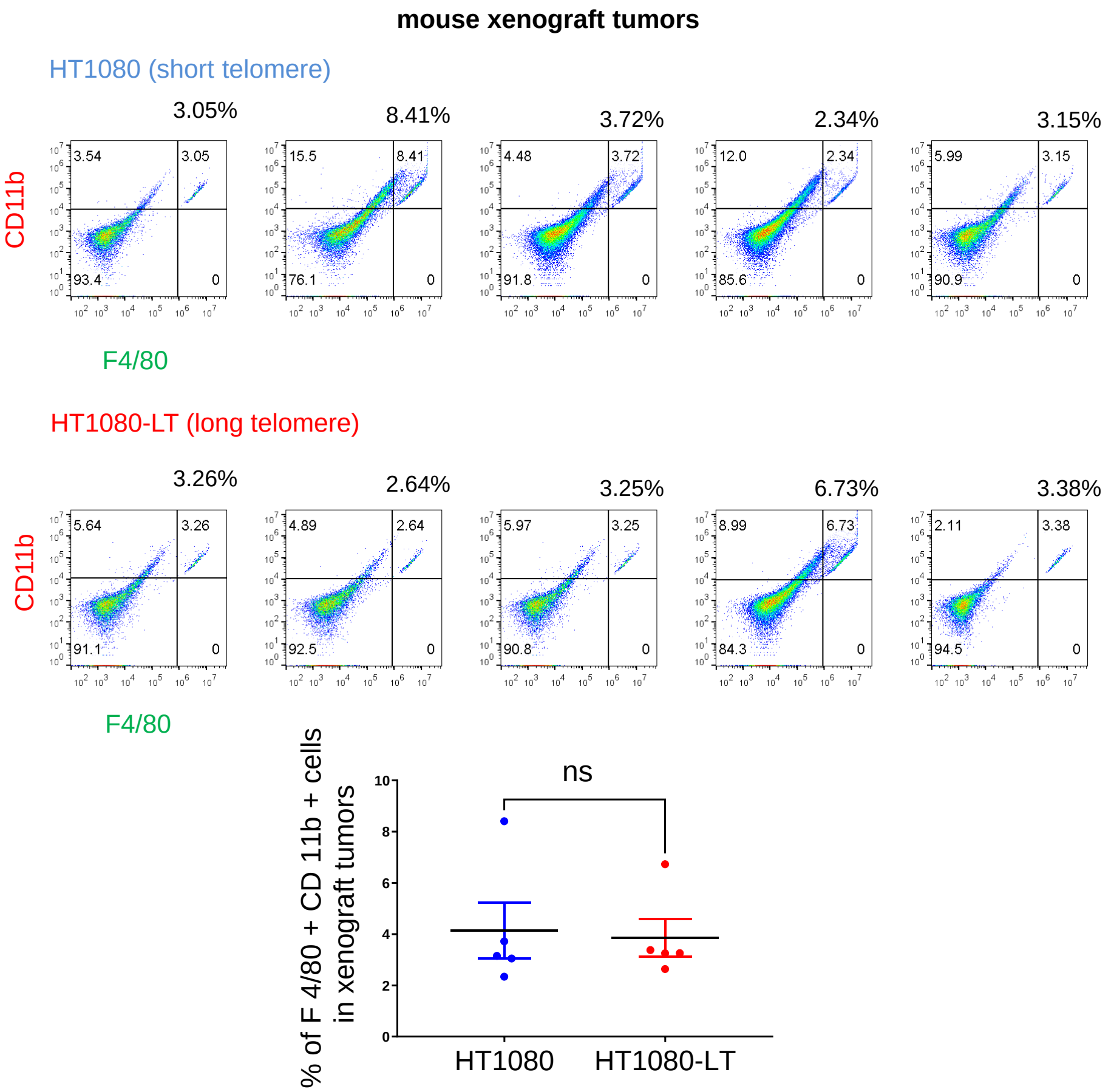

Supplementary Figure 1O:
Percentage of F4/80^{+} CD11b^{+} cells was estimated in xenograft tumors from HT1080 or HT1080-LT cells in top right quadrant of individual plots; percentage values for HT1080 and HT1080-LT tumors shown in summary graph (bottom panel).

Supplementary Figure 1P

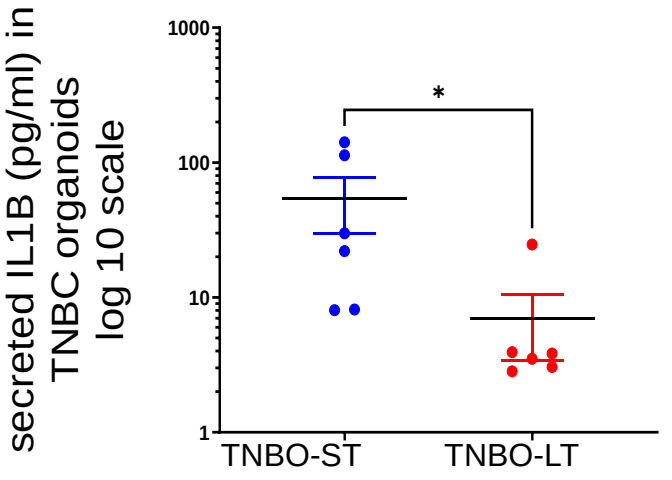

Supplementary Figure 1P:
Secreted IL1B (pg/ml) from organoids TNBO-ST or TNBO-LT by ELISA using media supernatant form organoid culture (see methods). Statistical significance was calculated using Mann-Whitney's non-parametric test (p values : * ≤ 0.05, ** ≤ 0.01, *** ≤ 0.001, **** ≤ 0.0001).

Supplementary Figure 1Q

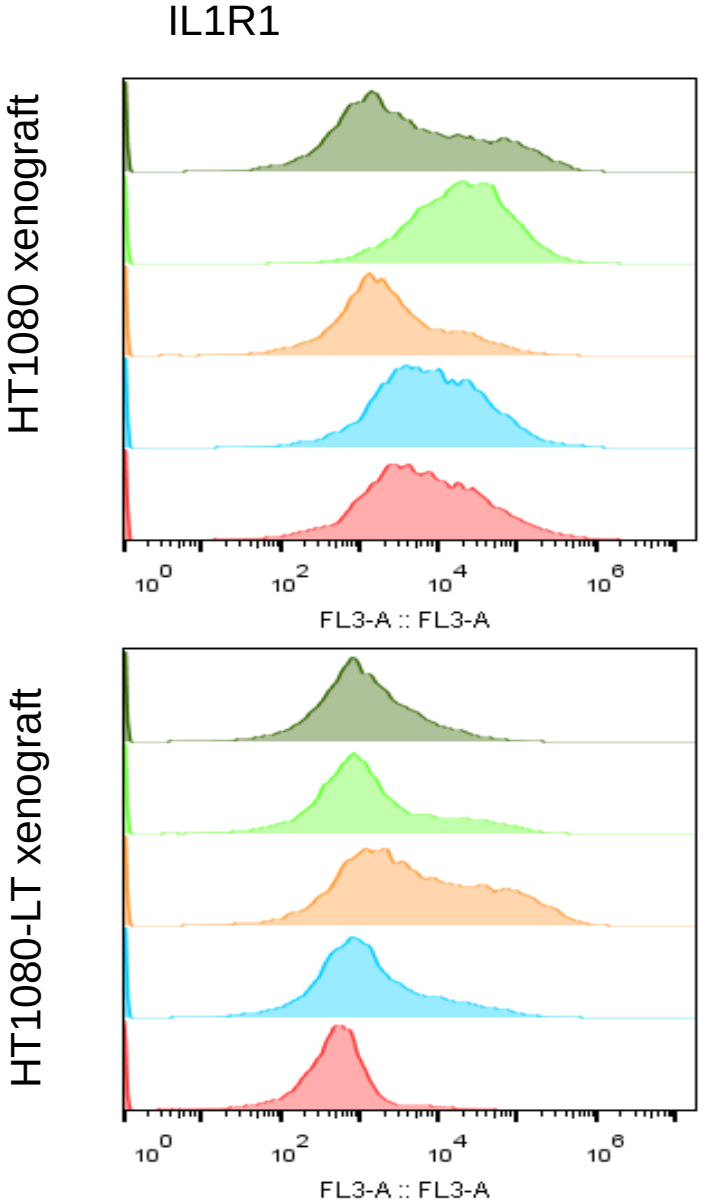

Supplementary Figure 1Q:
IL1R1 levels by immuno-flow cytometry in xenograft tumors from NOD-SCID mice injected with HT1080 or HT1080-LT cells plotted along X-axis in log scale.

Supplementary Figure 2

Supplementary Figure 2A

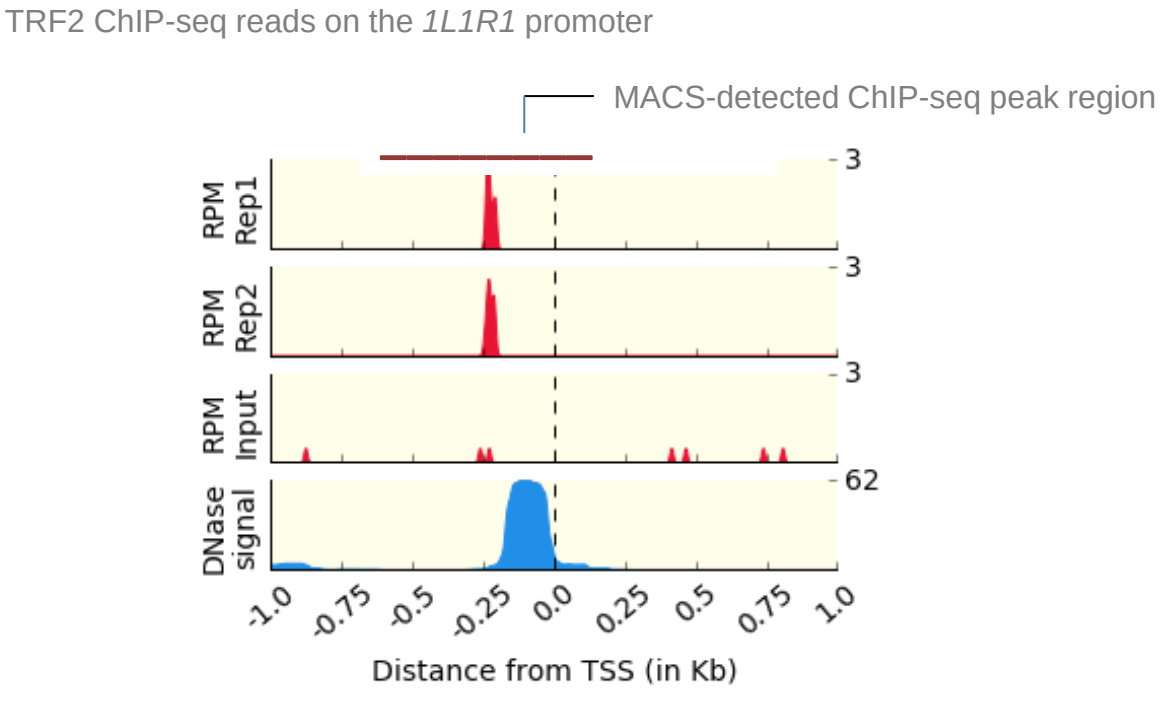

Supplementary Figure 2A:

Mapped reads (RPM: reads per million) on the *IL1R1* promoter from TRF2 ChIP-seq (Mukherjee et al, 2019) in HT1080 cells (replicate 1 and 2) and input DNA; plotted using publicly available software IGV (Integrated Genomics viewer) with sequence alignment files. The ChIP-seq peak (brown bar) detected using MACS 2.0 extended from +39 bp to -632 bp from the transcription start site (TSS).

Supplementary Figure 2B

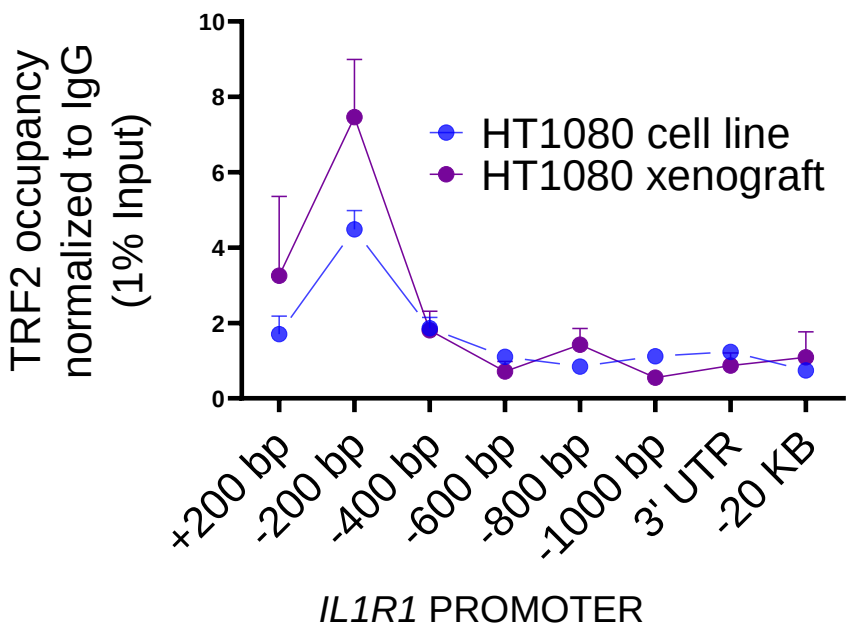

Supplementary Figure 2B:

Occupancy of TRF2 on *IL1R1* promoter in cells from xenograft tumors and ex-vivo HT1080 cells by chromatin-immunoprecipitation (ChIP) followed by qPCR. Primers spanning +200 bp from TSS (transcription start site) unto -1000 bp used for TRF2 enrichment on the *IL1R1* gene promoter. 3'UTR and -20 Kb upstream of TSS used as negative control for TRF2 binding; fold change of occupancy calculated over mock IgG after normalizing signal to 1% input .

Supplementary Figure 2C:

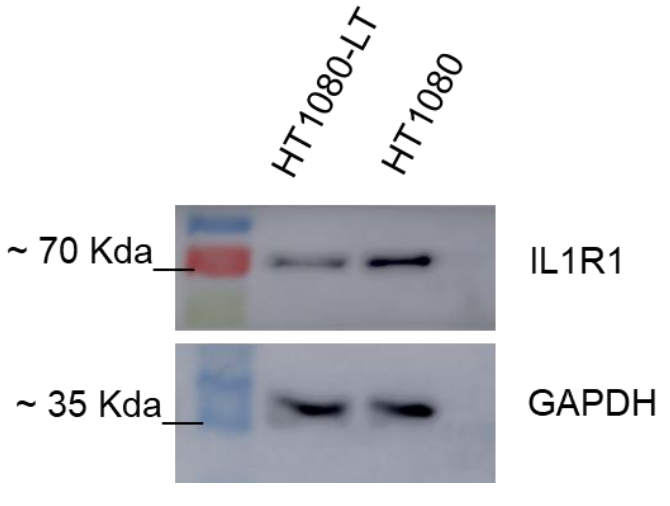

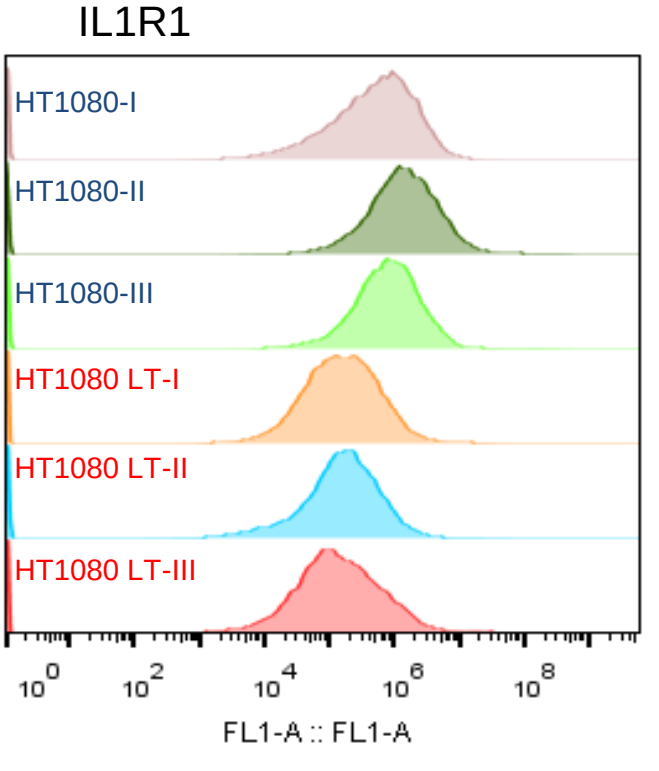

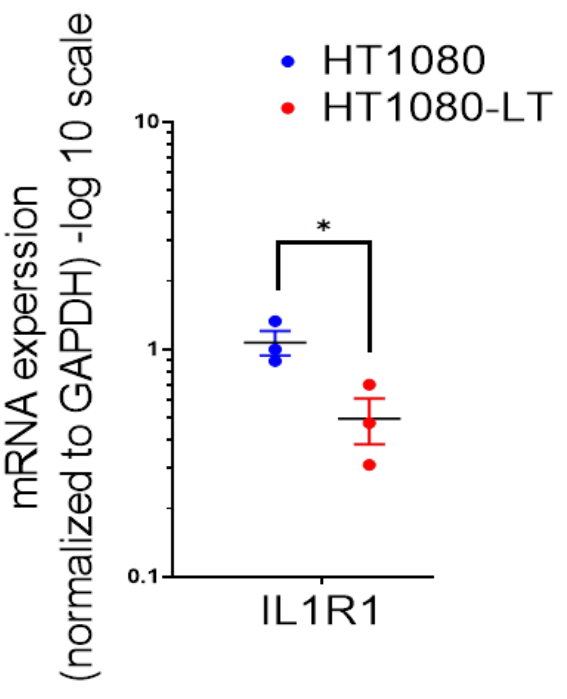

Supplementary Figure 2C:
IL1R1 protein levels in HT1080 and HT1080-LT cells by western blot (top eft panel); GAPDH was used as loading control. IL1R1 protein by immuno-flow cytometry in HT1080 or HT1080-LT cells in three independent replicates; IL1R1 plotted along the X-axis in log scale (top right panel).
IL1R1 mRNA expression in in HT1080 and HT1080-LT cells was checked by qRT-PCR. *GAPDH* was used for normalization (bottom panel)

Supplementary Figure 2D

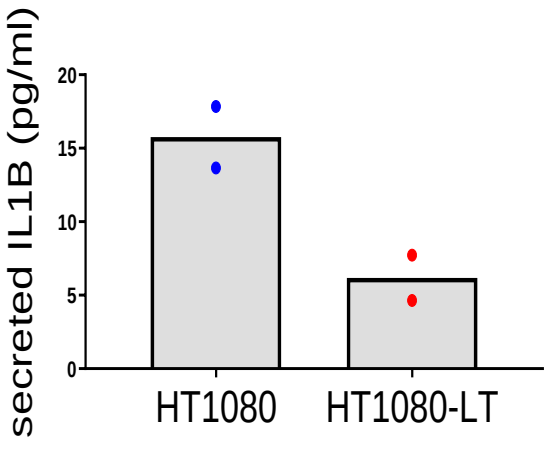

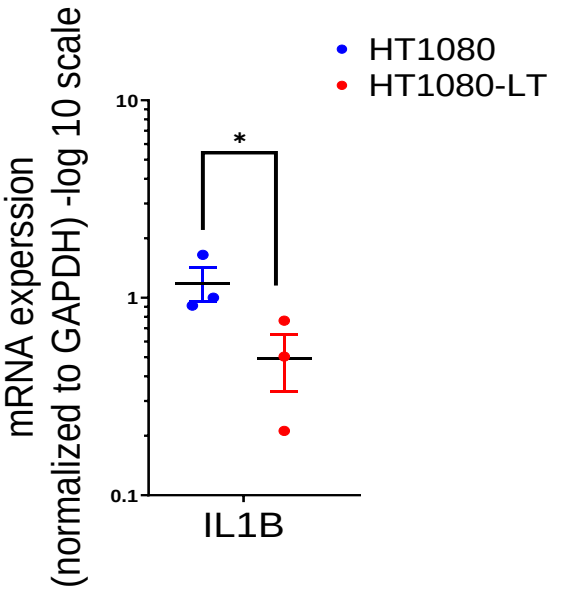

Supplementary Figure 2D:
Secreted IL1B (pg/ml) in supernatant media from HT1080 or HT1080-LT cells from two independent experiments. mRNA expression for *IL1B* in long or short telomere HT1080 or HT1080-LT cells respectively. *GAPDH* was used for normalization.
Statistical significance has been calculated using t-Test with Welch's correction (p values : * ≤ 0.05, ** ≤ 0.01, *** ≤ 0.001, **** ≤ 0.0001)

Supplementary Figure 2E

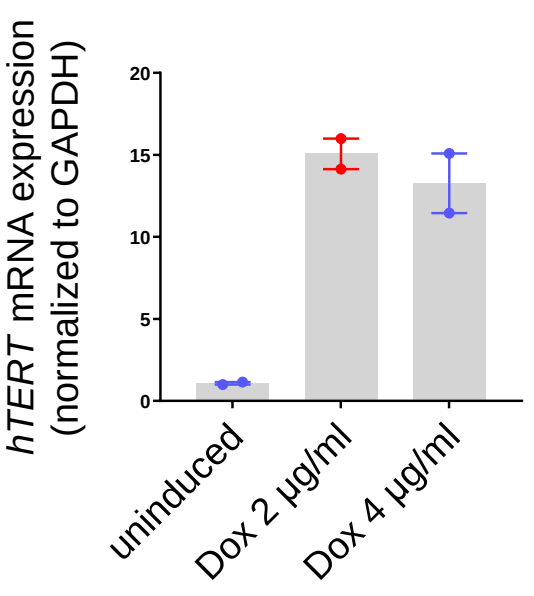

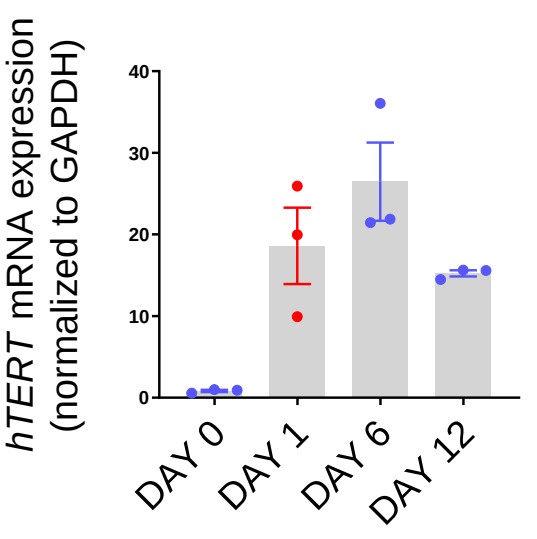

Supplementary Figure 2E:

hTERT mRNA expression in hTERT-inducible HT1080 cells on treatment with different concentrations of doxycycline (left panel) and at different days following induction (right panel). *GAPDH* was used for normalization.

Supplementary Figure 2F

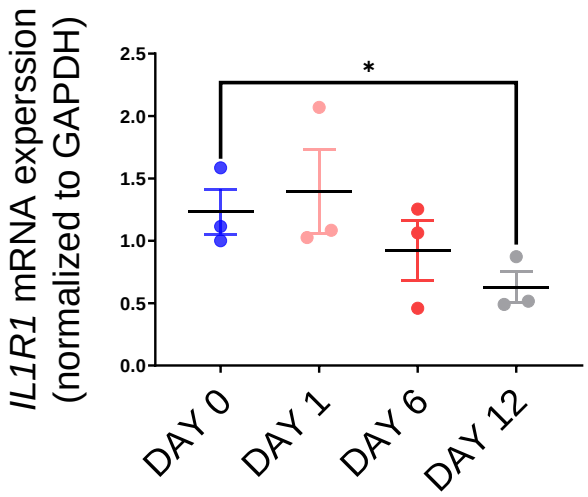

Supplementary Figure 2F:
IL1R1 mRNA expression (normalized to *GAPDH*) in HT1080 cells following 0, 1, 6 or 12 days of hTERT induction in ex-vivo culture. Statistical significance using t-Test with Welch's correction (p values : * ≤ 0.05, ** ≤ 0.01, *** ≤ 0.001, **** ≤ 0.0001).

Supplementary Figure 2G

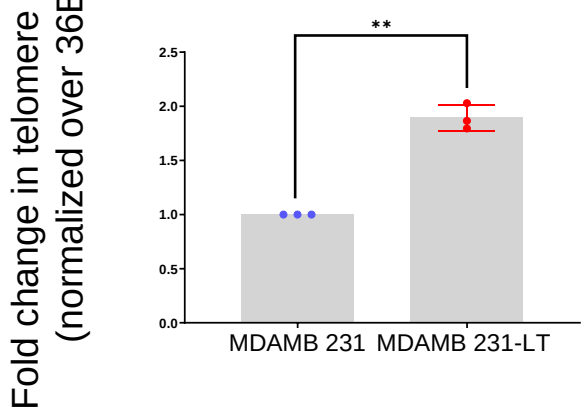

Supplementary Figure 2G:
Relative telomere length by qRT-PCR in MDAMB231 or MDAMD231-LT (long telomere) cells in two independent experiments. Statistical significance using t-Test with Welch's correction (p values : * ≤ 0.05, ** ≤ 0.01, *** ≤ 0.001, **** ≤ 0.0001).

Supplementary Figure 2H

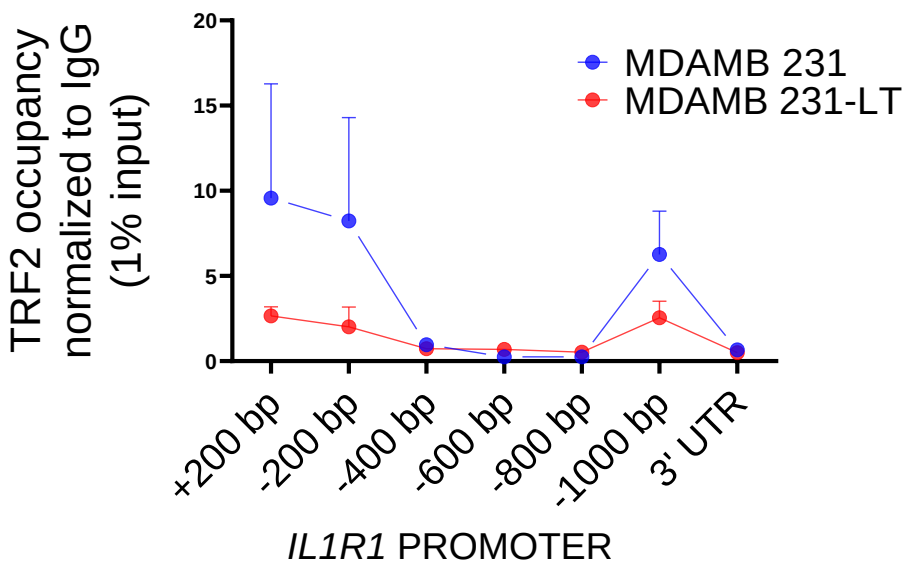

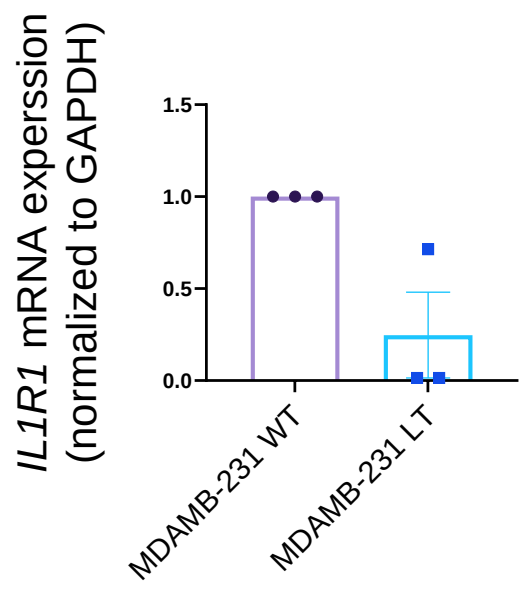

Supplementary Figure H:
TRF2 occupancy by ChIP-qPCR on the *IL1R1* promoter in MDAMB23 or MDAMD231-LT cells using primers and normalization described earlier (left panel). Expression for *IL1R1* in MDAMB231 cells or MDAMD231-LT cells; *GAPDH* was used for normalization (right panel).

Supplementary Figure 2I

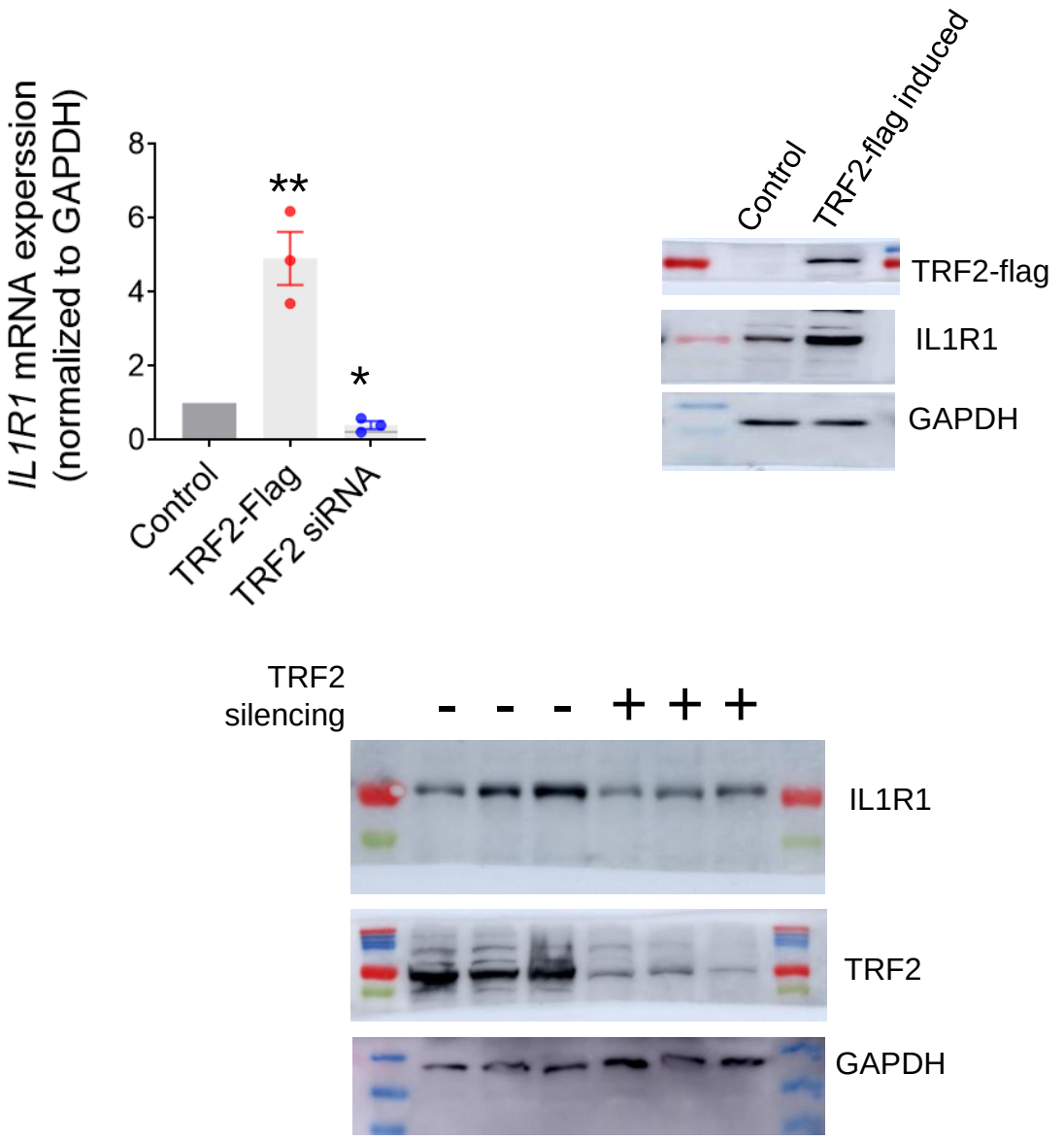

Supplementary Figure 2I:
IL1R1 expression by qRTPCR following expression of TRF2-flag or TRF2 silencing (top left), IL1R1 protein levels on TRF2-flag induction (top right) or TRF2 silencing (bottom panel) in HT1080 cells following 48 hrs of transfection.

Supplementary Figure 2J:

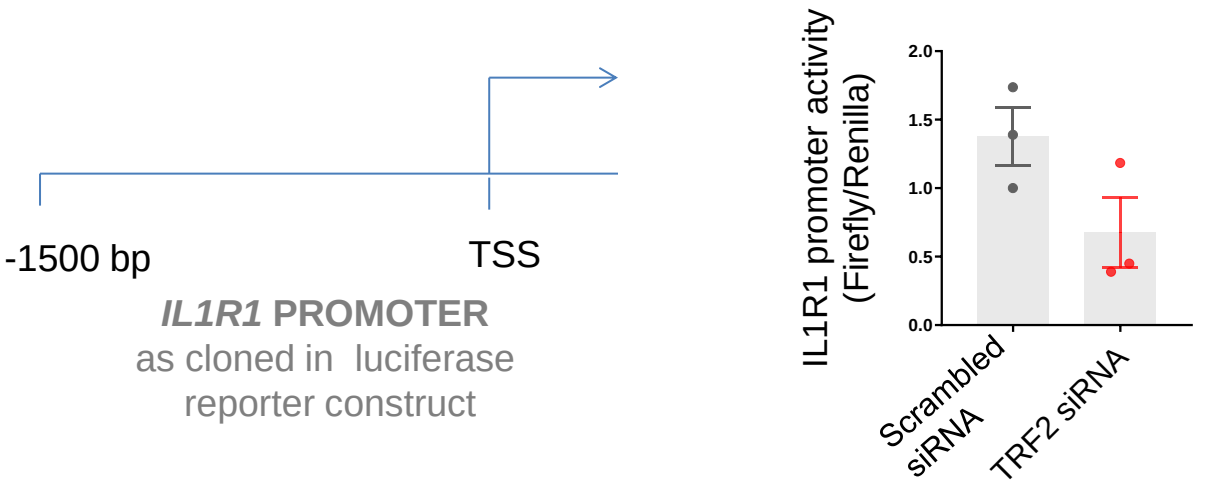

Supplementary Figure 2J:
IL1R1 promoter activity following transfection of control (scrambled) or TRF2-siRNA for 48 hrs in HT1080 cells.

Supplementary Figure 2K

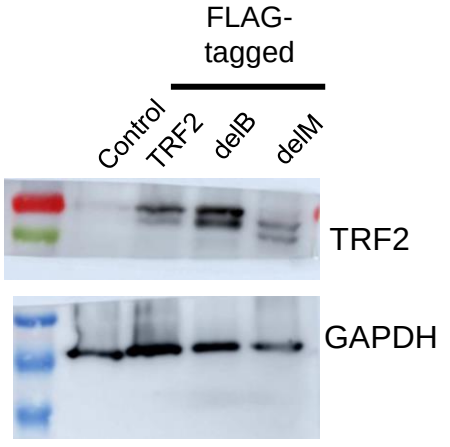

Supplementary Figure 2K:
Expression of flag-tagged TRF2-full length or DNA-binding mutants, delB or delM in HT1080 cells following 48 hrs of transfection.

Supplementary Figure 2L

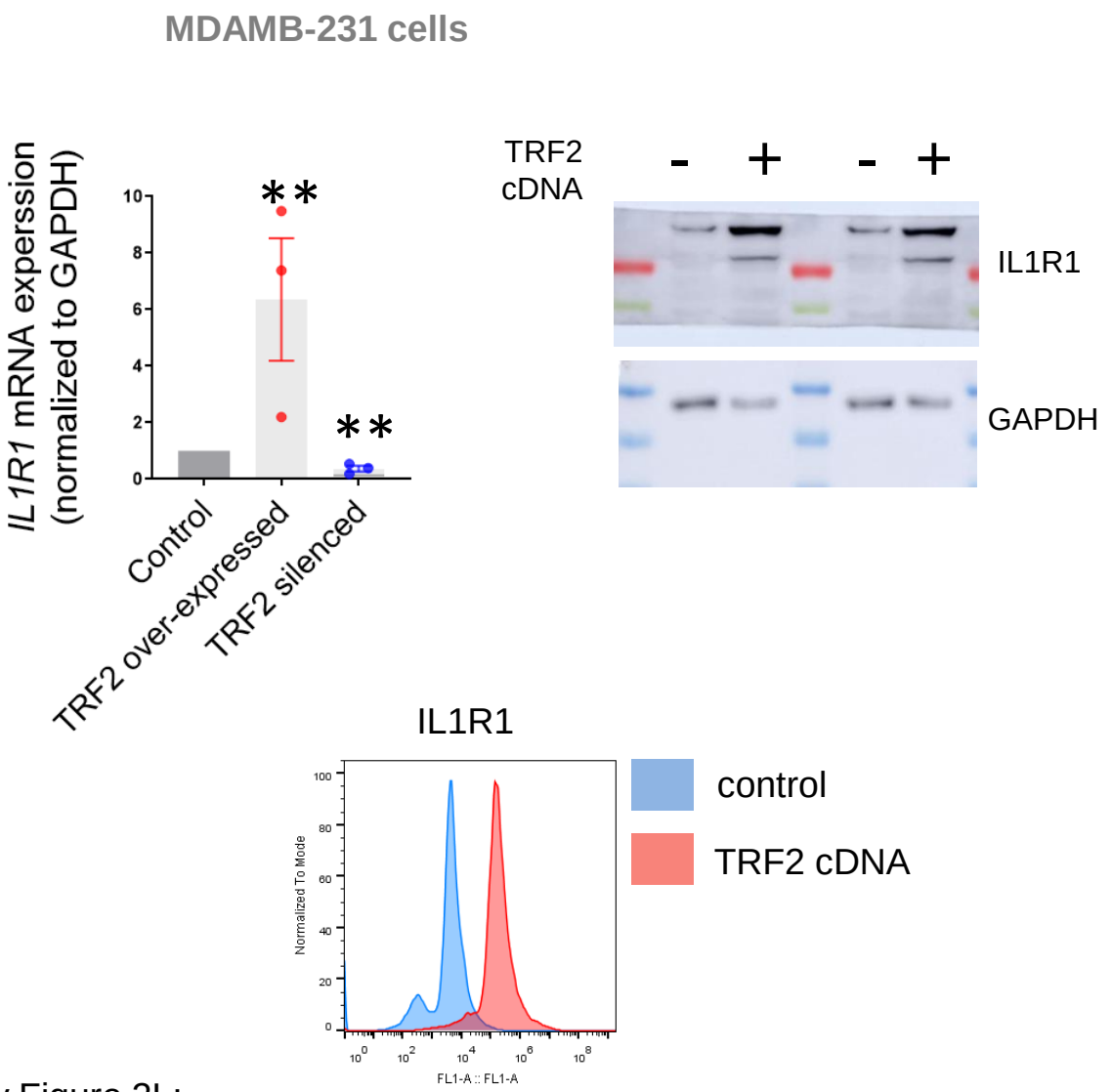

Supplementary Figure 2L:
IL1R1 mRNA expression in MDAMB231 cells following expression of TRF2 cDNA or TRF2 silencing for 48 hrs; *GAPDH* used as normalizing control (top left). IL1R1 protein levels in MDAMB231 cells following TRF2 induction for 48 hrs by western blot (top right) and immuno-flow cytometry (bottom panel).

Supplementary Figure 2M

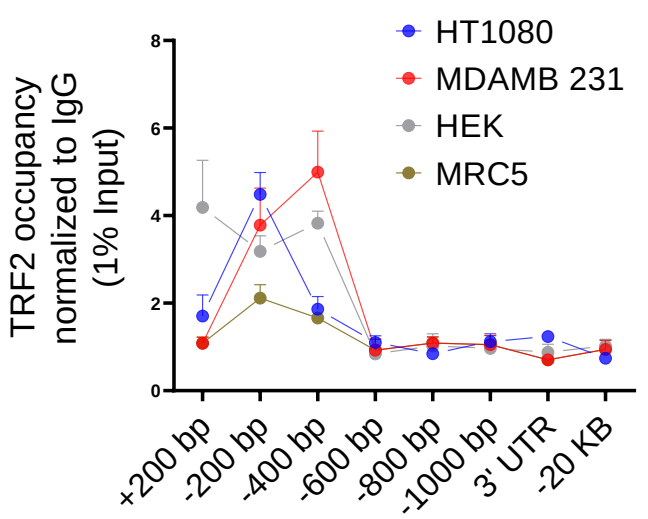

Supplementary Figure 2N

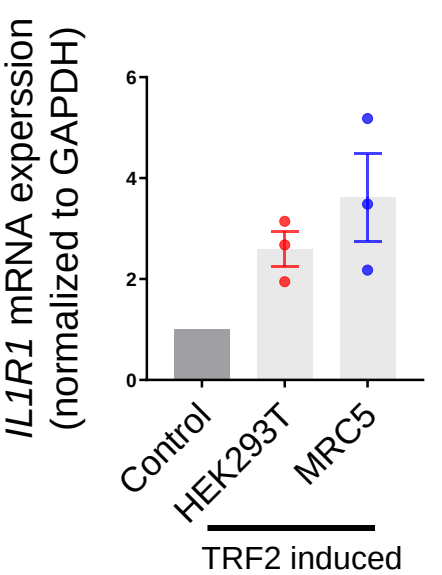

Supplementary Figure 2M-N:
TRF2 occupancy on the *IL1R1* promoter in HT1080, MDAMB231, HEK293T or MRC5 cells by chromatin-immunoprecipitation (ChIP) followed by qPCR. Primers spanning +200 to -1000 bp of TSS used for TRF2 enrichment on the gene promoter; 3'UTR and -20 Kb upstream of TSS used as negative control for TRF2 binding; fold-change of occupancy was calculated over mock IgG after normalizing signal to 1% input (M).
IL1R1 mRNA expression in HEK293T and MRC5 cells following transfection of TRF2-cDNA for 48 hrs; *GAPDH* was used as normalizing control (N).

Supplementary Figure 2O

TRF2 ChIP-seq peak sequence (+39 to -632 bp of TSS) shown below.
G4 motif A in red font (on + strand)
G4 motif B in green font (on - strand)

5'-
CCTCCTTAAGTGAAAAATCTGTGAGGAGTTTTCTATCTTTCT
AAGTCTTTGTGGCACACTTATCACATGCATAGTACTATTTCT
CAAGTTACCCAGGCACACACAGATGTATGGCTTTCAGGAA
GCCATACATCTGTGTAGCTCTGAGGCCCAGCCTTGTTCAA
CACTTCACTCAGAAGAATTGCTGGCCTGATGACCAACAATA
ATTGTCAACAACTTAAAACTTCATTGACGGCTCCTAAAAAA
AATCAGTGTGCATGTGTGTGTGTATGTGTGTGTGCGTGTGT
GTGTGTGTGTGTGTATGAGTGTGTGTATAACATTCATTACT
GCAAACT**GG**AAT**GG**AGT**GGGG**CT**GG**AAGGCAGCCCAGAA
GCAAGGCTCAGAGCCTGGAGCTGCTGACCTCTTGGGGAC
ACTGCAGCCCTGGCCTGGCCTACTTTTCTCTTCTCCCATAT
CTGGAAAATGAAAGTAGCCTGACGTAT**CC**GGGGA**CCC**GG
CCCAAGACT**CC**ACCCATTGGCAGCTCTTCACTTGTATCTTT
TCATATCAAAA – 3'

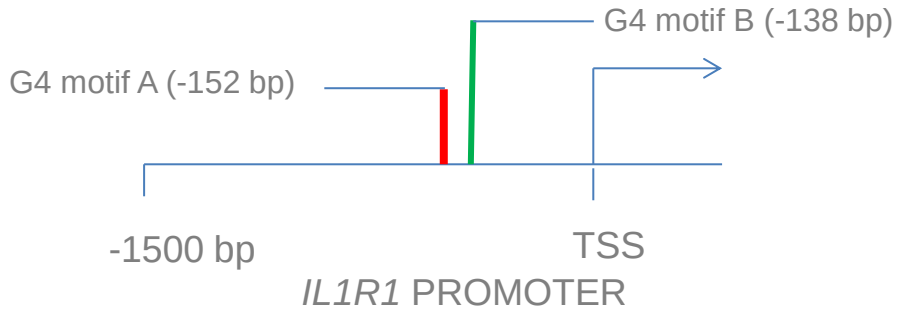

G4 sequence:
GG-(X)n-**GG**-(X)n-**GG**(X)n-**GG**

The repetitive G-tracts or stems marked by underlining, intervening variable sequences are called loops.

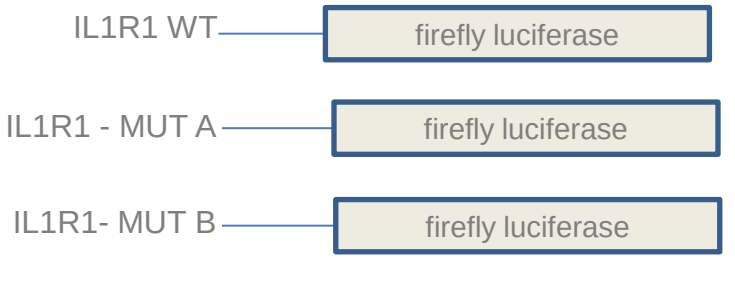

G4 A: GGAATGGAGTGGGGCTGG
G4 A mutant: GGAATGTAGTGTGGCTGG

G4 B: GGAGTCTTGGGCCGGGTCCCCGG
G4 B mutant: GGAGTCTTGTGCCGTGTCCCCGG

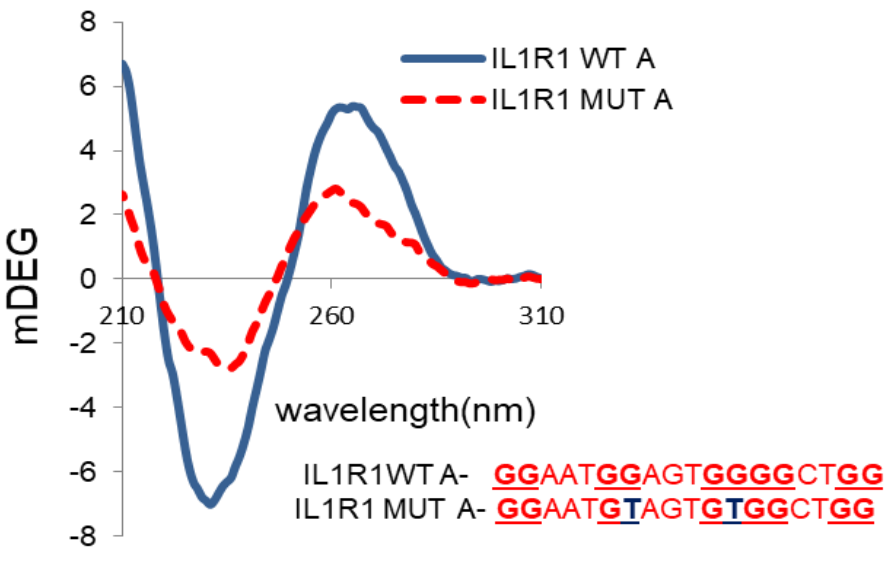

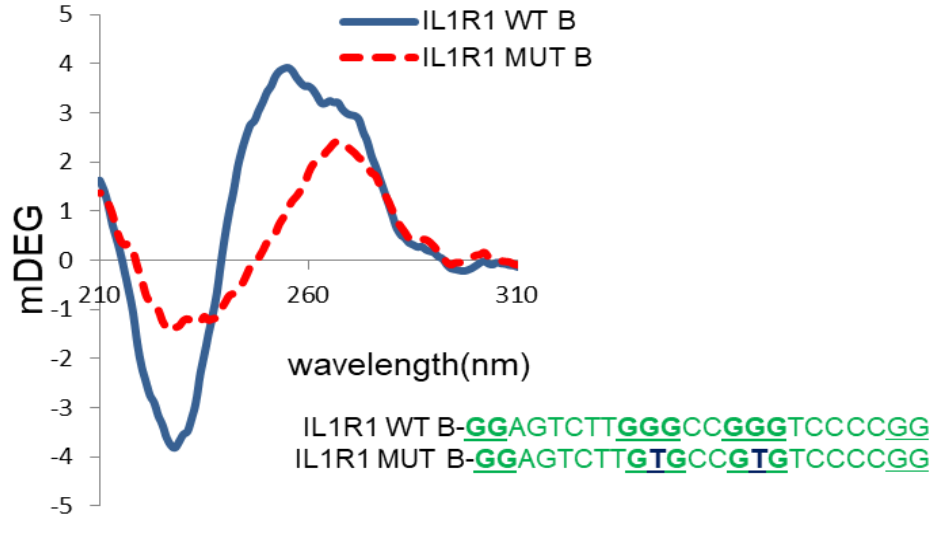

Supplementary Figure 2O:
TRF2 ChIP-seq peak with sequence of the G4 motifs (A and B) and their respective positions on the *IL1R1* promoter; sequence scheme depicting generic G4 motifs; specific G4-disrupting substitutions shown for respective motifs; and the scheme for firefly luciferase reporter constructs (top panels).
Circular dichroism profile (220-310 nm wavelength) of oligonucleotides (5 µM) with sequence of the G4 motifs A or B (or respective mutants with base substitutions) in solution (bottom panels).

Supplementary Figure 2P

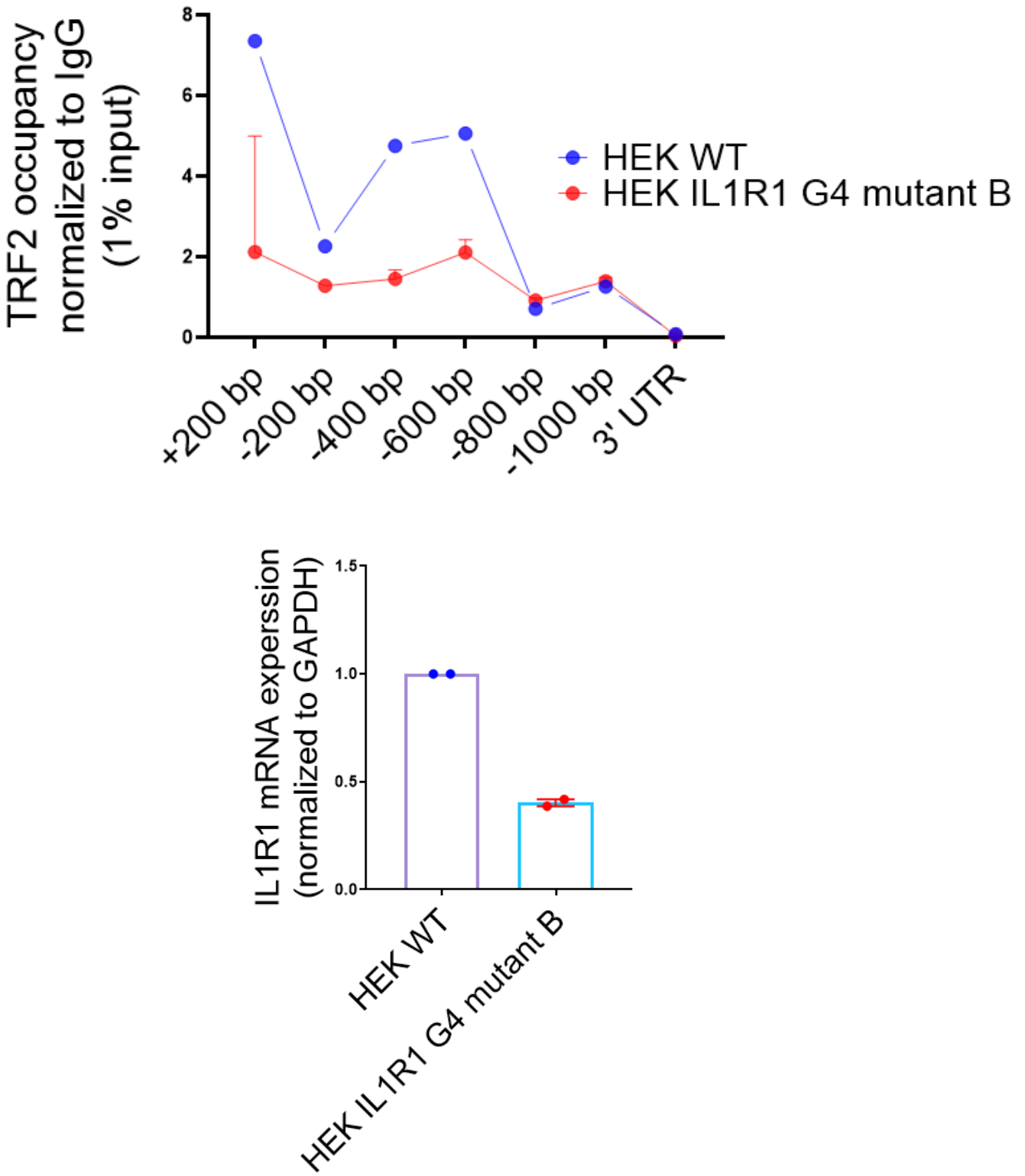

Supplementary Figure 2P:
Base substitutions for the G4 motif B in the IL1R1 promoter (as shown in Supplementary Figure 2O) were introduced using CRSIPR in HEK293T cells. TRF2 ChIP-qPCR spanning the IL1R1 promoter (top panel) and *IL1R1* mRNA expression (bottom panel) in HEK293T cells with or without the G4-disrupting substitution in two replicates.

Supplementary Figure 3

Supplementary Figure 3A

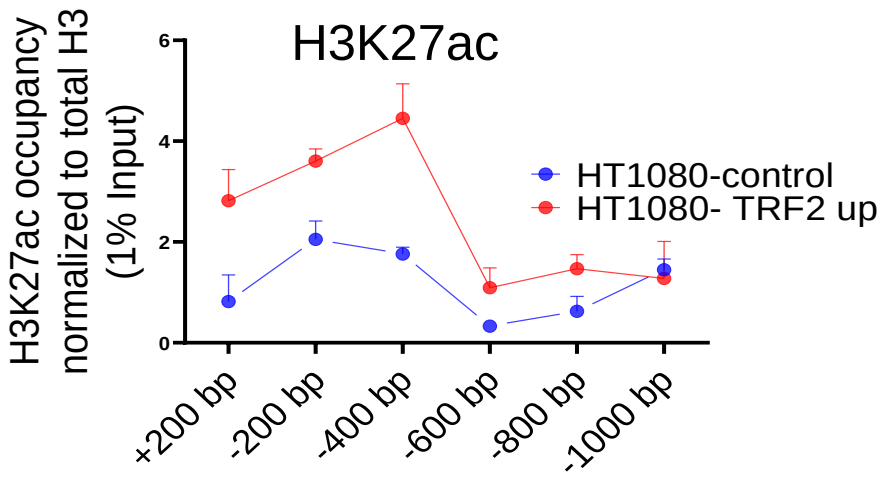

IL1R1 PROMOTER

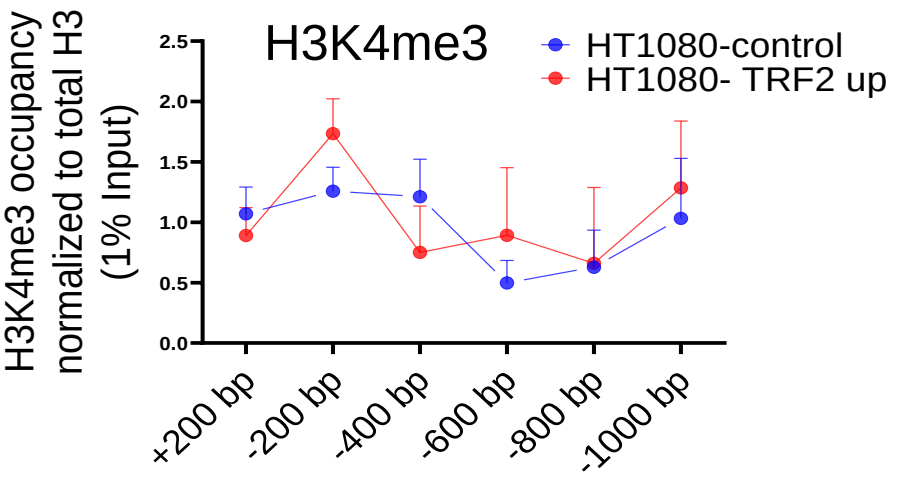

IL1R1 PROMOTER

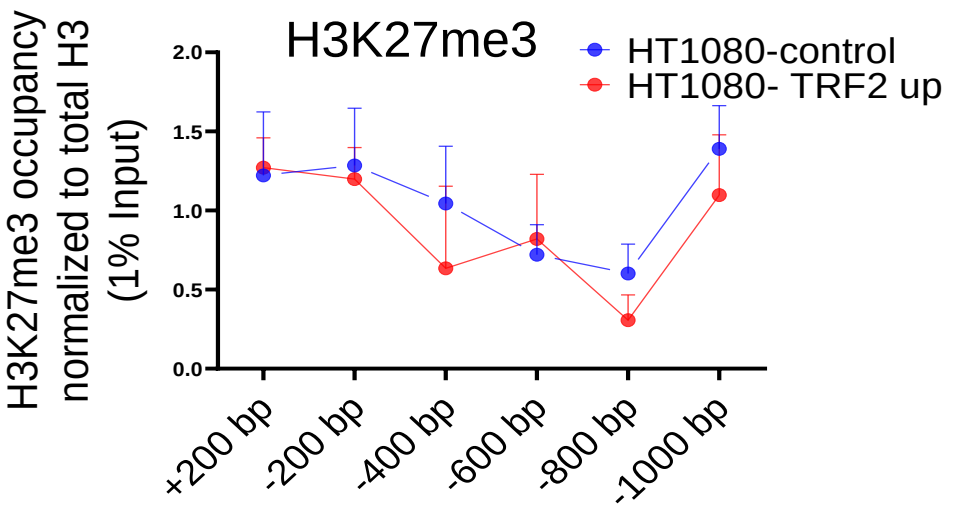

IL1R1 PROMOTER

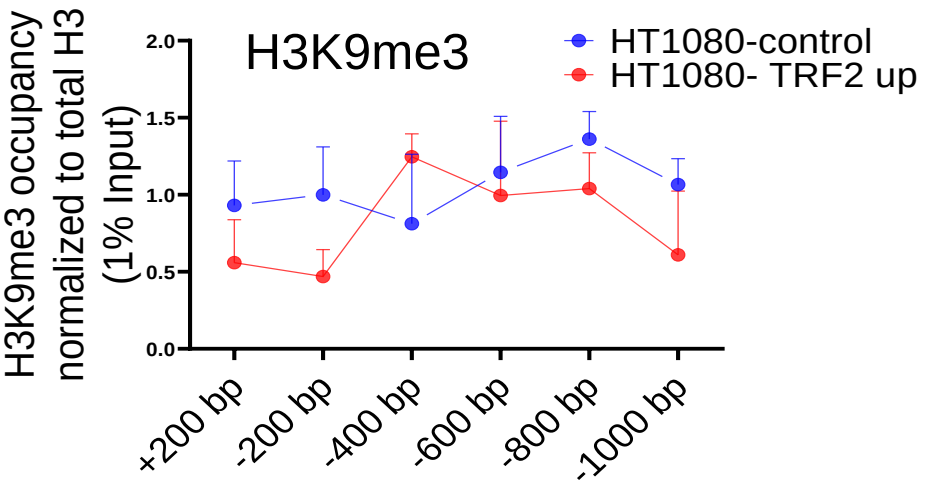

IL1R1 PROMOTER

Supplementary Figure 3B

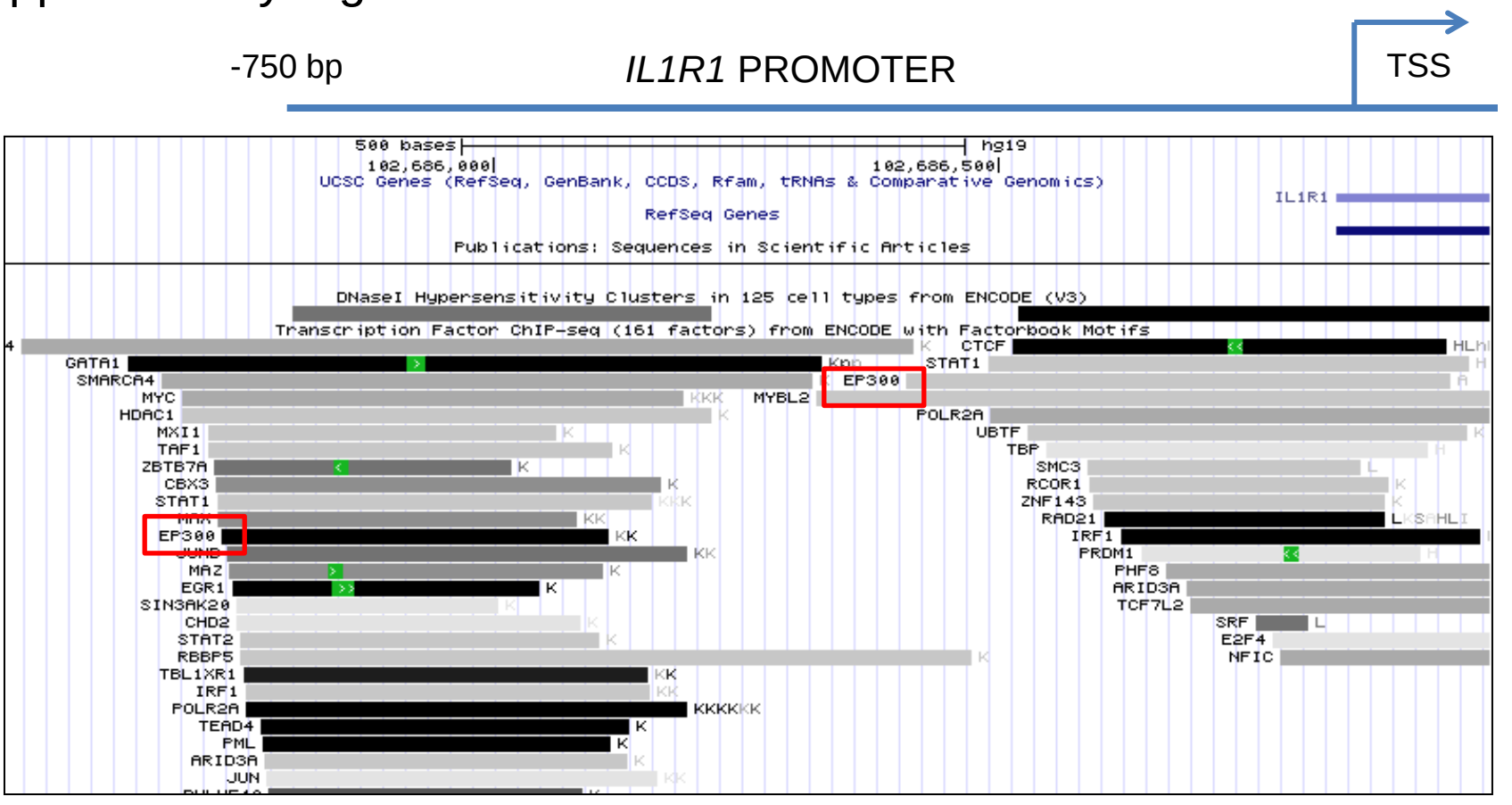

P300 marked in red box

Supplementary Figure 3C

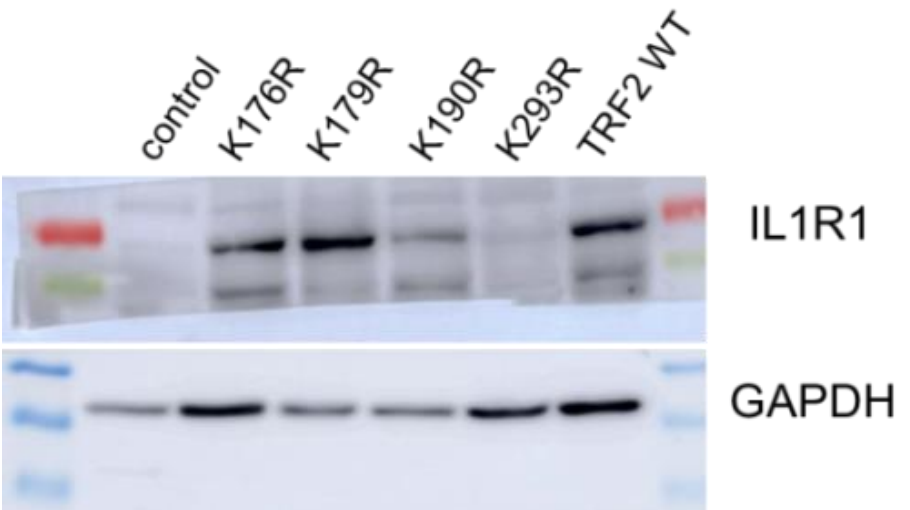

Supplementary Figure 3

A. Enrichment of histone marks H3K27ac, H3K4me3, H3K27me3, H3K9me3 (normalized to total H3) by ChIP-qPCR on the *IL1R1* promoter in HT1080 cells in TRF2-up (induced) condition or un-induced corresponding control cells.

B. Transcription factors/histone remodelers on the *IL1R1* proximal promoter (-750 bp) across seven cell lines curated from ENCODE was plotted using UCSC genome browser hg19 human genome assembly. P300 enrichment marked in red box.

C.IL1R1 protein level following induction of TRF2 mutants; GAPDH used as loading control.

Supplementary Figure 4

Supplementary Figure 4A

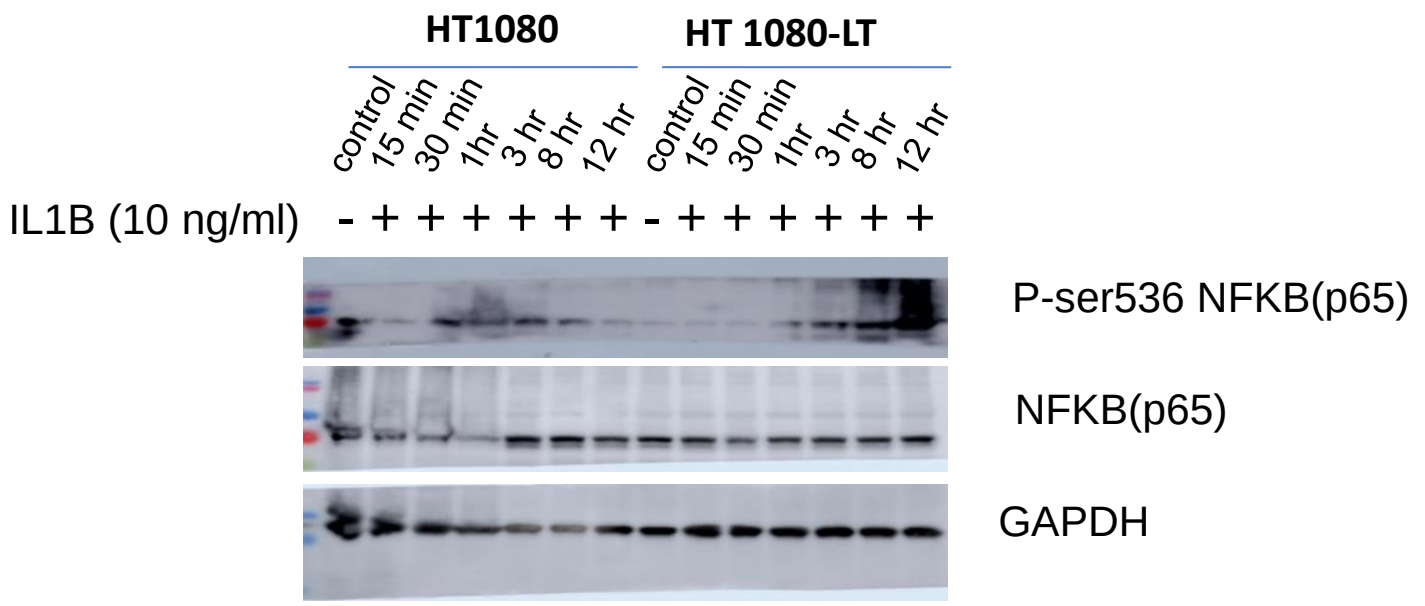

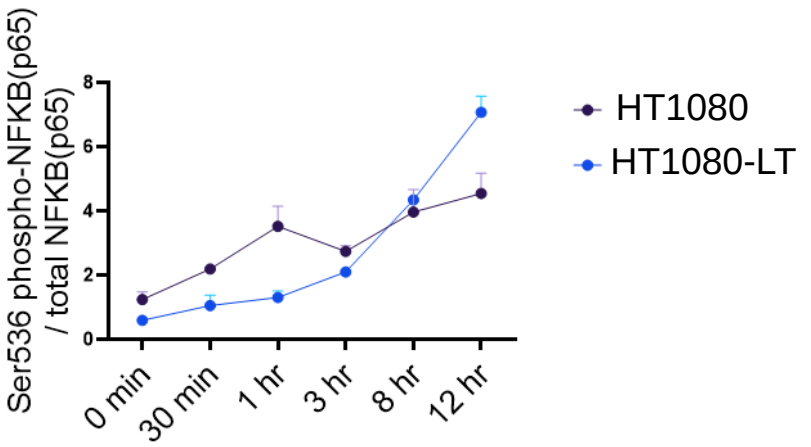

Supplementary Figure 4A:
Phospho-NF-Kappa-B-(Ser-536p) and NFkappaB in HT1080 or HT1080-LT cells with or without IL1B stimulation (top panel); ratio of p-NFKB to total NFKB from above western blots plotted from two independent experiments (bottom panel).

Supplementary Figure 4B

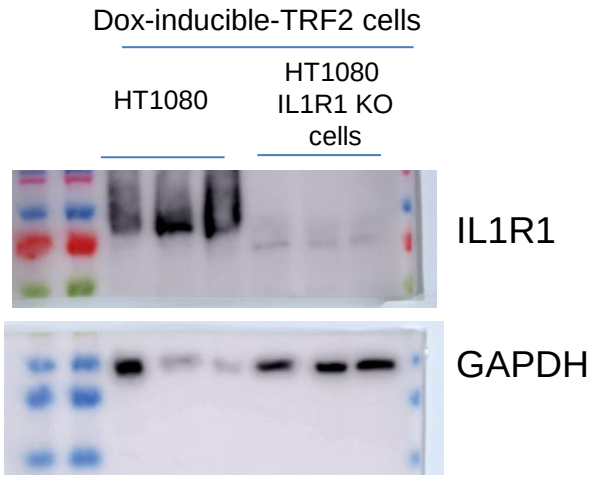

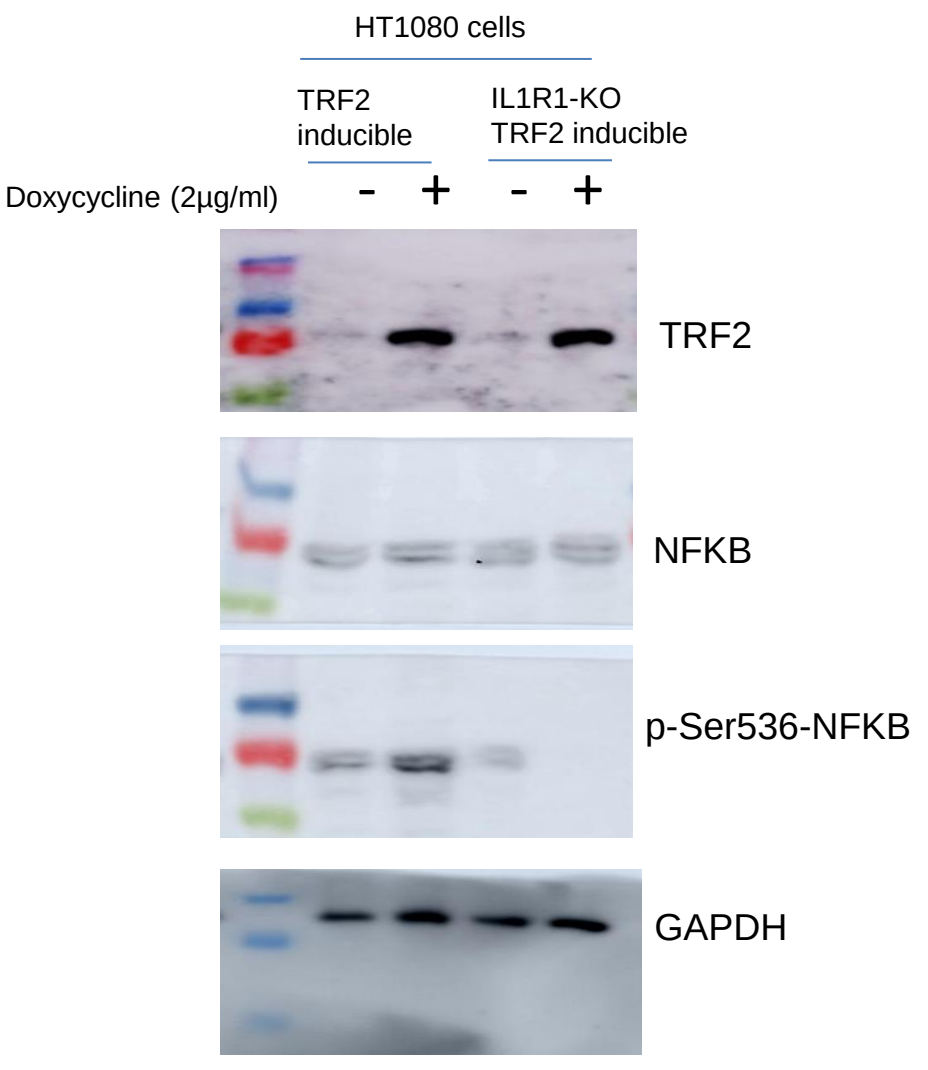

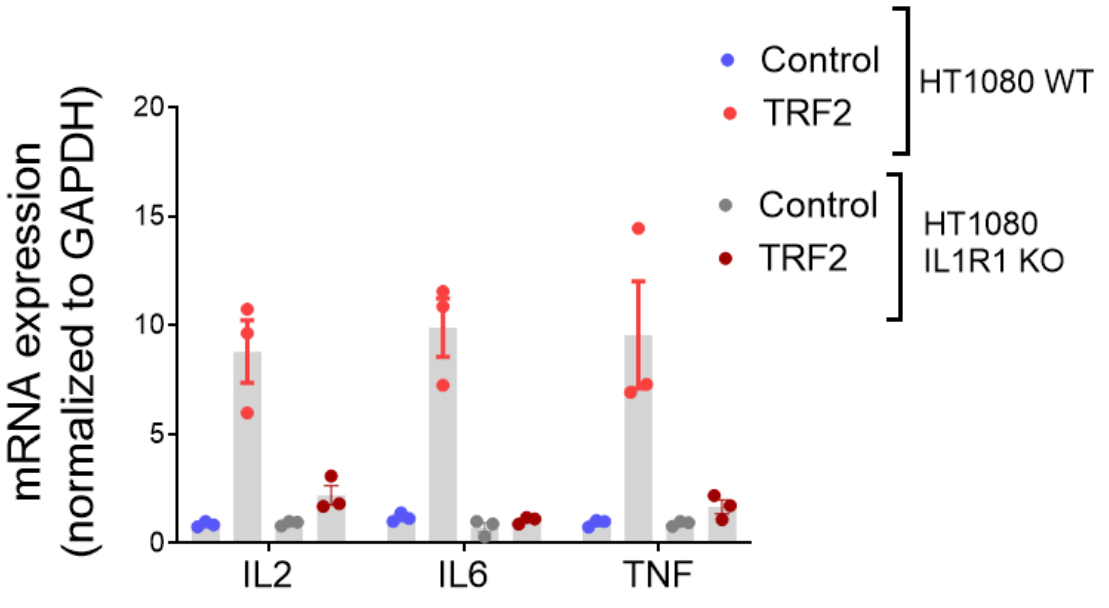

Supplementary Figure 4B:
IL1R1 knockout (KO) HT1080 cells using CRISPR were made and were transduced (lentiviral) to a doxycycline-inducible-TRF2 stable line (top left). TRF2, NFKappa-B and Ser536p-NFKappa-B in IL1R1 knockout or control HT1080 cells with or without TRF2 induction by doxycycline; GAPDH used as loading control (top right)

Induction of TRF2 in HT1080 WT and IL1R1 KO cells to check for NFkappaB downstream target gene expression(bottom). Activation of NFKB target genes (~ 2-5 fold) post-TRF2 over-expression was lower in IL1R1KO cells compared to WT cells (~ 10 fold)

Supplementary Figure 4C

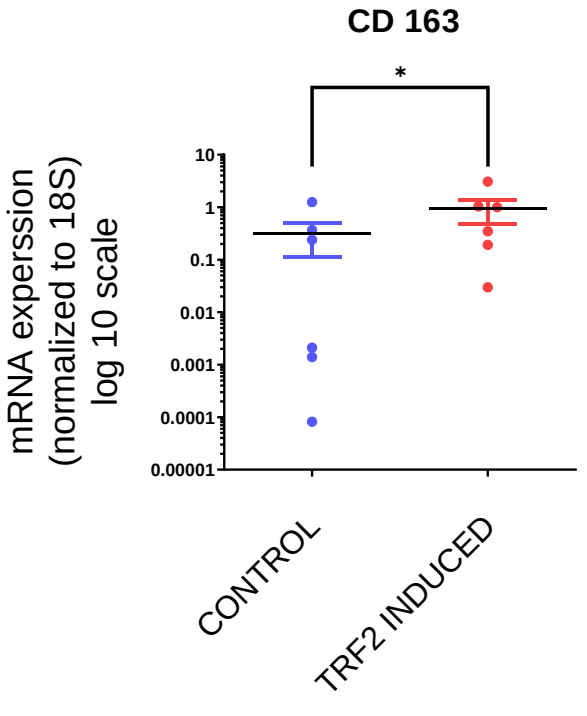

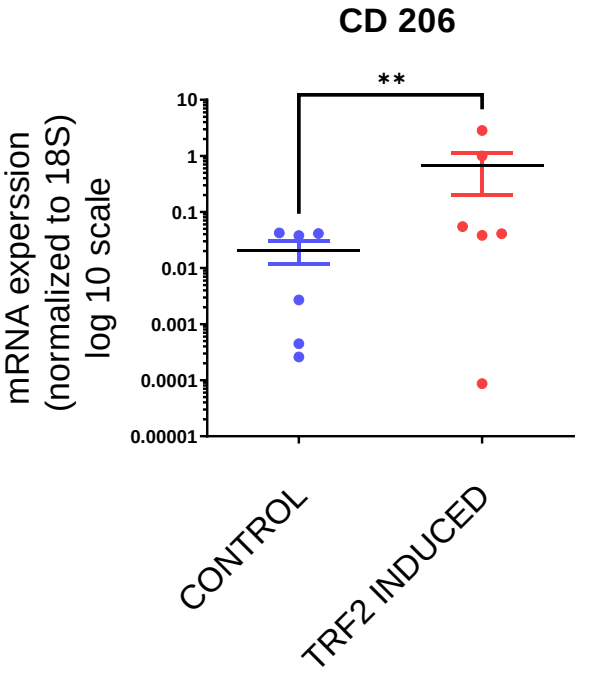

Supplementary Figure C:
mRNA expression of mouse M2 macrophage markers *CD163* or *CD206* in xenograft tumors made from HT1080-controlor HT1080-TRF2-induced cells; human *18S* was used for normalization.

Supplementary Figure 4D

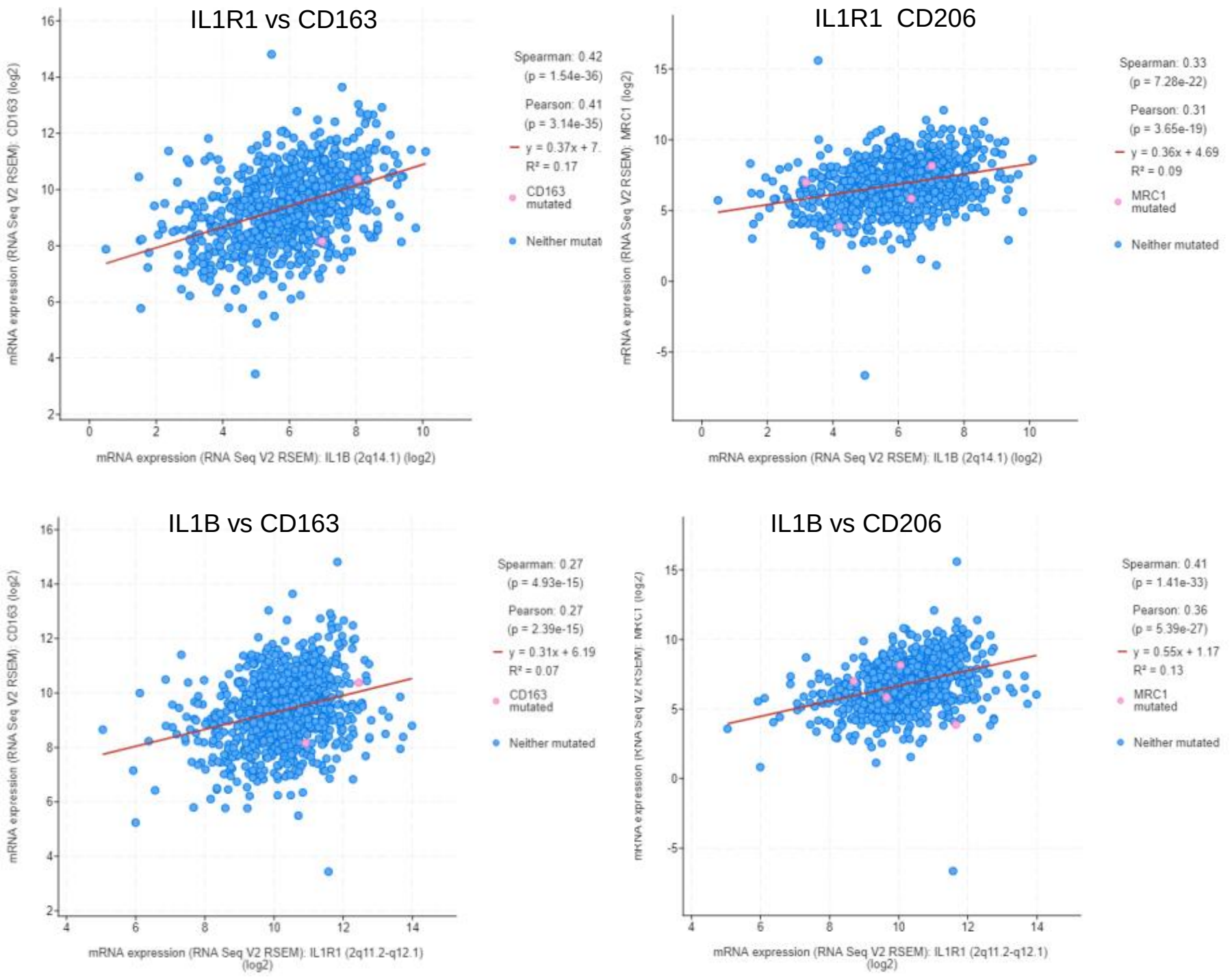

Supplementary Figure 4D:

Correlation of *IL1R1/L1B* with *CD163/CD206* from publicly available breast cancer microarray dataset of 817 TNBC patients (available from cBIOPORTAL; see methods for analysis details).

Supplementary Figure 4E

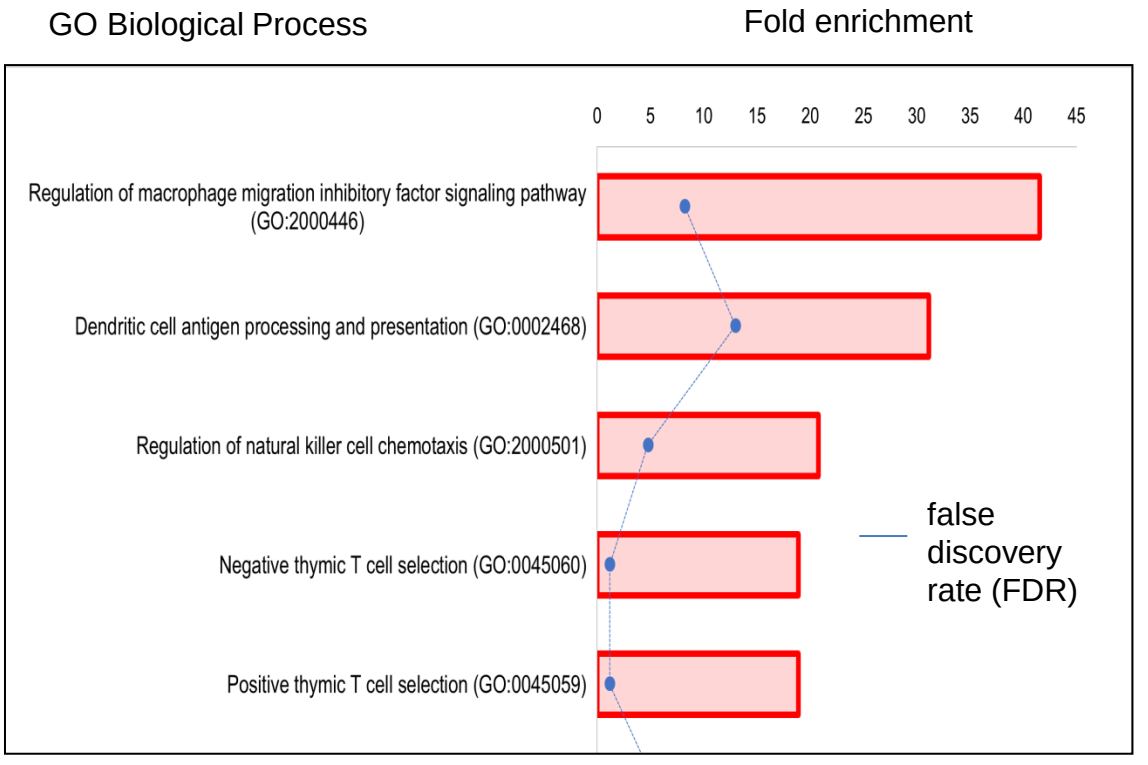

Supplementary Figure 4E:
Gene Ontology (GO) analysis of top 500 genes correlated with telomere elongation across 31 cancer types(as reported in Barthel e*t al.,* 2017) Top 5 hits for 'biological processes' represented in descending order of enrichment; respective fold enrichments shown by individual bars (x-axis – top); the false discovery rate (FDR) shown by blue line.

Supplementary Figure 5

Supplementary Figure 5A

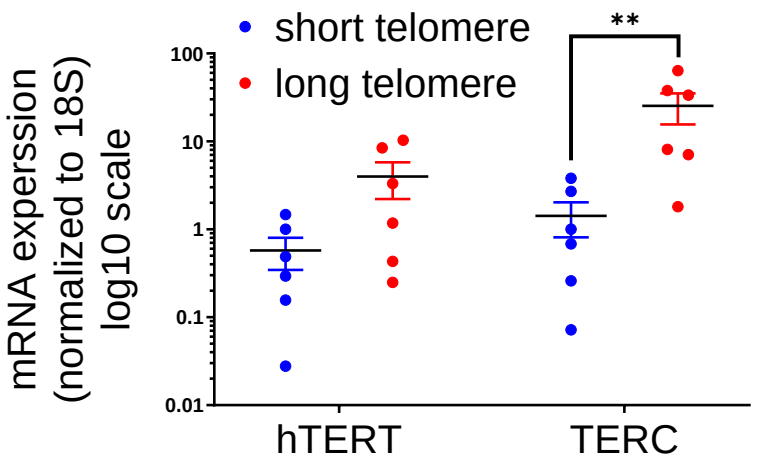

Supplementary Figure 5A:

mRNA expression of *hTERT* and *TERC* in six TNBC samples (long or short telomeres) normalized to the *18S* gene in respective samples. Statistical significance was calculated using Mann-Whitney's non-parametric test (p values : * ≤ 0.05, ** ≤ 0.01, *** ≤ 0.001, **** ≤ 0.0001).

Supplementary Figure 5B

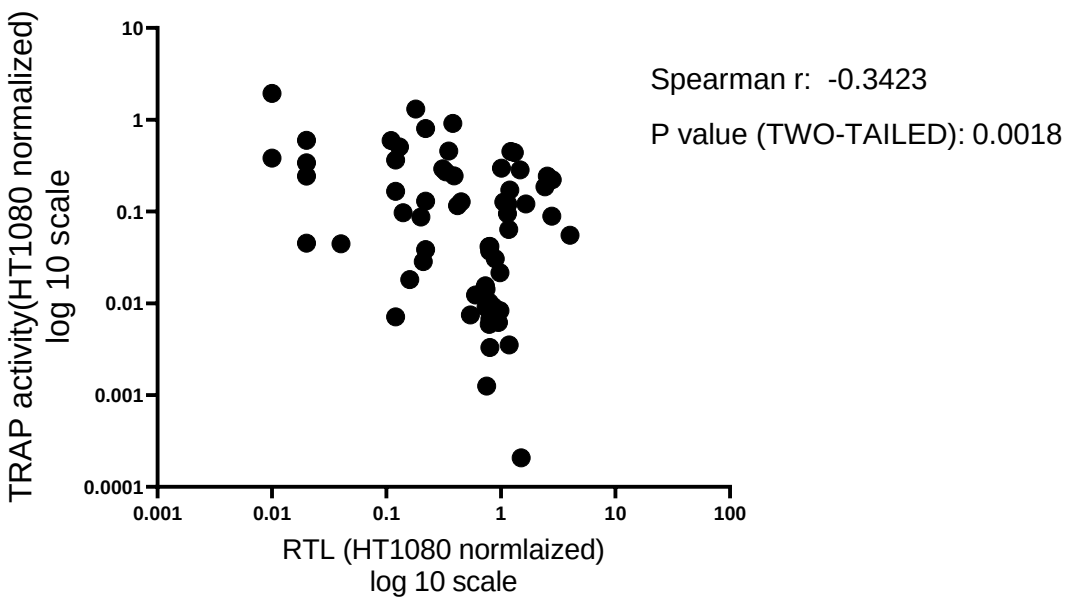

Supplementary Figure 5B:

Telomerase activity was measured from protein lysates across 64 TNBC samples (long or short telomeres) normalized to the telomerase activity of HT1080 cells for the same amount of protein; spearman correlation was calculated between RTL (relative telomere length) and telomerase activity.